PREPARATION AND CHARACTERIZATION OF POLYARYLSULFONE BASED MEMBRANES FOR WATER PURIFICATION

Thesis

Submitted in partial fulfillment of the requirements for the degree of

DOCTOR OF PHILOSOPHY

by

IRFANA MOIDEEN K
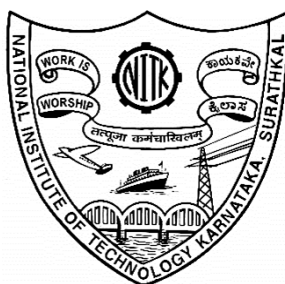
DEPARTMENT OF CHEMISTRY

NATIONAL INSTITUTE OF TECHNOLOGY

KARNATAKA, SURATHKAL, MANGALORE - 575025

December, 2017

DECLARATION

I hereby *declare* that the Research Thesis entitled **"Preparation and characterization of polyarylsulfone based membranes for water purification"** which is being submitted to the National Institute of Technology Karnataka, Surathkal in partial fulfillment of the requirements for the award of the Degree of ***Doctor of Philosophy*** in Chemistry is a *bonafide report of the research work carried out by me.* The material contained in this Research Thesis has not been submitted to any University or Institution for the award of any degree.

Reg. No. 135036CY13F01, Irfana Moideen K

Department of Chemistry

Place: NITK, Surathkal

Date:

CERTIFICATE

This is to *certify* that the Research Thesis entitled **"Preparation and characterization of polyarylsulfone based membranes for water purification"** submitted by **Irfana Moideen K (Register Number: 135036CY13F01)** as the record of the research work carried out by her is *accepted as the Research Thesis submission* in partial fulfillment of the requirements for the award of degree of **Doctor of Philosophy**.

Dr. Arun M. Isloor

Research Guide

Chairman- DRPC

ABSTRACT

The membrane technology has gained prominence in water purification because of its energy efficiency. However, the lack of suitable membrane is a major technological hurdle in its acceptance as a primary tool for water purification. The polyarylsulfone based membranes are widely used due to its superior thermal and mechanical stability. However, its poor hydrophilicity and fouling nature have driven further research in this area. Therefore, the present work is an attempt to improve the performance of polyarylsulfone based membranes for water purification.

In this research work, the polyarylsulfones such as polysulfone and polyphenylsulfone (PPSU) were used for the fabrication of novel membranes. The performance of membranes was improved by different modification techniques such as blending, chemical modifications, coating, or nanocompositing. The prepared membranes were characterized by analyzing their morphology, topography, surface hydrophilicity, water uptake capacity, and porosity. The membrane performance was further evaluated by the permeability, selectivity, and antifouling studies. The water purification capability of these membranes was studied by the rejection of heavy metal ions, salts, proteins, and dyes present in the aqueous feed.

The ultrafiltration flat sheet membranes prepared using hydrophilic modifiers such as sulfonated PPSU, polyethylene glycol-1000, and glycine betaine showed good heavy metal rejection than their pristine counterparts. The studies on the bath composition on sPPSU based membranes also showed to affect the membrane morphology and porosity. The nanoparticles (NP) such as chitosan NPs (CNP), silver-loaded CNPs, and MoO_3 NPs were prepared and used as additives to fabricate nanocomposite hollow fiber membranes. These modified membranes showed better antifouling and antibiofouling properties. The thin film composite nanofiltration membranes were also prepared by incorporating glycine and L-glutamine as hydrophilic additives. The addition of these additives improved the water flux without compromising the salt rejection. Overall, the modified membranes exhibited an enhancement in the hydrophilicity which resulted in the superior antifouling property.

Keywords: Polyarylsulfone, membrane modification, nanoparticles, antifouling, water purification

CONTENTS

CHAPTER 3

EFFECTS OF BATH COMPOSITION ON SULFONATED POLYPHENYLSULFONE ULTRAFILTRATION MEMBRANES FOR ENHANCED REJECTION OF PROTEIN AND TOXIC HEAVY METAL

CHAPTER 4

FABRICATION OF ANTIFOULING HOLLOW FIBER MEMBRANES EMBEDDED WITH CHITOSAN AND SILVER-LOADED CHITOSAN NANOPARTICLES FOR DYE REJECTION

CHAPTER 5

FABRICATION OF NOVEL HOLLOW FIBER MEMBRANES CONTAINING MOLYBDENUM TRIOXIDE NANOPARTICLES FOR THE EFFICIENT REMOVAL OF DYE AND HEAVY METAL

LIST OF FIGURES

viii

LIST OF SCHEMES

LIST OF TABLES

NOMENCLATURES

A) List of Abbreviations

AA	Acetic acid
AAS	Atomic absorption spectroscopy
AFM	Atomic force microscopy
AHM	Ammonium heptamolybdate tetrahydrate
ATR-FTIR	Attenuated total reflectance Fourier transform infrared
BER	Bore extrusion rate
BSA	Bovine serum albumin
CA	Cellulose acetate
CDH	Central Drug House
CNP	Chitosan nanoparticles
DER	Dope extrusion rate
DI	Deionized
DS	Degree of sulfonation
DSC	Differential scanning calorimeter
E. Coli	*Escherichia coli*
EDX	Energy dispersive X-ray
FDR	Flux decline ratio
FRR	Flux recovery ratio
FS	Flat sheet
FTIR	Fourier transform infrared

GB	Glycine betaine
HA	Humic acid
HF	Hollow fiber
IPA	Isopropyl alcohol
MB	Methylene blue
MF	Microfiltration
MPD	m-Phenylenediamine
M. smegmatis	*Mycobacterium smegmatis*
NF	Nanofiltration
NIPS	Non-solvent induced phase separation
NMP	N-methyl-2-pyrolidone
NMR	Nuclear magnetic resonance
NP	Nanoparticle
PA	Polyamide
PAN	Poly(acrylonitrile)
PANI	Polyaniline
PEG	Polyethylene glycol
PEI	Polyethyleneimine
PES	Polyethersulfone
PEUF	Polymer enhanced ultrafiltration
PIP	Piperazine
PMMA	poly (methyl methacrylate)
PPSU	Polyphenylsulfone
PSF	Polysulfone

PU	Polyurethane
PVA	Polyvinyl alcohol
PVDF	Polyvinylidene fluoride
PVP	Poly(1-vinylpyrrolidone)
PWF	Pure water flux
RB 5	Reactive Black 5
RO	Reverse osmosis
RO 16	Reactive Orange 16
RT	Room temperature
S. aureus	*Staphylococcus aureus*
SEM	Scanning electron microscopy
sPES	Sulfonated polyethersulfone
sPPSU	Sulfonated PPSU
sPSF	Sulfonated polysulfone
TEA	Triethylamine
TEM	Transmission electron microscopy
TFC	Thin film composite
TGA	Thermal gravimetric analysis
TMC	Trimesoyl chloride
TMP	Transmembrane pressure
TPP	Sodium tripolyphosphate
UF	Ultrafiltration
UV	Ultraviolet
UV-Vis	Ultraviolet-Visible

WCA	Water contact angle
XRD	X-ray diffraction
ZP	Zeta potential

B) List of Symbols

aq.	Aqueous
T_g	Glass transition temperature
ΔC	Concentration gradient
ΔP	Pressure gradient
ΔT	Temperature gradient
ΔE	Electric potential gradient
J_w	Water flux
Q	Amount of water passing through the membrane
Δt	Change in time
A	Area of membrane sample
R	Rejection
C_p	Concentration of the solute in permeate
C_f	Concentration of the solute in feed
$wt.$	Weight
W_w	Wet weights of membrane samples
W_d	Dry weights of membrane samples
E	Porosity
L	Thickness of the membrane sample
P	Density of water
Mw	Average molecular weight

R_a	Average roughness
R_q	Root mean square roughness
R_{irr}	Irreversible fouling ratio
R_{rev}	Reversible fouling ratio
r_m	Mean pore radius

CHAPTER 1

INTRODUCTION

Abstract: *This introductory chapter display, the significance of present research work on the use of membranes for water purification. It gives concise details on the membrane fabrication, modification, types and its applications. This chapter also comprises of a literature survey that enlightens the usage of polyarylsulfone polymers such as polysulfone and polyphenylsulfone as the membrane material.*

1.1 GENERAL INTRODUCTION

Water is a lifeline for all the living beings and one of the most important natural resources. Water exists in abundance on Earth as it covers 70 % of its surface, and the total volume is estimated to be about 1.4 billion km^3. However, most of it is saline water, and only about 2.5 % of the global water resources (about 35 million km^3) is constituted by fresh water, of which 69 % is bound as snow and ice, and 30 % is stored as groundwater (Figure 1.1). The annual consumption of groundwater is generally considered to be 1000 km^3, and global groundwater recharge is 12,700 km^3 per year. However, the global demand for water is barely about 11 % of the average water released from the rivers, where, 70 % is utilized for agriculture, 20 % for industrial activities and 10 % for household and municipal uses (Figure 1.2). Therefore, the crisis is not in terms of global water scarcity, but in its uneven distribution. Moreover, the unmet demands of water lead to the deprivation of fresh water levels in both urban and rural regions.
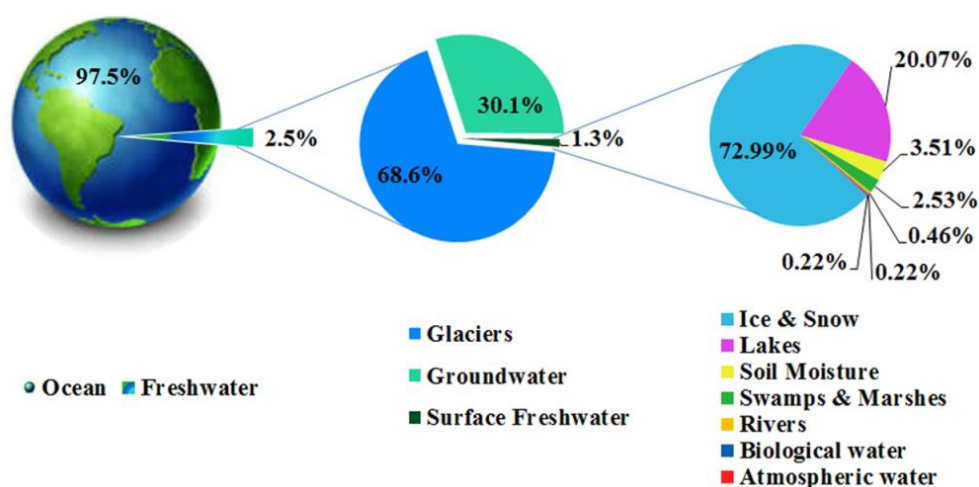
Figure 1.1 Pi-chart of distribution of water on the Earth (Gleick 1993)
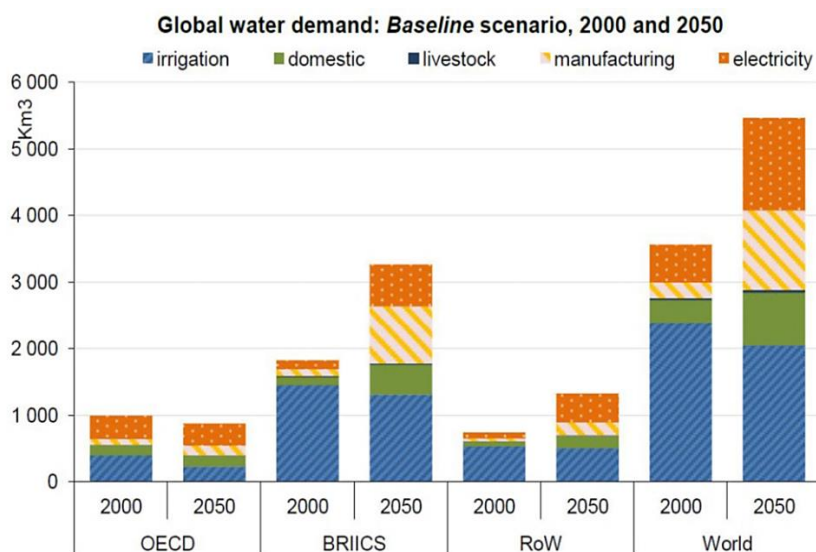
Figure 1.2 Graphical illustration of global water demand (OECD)

Water has turned out to be the limiting resource for urban development as the demand for clean water for human consumption, agriculture and industrial purpose has risen due to rapid growth in human population. Need for clean water is increasing every year and it is a fact that clean water is not available to 1 out of 5 people on Earth. Moreover, the water resources, such as rivers, lakes, and oceans are continuously being polluted by discharge of agricultural, industrial and municipal waste in large quantity; whereas the atmospheric deposition of gaseous emissions pollutes the water sources indirectly. Deposition of toxic and carcinogenic substances like pesticides, herbicides, heavy metals (such as mercury, zinc, and lead), detergents, and oil wastes into the water bodies has been posing a threat to aquatic health and welfare of population (Pollack *et al.* 2003). It is reported that 80-90 % of diseases and 30 % of death in developing countries are due to the poor quality of water.

Unfortunately, it is very easy to contaminate, but often hard, costly, and at times even impossible to decontaminate (Begon *et al.* 2006). Furthermore, water scarcity is an issue affecting the quality of our environment, drinking water supplies, food production, energy, and industrial output (Shannon *et al.* 2008). This crisis with water is anticipated to intensify in the future. Thus, scarcity of fresh water and pollution of the freshwater resources due to the rapid growth in population and economic

development raise the need for efficient and low-cost methods to purify polluted water and desalinate the sea and brackish water. Presently, a huge amount of money is invested every year in the conservation, recycle, and purification of water. Hence, membrane technology which is much simpler and energy efficient method over the conventional methods has been developed and employed for the water treatment, as a solution to the limiting freshwater resources.

1.2 HISTORICAL DEVELOPMENT OF MEMBRANE

The membrane technology has gone through a prolonged historical advancement in laboratory study before achieving the pioneer industrial application since 1960 (Fane *et al.* 2011). Today the membrane technology has undergone rapid development that its application has paved way for better tomorrow.

The membrane technology emerged from the 18th century when the philosopher-scientist Abbe Nollet in 1748 discovered the phenomenon referred as "Osmosis" where the animal bladder served as semipermeable membrane when in contact with the spirit of wine in a container (Nollet 1995). In 1855, Fick introduced a novel synthetic membrane using nitrocellulose (Fick 1855). Graham in 1833, studied gas permeation and proposed Graham's law in 1866 (Graham 1866). He was also first to carry out the dialysis experiment. Traube (1867) developed a semipermeable membrane by precipitating cupric ferrocyanide in a thin layer of porous porcelain and later the membrane was used by Pfeffer in his primary investigations of osmosis. In 1908, the term ultrafiltration (UF) was coined by Bechold as he devised a technique of developing synthetic membrane by infusing filter paper in a solution of nitrocellulose in glacial acetic acid (Bechhold 1908). Around 1920's, the reverse osmosis (RO) membranes were in its infancy until it was retrieved by Reid and co-workers after 30 years (Reid and Breton 1959). The hemodialyzer developed by Kolff *et al.* (1944) lead to the extensive application of membranes in the biomedical field.

By the 20th century, the modern membrane science entrenched its place in industrial application from the laboratory scale. In early 1960's, the discovery of cellulose based anisotropic RO membranes, which were defect-free and hydrophilic via phase inversion by Loeb–Sourirajan was a key to the establishment of the

significant membrane based industries (Loeb and Sourirajan 1962). It was a significant breakthrough in the application of the RO membrane as an effective means to produce drinking water from the seawater. Shortly, various other synthetic polymers like polyamides (PA), polyacrylonitrile (PAN), polysulfone (PSF), polyethylene (PE), etc. were used as a basic material for the preparation of synthetic membranes. The development of self-supporting hollow fiber (HF) membranes by Mahon (1966) paved the way for a different approach to the geometry of the membrane. Thereafter, diverse membrane configurations such as flat sheets (FS), tubes, and HF or capillaries tubes were reported.

The status of membrane technology has been changed significantly during the period from 1960 to 1980. The Loeb–Sourirajan technique was then considered as a milestone for the development of several other membrane preparation techniques, such as interfacial polymerization and multilayer composite casting and coating, to create membranes with high performance. The development of thin film composite (TFC) membranes by Cadotte *et al*. (1980) led to a crucial breakthrough in the commercial application of RO. By 1980, large plants were installed globally for microfiltration (MF), UF, nanofiltration (NF), RO, and electrodialysis processes. As a result of which, a promising growth has been observed in the membranes and membrane-based process since 1960's, where its application expanded from laboratory scale to commercial level.

Today, membrane plays a dominant role in the treatment of seawater and wastewater, in chemical and pharmaceuticals process, in medical applications, in food processing, in the separation of gas and vapors, and in fuel cells etc. Furthermore, the emergence of gas separation by Monsanto Prism membrane for hydrogen separation was the principal development in 1980. Therefore, membrane technology is indispensable in the current situation, where the growing population and water scarcity are major concerns. Moreover, membrane technology is expected to tackle the challenges in the field of energy, water, and environment in coming years.

1.3 FUNDAMENTAL ASPECTS OF MEMBRANES

A membrane is a semipermeable barrier that separates two vicinal phases and controls the selective transport of various components under the influence of driving force across it in a specific manner (Lonsdale 1982). The ability to regulate the rate of permeation of different species is one of the most important properties of the membrane. Hence, membrane separation process depends on the types of membranes used. Figure 1.3 is the schematic illustration of membrane separation, wherein the feed i.e. the solution which is to be treated by the membrane passes to give permeate i.e. the species passing through the membrane, while the components rejected by the membrane is called retentate.
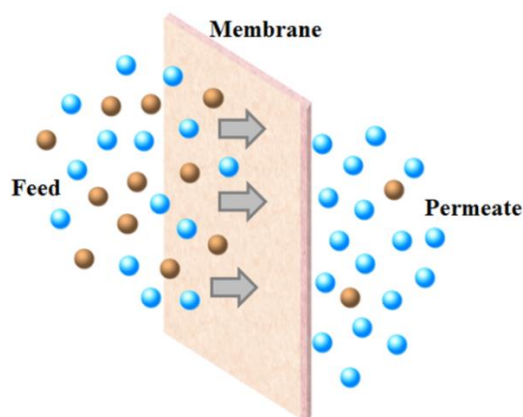
Figure 1.3 Schematic representation of membrane separation process

Even though there is a lot of competition between the membrane processes and the conventional water treatment techniques, there are significant advantages of using membrane processes over the conventional methods, which is summarized below:

- It is very energy efficient and economical.
- Simple to operate and produces high-quality water.
- Membrane processes in combination with other conventional water treatment methods are more reliable and cost-effective.
- Separation can be carried out under mild conditions.
- They have a lower environmental impact as there are no toxic chemicals used in the process and no heat is generated.

- Properties of the membranes are variable and can be altered based on necessity.

- Easy to control and scale up.

However, it also suffers from certain drawbacks such as,

- The long-term reliability of membrane processes is not completely proven.

- Need for pre-treatment due to sensitivity to fouling and concentration polarization.

- The low mechanical strength of membrane, which may lead to damage under the extreme operating conditions.

1.3.1. Membrane transport mechanism

The transport of species across the membranes is controlled by the driving force such as concentration (ΔC), pressure (ΔP), temperature (ΔT) and electrical potential (ΔE) gradients in the membrane matrix. There are two types of models that describe the working mechanism of the membranes. They are pore flow model and solution-diffusion model.

In pore flow model, the separation process occurs as permeates are transported by pressure-driven convective flow through pores. Here the molecules get rejected based on the sieving mechanism wherein, the permeate is separated by size exclusion and pore flow. This mechanism is typically observed in case of porous, MF, and UF membranes. The pressure-controlled separation process describes the pore flow model and is expressed in Darcy's law;

$$J_i = K'c_i \frac{dp}{dx}$$

Where $'dp/dx'$ is the pressure gradient present in the porous medium, $'c_i'$ is the concentration of component $'i'$ in the medium and $'K''$ is a coefficient revealing the nature of the medium (Baker 2004).

In nonporous dense membranes, separation is based on a solution-diffusion mechanism. In solution-diffusion model, the permeate dissolve in the membrane material and then diffuse through the membrane. The selectivity is based on the difference in solubility and differences in the rates of diffusion taking place through

the membrane. The transport of permeate by solution-diffusion is described by Fick's law of diffusion. According to the Fick's law of diffusion the transport rate i.e. flux $'J_i'$ (g.cm^{-2}s^{-1}) of species (*i*) is correlated to the concentration gradient (*dc$_i$/dx*). It is expressed as follows;

$$J_i = -D_i \frac{dc_i}{dx}$$

Where, the term 'D_i' is the diffusion coefficient (cm^{2}s^{-1}) which is a measure of the mobility of the individual molecules. The negative sign indicates that the diffusion is down the concentration gradient, i.e. from a region of high concentration to low concentration.

The basic differences between these models are the relative size and permanence of the pores. The size and position of free-volume elements (pores) are fixed in the pore flow model. In solution-diffusion model, the dense membranes have no fixed the free-volume elements (pores). Here, permeates passes through the spaces between polymer chains caused by thermal motion of the polymer molecules. These free-volume elements disappear after the passage of permeates. Moreover, the pore flow model which is a pressure driven process results in higher flux than the diffusion model which works on concentration gradient.

1.3.2 Classification of membranes

Membranes can be classified in many ways such as biological or synthetic, homogeneous or heterogeneous, porous or non-porous, symmetric or asymmetric in structure, solid or liquid in nature. It may contain organic or inorganic materials or functional groups with specific binding or complexing abilities. Therefore, the term "membrane", is complex as it has extensively diversified materials and structures.

The membranes can be classified as follows according to their morphology:

- *Symmetric membrane:* In symmetric membranes, the structure and the transport properties are identical across the cross-section with a uniform pore size (Figure 1.4). The thickness of the entire membrane determines its flux. They may have either porous or dense structure which can be tuned as per the requirement.
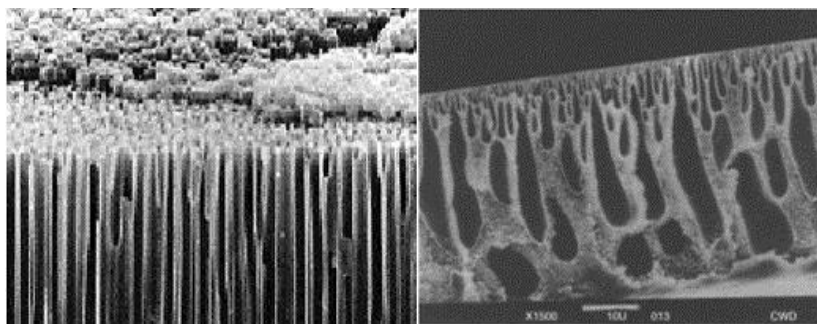
Figure 1.4 Cross-sectional images of symmetric (left) and asymmetric (right) membranes.

- *Asymmetric membrane:* Asymmetric membranes are one, in which structural and transport properties vary across the membrane cross-section (Figure 1.4). These membranes are widely used for separation processes. It's composed of a dense thin active layer on a porous sub-layer as support. The nature of the membrane material or the pore size of the skin-layer affects the separation processes. High mass transport rate and good mechanical strength are the two main properties required for this type of membrane. They are further sub-branched into the integrally skinned asymmetric membrane and TFC membrane.
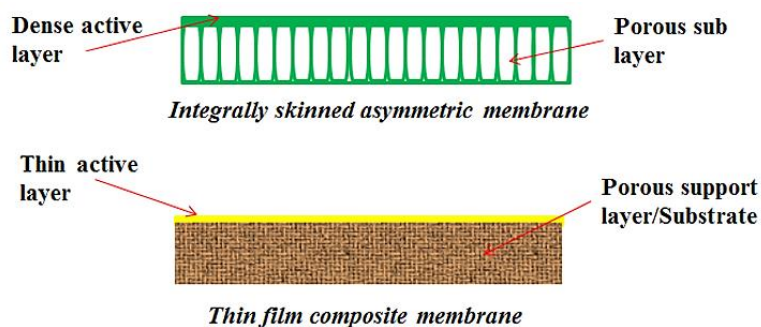
Figure 1.5 Schematic representations of integrally skinned asymmetric membrane and TFC membrane

- *Integrally skinned asymmetric membrane:* This kind of membrane is composed of an identical material in its dense top active layer and the porous sublayer, which are formed during the phase inversion (Figure 1.5).
- *Thin film composite membrane*: Here, the dense active thin coating and the porous support are made of two different compositions. An ultra-thin layer of a

polymer is deposited on the top of a porous support which is physically separated (Figure 1.5).

The membrane processes have four main driving forces which determine the transport rate of the membrane, namely ΔP, ΔC, ΔT, and ΔE (Table 1.1). If the flux is directly associated with the driving force then it is denoted as "corresponding" flux. Thus, the flux associated with ΔP, ΔC, ΔT, and ΔE is denoted as the volume flux, flux of individual molecules, flux of heat, and an electrical current, respectively. There are cases of flux-force relationship which is indirectly related. For example, flux of individual components or a volume associated with forward osmosis, RO and electrodialysis are the results of ΔC, ΔP, and ΔE, respectively.

Table 1.1 Classification of membranes based on driving force (Mulder 1996).

ΔP	ΔC	ΔT	ΔE
MF	Pervaporation	Thermo-osmosis	Electrodialysis
UF	Gas separation	Membrane distillation	Membrane electrolysis
NF	Dialysis		
RO			

Typically, pressure-driven membrane processes are classified into MF, UF, NF, and RO membrane based on the pore size of the membrane (Figure 1.6).

1. *Microfiltration:* Membrane that uses low pressure i.e. less than 2 bar to separate suspended particles solely according to their dimensions. The average pore size of these membranes ranges from 0.05 to 10 μm. These membranes sieves bacteria present in water to give pure water.

2. *Ultrafiltration:* The term UF membrane is used when the pore size of membranes is between 1 nm to 100 nm and operating pressure is from 1 to 10 bar. They retain particles and micro solutes by sieving mechanism.

3. *Nanofiltration:* NF membranes are membranes with a pore size less than 2 nm and the operating pressures range from 10-25 bar. NF membranes can reject organics, multivalent ions, and micropollutants.

4. *Reverse osmosis:* RO membranes operate at a higher pressure up to 80 bar and having a pore size less than 1 nm. The seperation process in these membranes are based on solution diffusion. They are mainly used for desalination of brackish water and seawater.
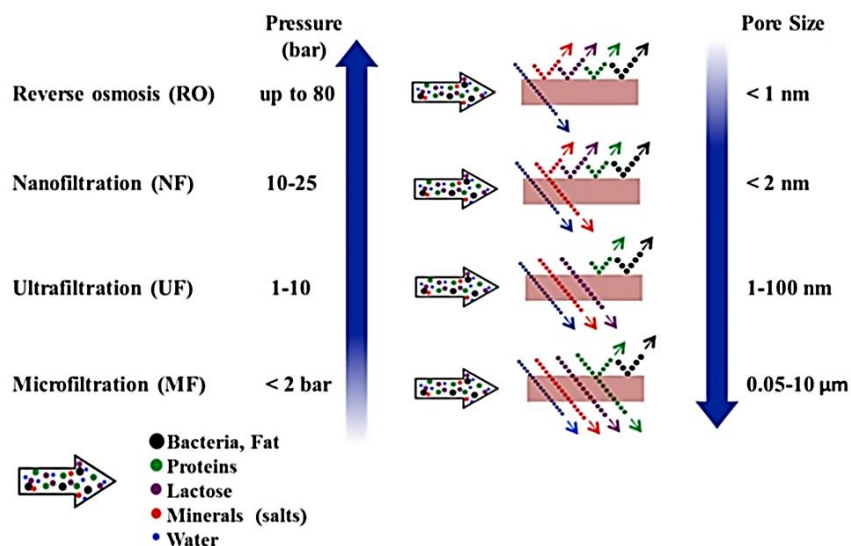
Figure 1.6 Classification of membranes based on pore size (Wu and Imai 2012)

1.3.3 Modes of filtration

The two modes of filtration process in membrane technology are dead-end filtration and cross-flow filtration (Figure 1.7).
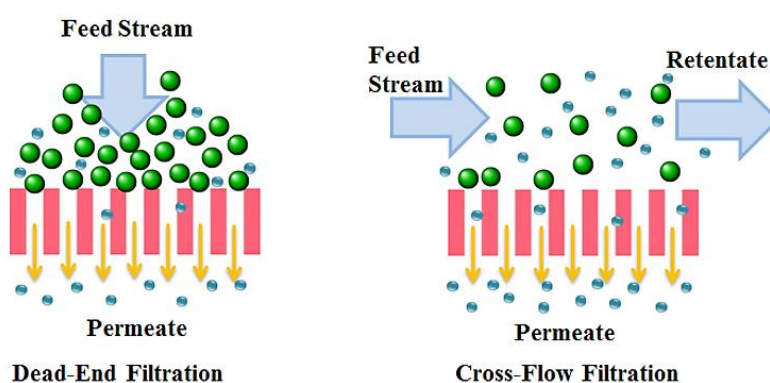
Figure 1.7 Schematic illustration of modes of filtration

- *Dead-end/Direct-flow filtration:* Here the feed solution flow perpendicular to the surface of the membrane. This causes the particulate to get accumulated on the surface, hence results in low permeability due to concentration polarization.

- *Cross-flow filtration:* In this mode, the feed solution flows along or parallel to the membrane surface. Here the accumulation of the particulates is less and hence causing low fouling as the concentration polarization is decreased due to the continuous flow of feed. However, cross-flow requires higher energy than the dead-end filtration as the feed solution is circulated at high velocity.

1.3.4 Basic terminologies in membrane process

Some of the common terminologies which are used in the membrane process are listed as follows:

- *Flux:* Flux is defined as the amount of water passing through a unit area of the membrane per unit time. The flux is a parameter by which the productivity of the membrane is determined.

$$J_w = \frac{Q}{\Delta t \times A}$$

Where,

$'J_w'$ is water flux expressed in $Lm^{-2} h^{-1}$,

$'Q'$ is amount of water passing through the membrane in Litre (L),

$'\Delta t'$ is the time in hours (h),

$'A'$ is the effective membrane area responsible for the filtration, expressed in (m^2).

- *Solute rejection:* The membrane perm-selectivity is the most important property of membrane and it is expressed in terms of rejection (R).

$$R = \left(1 - \frac{C_p}{C_f} \right) \times 100$$

Where,

$'C_p'$ is the concentration of the solute in permeate (can be expressed in M, mM, or %),

$'C_f'$ is the concentration of the solute in feed solution.

- *Swelling:* The water uptake capacity of the membrane is expressed as

$$Water\ Uptake\ = \left(\frac{W_w - W_d}{W_d}\right) \times 100$$

Where,

$'W_w'$ is the weight of swollen/wet membrane (g),

$'W_d'$ is the weight of dry membrane (g).

- *Porosity:* Porosity (ε) of a membrane is defined as the ratio of the pore volume to geometrical volume. It is as follows:

$$\varepsilon\ = \left(\frac{W_w - W_d}{Al\rho}\right) \times 100$$

Where,

$'W_w'$ is the wet weight (g) of membrane samples,

$'W_d'$ is the dry weight (g) of membrane samples,

$'A'$ is the area of the sample (cm^2),

$'l'$ is the thickness (cm) of the membrane sample,

$'\rho'$ is the density of water (0.998 gcm^{-3}).
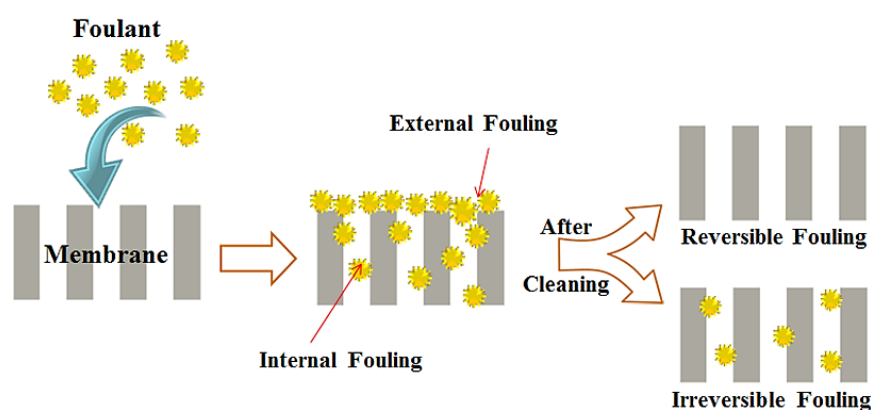
Figure 1.8 Mechanism of membrane fouling

- *Membrane fouling:* Membrane fouling is the phenomena where the particles in the feed solution such as, colloids, emulsions, suspensions, macromolecules, salts etc. deposit on (external fouling) or in (internal fouling) the membrane which in turn affects the efficiency of the separation process. The flux decline

takes place due to adsorption, pore blocking, precipitation, and cake formation (Pabby *et al.* 2015). The fouling can be classified as reversible and irreversible fouling based on the nature of fouling (Figure 1.8). If the foulant adsorbed on membrane surface could be removed by simple hydraulic washing or chemical cleaning, it is reversible fouling. While the irreversible fouling is when the foulant is strongly adhered to the membrane and can't be removed by cleaning.

- *Concentration polarization:* During membrane filtration, the concentration of the non-permeating solute increases on the feed side due to the formation of a layer at the membrane surface. Moreover, the concentration of the permeating solute reduces on the fluid adjacent to the feed side than the bulk solution. Hence, there develops ΔC in the fluid adjacent to the membrane surface which is known as concentration polarization. The fouling of membranes takes place due to the concentration polarization.

1.3.5 Membrane preparation

The membrane processes mainly depend on the structure and transport property of membrane. It is observed that different methods of membrane preparation resulted in different types of membranes with various pore sizes from the same materials (Pinnau and Freeman 2000). The membrane preparation can be performed by various techniques, which in turn helps in modifying the membranes based on the requirements. The main criterion to choose the membrane preparation technique depends on the selection of the polymer, preferred structure of the membrane and also application of the membrane (Lalia *et al.* 2013). Some of the membrane preparation techniques are listed as follows:

- Sintering
- Track etching
- Stretching
- Phase inversion
- Solution coating
- Vapor deposition
- Template leaching

Amongst these, the phase inversion technique is very important and frequently used due to its simplicity. It is a flexible technique resulting different kinds of membrane morphologies. Normally, this technique results in asymmetric membranes with a fairly thin selective active layer sustained on a thick porous sub-layer (Jansen *et al.* 2005). Here polymer solution prepared by dissolving it in a suitable solvent is cast onto a plate, a belt, or a fabric support. This liquid film cast was precipitated by precipitant in phase inversion process. The membrane morphology can be reformed by altering the polymer, the polymer concentration, the precipitation medium, and the precipitation temperature (Strathmann and Kock 1977). The different techniques for membrane preparation controlled by phase separation are discussed below:

1. ***Immersion precipitation/Non-solvent induced phase separation:*** The non-solvent induced phase separation (NIPS) is the process where the polymer cast is dipped in the non-solvent coagulation bath. The membranes are obtained as the polymer gets precipitated due to liquid-liquid demixing. This method is one of the most commonly used techniques to prepare polymeric membranes with different morphology. In this process, precipitation of the polymer occurs due to the separation of the homogeneous polymer solution into two phases, i.e. a solid polymer rich and a liquid solvent rich phase during diffusion of solvent from the polymer dope solution to the coagulation bath and flow of non-solvent from the coagulation bath to the polymer matrix, resulting in the solidification of polymer rich phase with a porous structure comprising of the network with relatively uniform pores. The rate of diffusion of the solvent and non-solvent at the membrane interface determines the membrane morphology. Hence, the composition of solvent/non-solvent system and polymer dope concentration is an important factor that affects the membrane morphology.

2. ***Thermally induced phase separation:*** This method involves a reduction in the solvent quality on lowering the temperature. Here, the thermal energy is responsible for phase separation. Once the demixing occurs, the solvent is extracted, evaporated off or frozen to give the membrane.

3. ***Evaporation induced phase separation:*** Here, the polymer is dissolved in a mixture of a volatile solvent and a less volatile non-solvent. The phase separation takes place as the volatile solvent evaporates.

4. ***Vapor induced phase separation***: The phase separation of the dope solution is generated by subjecting the polymer solution to vapors containing non-solvent (typically water). The polymers get precipitated on adsorption of non-solvent.

1.3.6 Membrane properties and materials

Membranes could be prepared from different materials with a wide variety of properties. Therefore, the selection of membrane materials should be unambiguous based on specific properties that are essential for the membranes. On the basis of materials used, synthetic membranes are grouped into organic and inorganic membranes, where the former is considered highly significant due to its wide application in water treatment.

The selection of a suitable material for the membrane depends on following properties.

1. Film forming ability of the material is a very significant parameter that has to be considered while the selection of membrane material since it is essential for the formation of a cohesive film.

2. The mechanical strength of the material should be good enough to tolerate high operating pressure due to its strength, flexibility, and stability.

3. Membrane material should be thermally stable so that it can withstand temperature variation. Therefore, the thermal stability of the polymer is determined by its glass transition temperature (T_g) and it should be higher than that of the process temperature.

4. Chemical stability is another factor that membrane material should possess in order to sustain extreme pH and chemical condition of feed solution.

5. There must be balance in hydrophilic and hydrophobic nature of the material so as to obtain higher flux, better rejection, and minimal fouling during operation.

However, there are many membrane materials investigated till date which exhibits a few of the above-mentioned material properties. Some of the polymeric

materials that are widely used for the membrane synthesis are PSF, poly(vinylidene fluoride) (PVDF), PAN, polyethersulfone (PES), chitosan, cellulose acetate (CA). The polymers such as PVDF, PSF, PAN, and PES usually result in MF and UF membranes (Baker 2004) (Figure 1.9). However, each one of them has its own merits and demerits. For example, CA and chitosan are biodegradable and hydrophilic polymers, while the former having low chemical resistance and later being insoluble in organic solvents. PVDF and polyetherimide have good thermal and chemical resistance, while the hydrophobicity of the polymer is its limitation.

Polysulfone

Cellulose Acetate (R: CH₃CO or H)

Polyethersulfone

Chitosan

Poly(vinylidene fluoride)
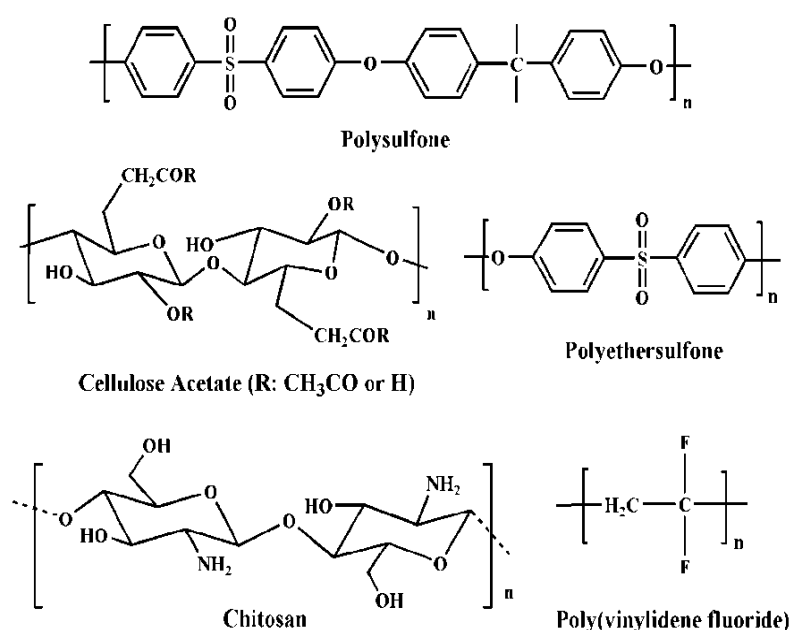
Figure 1.9 Structures of some commonly used polymers in membrane technology

Polyarylsulfones are polymers consisting mainly of phenyl and biphenyl groups linked by ether and sulfone groups, which include PSF, PES, and polyphenylsulfone (PPSU). These polymers have gained prominence in the field of engineering plastics. These materials exhibit high thermal stability, mechanical strength, and chemical stability, that is, resistance to temperature, stress, and oxidation, respectively. Polyarysulfone polymers are utilized to fabricate FS, HF, and tubular membranes due to their solubility in conventional processing solvents. Higher molecular weight of these polymers results in improved fiber strength and minimized fiber breakage. Their unique features such as hydrolytic stability and highly desirable transparency make polyarylsulfone polymers stand out among other high-performance thermoplastic

polymers. The Food and Drug Administration declared sulfone-based polymers as an ideal material for food and medical applications due to its ability to withstand repeated steam sterilization. Furthermore, exceptional electrical properties, flame retardancy, and resistance to radiation make them suitable for several electrical and electronic applications. Good dimensional stability and close tolerances also make sulfone-based polymers highly desirable for other industrial applications, which demands toughness, long-term creep resistance, and low mould shrinkage.

The basic features of the polyarylsulfone polymers that make it excellent membrane material are as follows:

- Extraordinary mechanical properties.
- Excellent hydrolytic stability.
- Stable within pH levels from 2 to 13.
- Ease of MF and UF membrane formation.
- Soluble in conventional processing solvents.
- Excellent biocompatibility.
- Outstanding thermal and chemical stability.
- Transparency and superior resistance to environmental stress cracking.

However, the main drawback of these polymers is their hydrophobicity as membrane fouling is directly related to the hydrophobic nature of the material. In this work, the polysulfone and polyphenyl sulfone were chosen as the membrane material and their properties are discussed below.

1.3.5.1 Polysulfone as membrane material

PSF (Figure 1.10) is a rigid, high strength, semi-tough, and transparent polymer. It offers higher thermal stability with T_g of 195 °C and better hydrolytic and oxidative stability than polycarbonate. PSF is obtained from the reaction between bisphenol A and dicholorodiphenyl sulfone. The presence of ether group in the backbone provides good flexibility and toughness to the polymer. The membranes made from PSF exhibit resistance to high energy radiation due to the aromatic moieties present in the polymer. It retains its good mechanical properties when exposed to steam and other

sterilization techniques. Resistance to extreme pH, chlorine, and low creep at high temperature makes it an outstanding membrane material. The poor hydrophobicity of PSF membrane restricts its utilization in membrane application; hence there is a demand for its modification to attain desired properties suitable for membrane operations. Membranes obtained from PSF may be used as MF, UF, NF, RO, and gas separation membrane. They are extensively used as a support layer in TFC membranes (Yang *et al.* 2017).
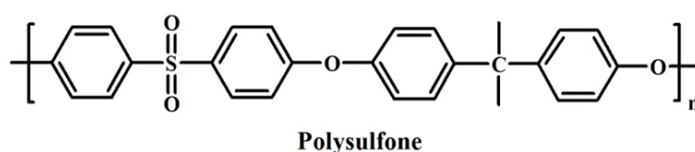
Polysulfone

Figure 1.10 Structure of polysulfone

1.3.5.2 Polyphenylsulfone as a membrane material

PPSU (Figure 1.11), also known as polyarylethersulfone, exhibits superior performance among the polyarylsulfone polymers with better mechanical and chemical resistance than PSF. It is capable of operating at high temperatures as its T_g is 220 °C which is higher than that of PSF (190 °C) and equivalent to PES (220 °C) (Darvishmanesh *et al.* 2011). It also shows high resistance to hydrolysis, plasticization, and stress p-cracking caused by numerous organic solvents. However, the poor hydrophilicity of this polymer is its major limitation that can be overcome by the modification (Shukla *et al.* 2017). In addition to the outstanding chemical and physical properties, the fairly low price of PPSU tags it as an ideal material for the preparation of next-generation membranes.

Polyphenylsulfone
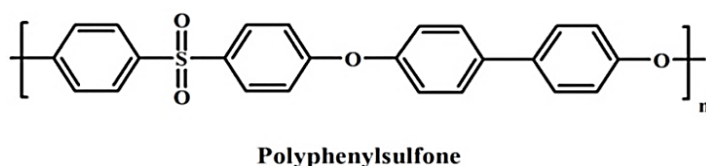
Figure 1.11 Structure of polyphenylsulfone

1.3.7 Modification of the membranes

The characteristic features discussed earlier, makes the PSF and PPSU, a potential membrane material. However, the hydrophobic nature of these polymers is

the major drawback as it affects the performance of membranes due to the fouling of the membrane. Hence there is need to modify the membrane material to reduce the adsorption of undesirable substance on the surface of the membranes. Apart from this, the selectivity of the membrane has to be improved since the polymer lacks the desired properties for the separation and purification applications.

The membrane can be modified by processes like coating, blending, compositing, chemical modification, grafting, or their combination. However, the uniformity, reproducibility, stability, process control, and cost-effectiveness are the factors that have to be considered while choosing the modification techniques.

1. *Coating:* It is a type of membrane modification where a thin layer of coating material with the desired site like the hydrophilic site, charged site, and binding sites are non-covalently adhere onto the membrane substrate (Soroush *et al.* 2012). The membranes modified by this technique result in UF and NF membranes for the removal of the heavy metal and suspended solids in the feed. However, the stability of the coating is a major concern.

2. *Blending:* Blending technique is the simplest and most widely used method. The process includes mixing of two or more polymers to give rise to a homogeneous solution, which when casted result in the membrane with better performance (Susanto and Ulbricht 2009).

3. *Compositing:* A composite material is developed when two or more material with different physical or chemical properties is mixed to form a new material. Here the new materials possess distinct properties of the individual materials used. The thin film composite membranes i.e. the membranes formed by composite layer on the substrate and nanocomposite membranes i.e. the membranes obtained by incorporation of nanoparticles to the polymer dope solution are common composite membranes (Hebbar *et al.* 2014).

4. *Chemical modification:* This method involves treatment of the membrane materials with chemical reagents to introduce functional groups to the membranes. The chemical modifications include sulfonation, amination,

carboxylation, aminomethylation, etc. of the polymers (Breitbach *et al.* 1991, Staude and Breitbach 1991).

5. ***Grafting:*** Grafting is a method wherein monomers or polymers with low molecular weight are covalently bonded to the membrane (Shenvi *et al.* 2013). It is further classified into various techniques such as chemical, enzymatic, photochemical, and plasma technique, based on the structure of the polymer and desired characteristics of the modified membrane.

6. ***Combined methods:*** Here, a combination of two or more modification techniques is involved. For example, membrane modification can be carried by a combination of blending and chemical modification (Padaki *et al.* 2011) or by combining grafting on blend membranes (Fang *et al.* 2009) or a combination of chemical and grafting technique (Deimede *et al.* 2015). The combined modification technique is effective, in spite of being a complex process.

1.4 APPLICATION OF MEMBRANE TECHNOLOGY

The practical utilization of membrane came into existence only from the 18th century, even though the functions of membranes have been in nature since the dawn of life existed on Earth. An increasing scarcity of potable water led to the exploration of membranes in water treatment. The membrane processes being more economical and energy efficient has been widely used for various other applications. They are as follows:

1. ***Water purification process:***
   - *RO applications:* Majority of the RO membranes are applied for the desalination of sea and brackish water. Ultra-pure water is produced for the electronics, pharmaceuticals and power generation industry. Wastewater treatment is another major application for RO. Chemical processes industries also use RO membranes for effluent water reuse, organic solvent separation, and organic liquid mixtures separation (Li *et al.* 2011).
   - *NF applications:* The NF membranes are applied for the removal of micropollutants or microsolutes such as herbicides, insecticides, and pesticides and for other low molecular components such as dyes and sugars.

Their high rejection of bivalent ions makes them well suited for water softening. Other applications are purification of contaminated groundwater, removal of dyes and heavy metal from industrial effluents.

- *UF and MF process applications:* UF and MF are pre-treatment process prior to RO and also used to treat industrial wastewater i.e. effluent treatment like the leather and tanning effluents, bleach effluents from pulp and paper industry, and oily wastewater from washing operation.

- *Pervaporation:* Presently the pervaporation membranes are applied for the dehydration of solvents and organic/organic separations. The volatile organic compounds are removed from the water by this technique (Kim *et al.* 2002, Tang *et al.* 2012).

2. *Food process:* In the food industry, UF has found a major application in the production of cheese and it is now widely employed all over the dairy industry. Whey separation, yeast production, cleaning of fruit juice, separation of proteins etc. are the common application of UF membrane. MF membrane is used for the sterile filtration of pharmaceuticals, sterilization of beer and wine, and removal of bacteria and viruses from water.

3. *Gas separation:* Initially gas separation membranes focused on separation of nitrogen gas from air. These membranes are also employed for separation of other gases like oxygen, hydrogen, organic vapors from the air. The acid gas removal (Quinn *et al.* 1997), separation and removal of CO_2 from natural gas is another major application of gas separation membrane (Weng *et al.* 2008, 2010).

4. *Energy application:* Proton exchange membranes are used in the fuel cell which is an efficient energy conversion device and has become an economic technology for power generation (Peighambardoust *et al.* 2010, Park *et al.* 2016).

5. *Medical application:* Membranes are used in drug delivery, artificial organs, tissue regeneration, diagnostic devices, hemodialysis, as coatings for medical devices, bioseparations, etc. Out of which, hemodialysis (Bowry *et al.* 2011)

and drug delivery (Thombre *et al.* 1999) are few of the applications of synthetic membranes which are highly sought in the medical market.

1.5 LITERATURE SURVEY

Membrane technology has turned out to be a worthy separation technology over past decades. There has been a significant advancement in the research and development for better membrane materials. Polyarylsulfone polymer such as PSF and PPSU membrane has been widely used for water treatment application due to it's excellent mechanical, chemical, and thermal property. There are various techniques and modifications to develop novel polyarylsulfone membranes, some of which are mentioned below.

Majewska-Nowak *et al.* (1989) reported the synthesis of FS and tubular PSF membranes on a glass plate and poly (methyl methacrylate) (PMMA) bar support, respectively. They studied the performance of both FS and tubular membranes in the treatment of dyehouse effluents. The tubular PSF-PMMA UF membrane exhibited better hydraulic permeability and efficient dye rejection when compared to the FS membranes. This is because the tubular membrane brings in total membrane surface for fluid flow, thereby minimizing the fouling.

Rucka *et al.* (1996) studied the self-cleaning property of trypsin immobilized PSF/aminated PSF blend UF membranes fabricated by phase inversion technique. The blend membranes were reported to be good trypsin carrier. The immobilized membranes by dynamic sorption of trypsin showed higher flux and could effectively concentrate proteins.

Malaisamy *et al.* (2002) prepared UF membranes by blending polyurethane (PU), sulfonated polysulfone (sPSF) and polyethylene glycol (PEG) 600 using *N*, *N*-dimethylformamide (DMF) as a solvent by phase inversion technique. They studied the effect of the polymer composition and additive concentration on pure water flux (PWF), water content, and membrane resistance. The compatibility of sPSF in PU was observed for the composition such as 80:20 and 75:25 of PU/sPSF and 7.5 wt. % of the additive. The incorporation of sPSF in the casting solution increased the water

flux performance by introducing high pore size and reduced membrane resistance. Later they investigated the polymer enhanced ultrafiltration (PEUF) of toxic heavy metal ions such as Cu^{2+}, Ni^{2+}, Cd^{2+}, and Zn^{2+} complexed with polyethyleneimine (PEI) and proteins such as bovine serum albumin (BSA), egg albumin, pepsin, and trypsin. The blend showed higher rejection of both proteins and metal ions and lower flux than pure sPSF membrane (Malaisamy *et al.* 2003).

Sivakumar *et al.* (2005, 2006) studied the effect of concentration of polymer and additives in the UF membranes prepared by the blending of CA and PSF using polyvinylpyrrolidone (PVP) as pore former, on protein separation and heavy metal rejection. The increase in PWF and the water uptake results were observed with increase in the concentration of PSF in the blend. The molecular weight cut-off was calculated using the protein solution such as BSA, pepsin, and trypsin. It was found that BSA showed higher separation and lower flux due to it's higher molecular weight. The PWF increased on increasing the concentration of PVP and PSF due to the formation of a large aggregative pore. The PEUF of heavy metal ions such as Cu^{2+}, Ni^{2+}, Zn^{2+}, and Cd^{2+} was conducted by complexing it with 1 wt. % of PEI. The Cu^{2+} showed highest rejection (70 %) and lower flux (40 $Lm^{-2}h^{-1}$) than other metal ions due to the stable PEI-Cu^{2+} complex formation.

Intensive research has been taking place for the heavy metal removal by membrane filtration method which is more effective and economical option (Bodzek *et al.* 1999, Molinari *et al.* 2008, Huang *et al.* 2010). Due to the larger pore size of UF membrane, the heavy metal ions were complexed with complexing agents such as PEI, polyacrylic acid (PAA), and sodium dodecyl sulfate. (Ennigrou *et al.* 2009, Huang *et al.* 2010). Arockiasamy *et al.* (2008, 2009) also prepared blend membranes using CA and aminated polyetherimide, where the membranes showed better antifouling property due to the enrichment with amine. They also reported the preparation of CA/aminated PSF (Figure 1.12) blend membranes for polymer enhanced heavy metal separations, where rejection of Cu^{2+} was highest due to strongly bound Cu^{2+}-PEI. Incorporation of additive PEG-600 increased the hydrophilicity and flux.
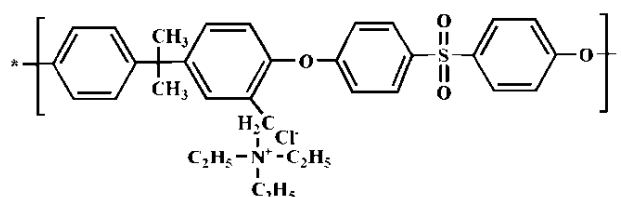
Figure 1.12 Structure of aminated polysulfone (Arockiasamy *et al.* 2009)

Ghosh and Hoek (2009) prepared PA membranes by interfacial polymerization of m-phenylenediamine (MPD) and trimesoylchloride (TMC) over the porous PSF substrate. The PSF support was prepared with different casting composition and studied for the influence of pore structure on the thin film layer properties. The pore structure of the substrate was varied by addition of pore formers such as PEG and PVP to casting solution or by adding solvent to coagulation bath. The TFC membranes displayed "ridge-and-valley" morphology on pure PSF as a substrate while "nodular morphology" for the blend PSF substrate. They observed that porous and rough support resulted in the permeable TFC membranes while larger pore size showed high salt permeability as the PA formation inside the pore is less (Figure 1.13).
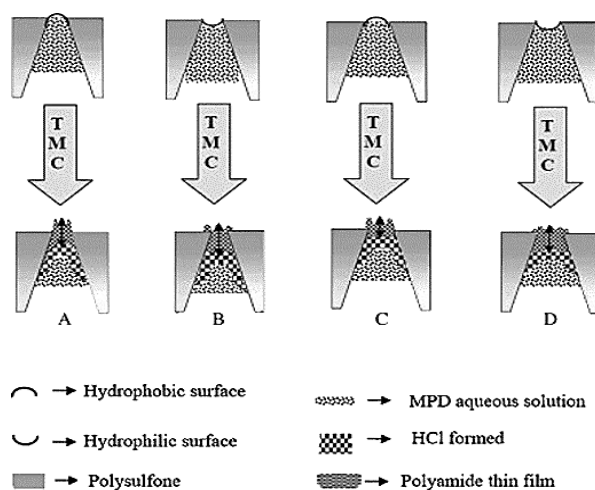
Figure 1.13 Illustration of the role of the pore structure of PSF membrane support during interfacial polymerization (Ghosh and Hoek 2009).

Mbareck *et al.* (2009) studied the heavy metal removal by PSF/PAA UF blend membranes fabricated by the phase inversion technique. The immobilization of the PAA in PSF membranes resulted in the decrease in pore size while the porosity and

permeability increased. The effect of pH, pressure, and concentration of metal ions on the rejection of heavy metal such as Pb^{2+}, Cd^{2+}, and Cr^{2+} was studied. The membrane showed high rejection at pH 5.7, which decreased on lowering the pH, while the rejection result decreased with increase in concentration and pressure. The PAA showed strong interaction with the Pb^{2+} which is confirmed with energy dispersive X-Ray (EDX) analysis.

Darvishmanesh *et al.* (2011) prepared PPSU based NF membranes of different composition (17 wt. %, 21 wt. % and 25 wt. %) using phase inversion method in a different solvent system such as N-methyl-2-pyrrolidone (NMP), dimethylacetamide (DMA) and a mixture of DMF and NMP on membrane performance. The morphology and performance of FS membranes were greatly influenced by the nature of solvent and polymer concentration. The increase in the concentration of polymer reduced the formation of macrovoids and increased the rejection of Rose Bengal dye. They also reported the preparation of PPSU based HF membranes by a dry-wet spinning technique (Darvishmanesh *et al.* 2011). The HF displayed asymmetric structure with dense skin layer and a porous sub-layer. The membrane was selective for the removal of Rose Bengal dye and found that dye rejection increased with increase in the concentration of the PPSU, which agreed with its lower pore size.

Hwang *et al.* (2011) reported the preparation of PPSU/polyetherimide blend membranes by blending hydrophobic PPSU and hydrophilic polyetherimide by non-solvent induced phase separation method. The membrane morphology and performance were tested to study the effect of the blend composition. It was observed that the hydrophilicity and pore size of the blend membranes increased with the increase in the polyetherimide concentration in the blend. The improvement in membrane hydrophilicity, in turn, resulted in resistance to the reversible fouling. The membranes also showed resistance to humic acid (HA) due to the electrostatic repulsion between the negatively charged HA and weak negative charge developed on the membrane.

Liu et al. (2012) prepared sulfonated TFC membranes on PPSU membrane support. The sulfonated diamine such as 2,5-bis(4-amino-2-trifluoromethyl-phenoxy)

benzenesulfonic acid and 4,4_-bis(4-amino-2-trifluoromethylphenoxy)biphenyl-4,4_-disulfonic acid along with piperazine (PIP) was reacted with TMC to form PA layer by interfacial polymerization. The TFC membrane surface was studied by attenuated total reflection Fourier transformed infrared (ATR-FTIR), scanning electron microscopy (SEM) and water contact angle (WCA) measurement. The dye rejection studies for Methyl Orange and Rhodamine B were conducted. The incorporation of the sulfonic group by sulfonated diamine resulted in higher water flux and hydrophilicity, without compromising the dye rejection.

Zhao *et al.* (2012) developed the polyaniline (PANI)−PVP nanocomposite and incorporated it into the PSF to prepare nanocomposite membrane by phase inversion method. The PANI-PVP additive used played the role of both hydrophilic additive and pore forming agent. The nanocomposite membranes were examined for its antifouling property using cross-flow filtration set up. The prepared membranes were compared with PSF/PVP and found that PSF/PANI−PVP membranes displayed higher flux, hydrophilicity and better antifouling nature with lower flux decline and higher flux recovery on water washing.
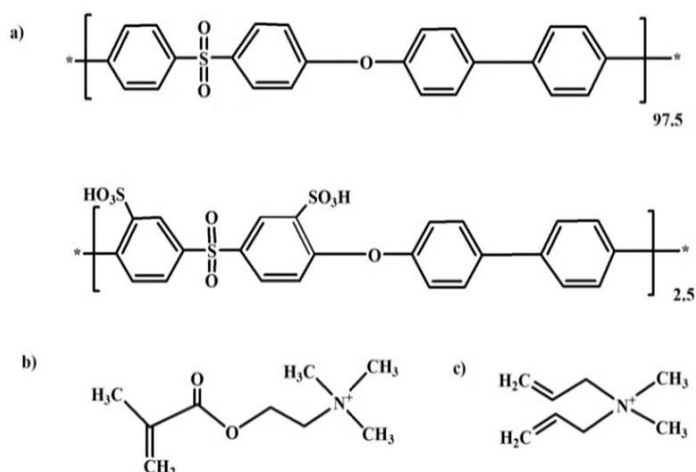
Figure 1.14 Structures of (a) sPPSU, (b) [2-(methacryloyloxy)ethyl] trimethyl ammonium chloride, and (c) diallyldimethylammonium chloride (Zhong *et al.* 2012)

Zhong *et al.* (2012) concocted positively charged NF membranes by grafting vinyl monomer such as [2-(methacryloyloxy)ethyl]trimethyl ammonium chloride and diallyldimethylammonium chloride (Figure 1.14) on the sPPSU membrane support.

The membranes displayed hydrophilic properties and sponge-like morphology. The zeta potential (ZP) value was measured to confirm the development of positive charge on the membrane surface. Among the salt solution tested for rejection, the membranes showed the maximum rejection of 95.20 % for $MgCl_2$. The positive surface charges of both the membranes and dye resulted in the 99.98 % rejection of Safranin O dye.

Alsalhy *et al.* (2013) prepared PPSU based nanocomposite membranes with different concentration of ZnO nanoparticles (NP) in 22 wt. % PPSU dope solution through non-solvent induced phase inversion method. The addition of ZnO NPs increased the membrane mean pore radius, flux, and hydrophilicity. However, the trend changed when the concentration of ZnO is above 0.03 %, as the mean pore radius and flux reduced. The rejection of Fw Direct Red 80 dye is performed and found that the addition of ZnO did not result in a reduction of solute separation performance by the PPSU membranes.

Hwang *et al.* (2013) fabricated composite polymer membranes by incorporating different ratios of activated carbon (AC) and PEG into PPSU/ polyetherimide polymers. The filtration flux and permeability of the composite membrane improved with this increase in AC concentration. The addition of hydrophilic pore-forming agent PEG also enhanced the surface hydrophilicity and porosity of the composite membranes. The resultant composite membrane with composition 0.25/35/5/6 wt. %, exhibited optimum membrane permeability and HA removal of 184 L m^{-2} h^{-1} and 80 %, respectively.

Kumar *et al.* (2013) prepared UF membrane by blending of PSF and chitosan by non-solvent induced phase separation technique. The blend membranes were characterized by SEM and studied for water uptake and WCA. The asymmetric structure with top dense layer and porous support layer with finger-like projections were observed for the pristine membrane, while the blend membranes develop voids in the sub-layer by reducing the finger-like projection (Figure 1.15). The blend membranes also showed better flux, hydrophilicity, and antifouling property than the pristine membrane.
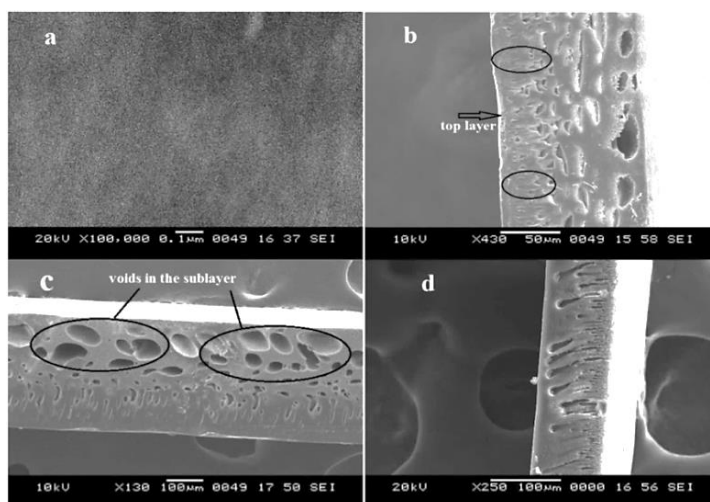
Figure 1.15 SEM images of (a) surface and (b-c) cross-section of PSF:CS blend membranes (d) cross-section of pristine PSF (Kumar *et al.* 2013)

Panda and De (2014) reported the use of PEG-200 and $ZnCl_2$ additive on PSF based NF membranes prepared by the phase inversion method. The addition of PEG-200 into the dope solution leads to the formation of porous membranes. The membranes morphology and performance of the membranes were further studied for varying concentration of $ZnCl_2$ additive. The WCA of the membranes decreased from $62°$ to $58°$ as the concentration of $ZnCl_2$ increased from 1 wt. % to 2 wt. %. The NF membranes formed were tested for salt rejection, with the maximum rejection of 43 % for NaCl. The membranes showed excellent rejection for dyes, i.e. 95 % of Chrysoidine R and more than 98 % of Crystal Violet and Congo Red were rejected.

Praneeth *et al.* (2014) reported the fabrication PPSU and PVDF-based HF by the dry-wet spinning process using a manual HF spinning machine incorporated with an inexpensive spinneret. The dope solutions were prepared by dissolving 20 wt. % of PPSU or PVDF in the DMA or NMP or DMF as a solvent. The HF membranes showed the outer diameter of 1.5 mm and the wall thickness of 0.25 mm. The PVDF and PPSU HF membranes demonstrated a turbidity rejection of 99.1 % and 93.9 %, respectively and flux of 73.9 Lm^2h^{-1} and 67.1 Lm^2h^{-1}, respectively, at 1 bar pressure. Both the HF membranes provided 5 log reductions for *Escherichia Coli* (*E. Coli*) bacteria at 1 bar pressure and a considerable water recovery of 80 %.

Arumugham *et al.* (2015) prepared sulfonated polyphenylsulfone (sPPSU) by chlorosulfonic acid through the bulk modification process (Scheme 1.1). The PPSU/sPPSU mixed matrix membranes were fabricated by varying the concentration of PPSU and sPPSU blend ratio in the dope solution. The sPPSU functions as both, a surface modifying agent and a macromolecular additive. The membranes showed improved finger-like pores and porosity with an increase in the concentration of sPPSU. The membranes with 25 wt. % of sPPSU showed high permeability and hydrophilicity with enhanced antifouling surfaces with a flux recovery ratio (FRR) of 79.6 %.
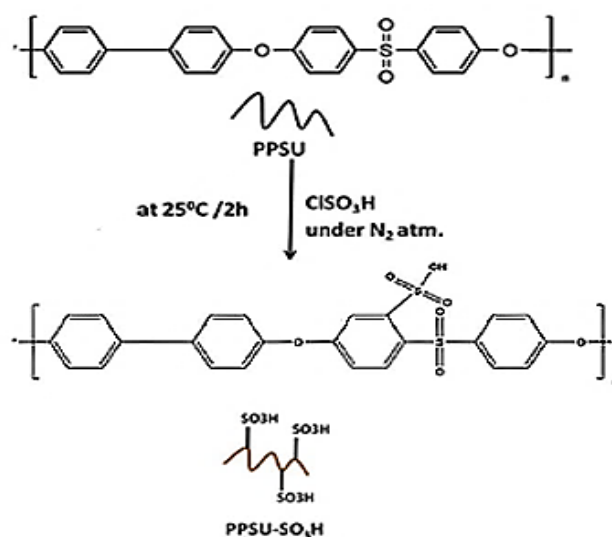
Scheme 1.1 Scheme of sulfonation of PPSU (Arumugham *et al.* 2015)

Kiani *et al.* (2015) prepared the PPSU nanofibrous membranes by blending PPSU (22 wt. %) with PEG 400. The effect of the concentration of PEG-400 in the membrane morphology and performance were studied by SEM, WCA measurement, and filtration study. The blending of PPSU with PEG-400 resulted in the hydrophilic nanofibrous membranes with remarkable PWF without compromising the rejection. Moreover, the membranes with 10 wt. % PEG-400 showed good antifouling nature with FRR of 83 %.

Arumugham *et al.* (2016) used the sPPSU as both an anchoring agent and an interlayer modifying agent and prepared nano MgO/sPPSU/PPSU membranes for

removal of oil from water. MgO NPs were dispersed in the membrane matrix which was confirmed by SEM and EDX analysis. The anchored nano MgO hydrophilic particles showed tremendous improvement in the membrane properties, such as interlayer distance, hydrophilicity, flux, rejection, porosity, pore size, and oleophobicity against oil/water emulsion.

Pereira *et al.* (2016) prepared PSF based PANI–TiO$_2$ nanocomposite HF membranes by dry-wet spinning technique. They investigated the effect of concentration of PANI–TiO$_2$ NP and different air gap distance i.e. 5 cm and 10 cm on the membrane morphology and performance. The membranes developed finger-like projections from both inner and outer surfaces with spongy layer sandwiched in between (Figure 1.16). It was observed that the increasing concentration of PANI–TiO$_2$ NP and higher air gap distance caused delayed demixing and poor finger-like projections. On testing the dye removal capacity of the HF membrane, the maximum rejection of 81.5 % and 96.5 % was observed for reactive dye such as Reactive Orange 16 (RO 16) and Reactive Black 5 (RB 5), respectively. This was due to the electrostatic interaction between anionic dye and NH$^+$ group present on the PANI–TiO$_2$ nanoparticle.
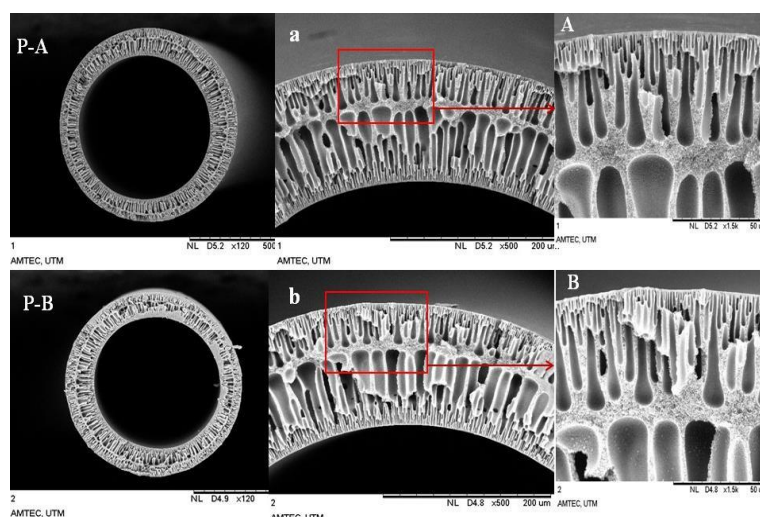
Figure 1.16 SEM images of PSF membranes at air gap 5 and 10 cm
(Pereira *et al.* 2016)

Arockiasamy *et al.* (2017) developed mixed matrix HF membrane using PPSU and sPPSU, and further studied the effect of additives such as PEG 600 and TiO_2 nanoparticle. The incorporation of TiO_2 NP into the PPSU and sPPSU dope solution resulted in improving the membrane characteristics such as mechanical properties, thermal properties, and permeability. The presence of sulfonated functional group on the surface of the HF could enhance membrane permeability and antifouling nature. The sulfonate group present on the membrane surface caused the formation of hydration layer on the surface, thereby inhibiting the protein adsorption.

Feng *et al.* (2017) compared the effect of PEG on the phase inversion process when added into PPSU and sPPSU dope solution. The addition of PEG to the dope solution increased the viscosity of the dope solution and suppressed the macrovoid formation as it slows down the phase inversion process. PEG could bring more evident changes in the sPPSU membrane than PPSU due to the hydrogen bond formation between the hydroxyl group of PEG and sulfonic acid groups. Moreover, the presence of PEG resulted in the membrane with improved mechanical strength, higher hydrophilicity, and permeation.

Shukla *et al.* (2017) developed antifouling PPSU based membranes by incorporating different concentrations of graphene oxide (GO) as a nano additive into 17.5 wt. % of the PPSU dope solution. The nanocomposite membranes were characterized with respect to ZP, pore radius, and porosity, while the membrane performance was evaluated by permeability, rejection, and antifouling studies. The incorporation of GO caused an increase in hydrophilicity and negative ZP. The membrane showed maximum flux of $171 \pm 3 \ Lm^{-2}h^{-1}$ on the addition of 0.5 % of GO, which is reported to be the optimum concentration. Moreover, the membranes showed good rejection for proteins such as BSA and pepsin, where BSA showed higher rejection than pepsin due to its higher molecular weight. The addition of GO could inhibit the interaction between the protein and the hydrophilic membrane surface, thereby resulting in its high antifouling nature.

From the above literature survey, it is evident that PSF and PPSU can be employed as an excellent membrane material. However, limited research has been

done on PPSU as membrane material due to its lower hydrophilicity and flux. Hence more research is needed to overcome its drawbacks, as PPSU being cheaper than other commonly used polymer would make an economical membrane material. Following work has been proposed by taking these arguments into account.

1.6 SCOPE AND OBJECTIVES

The scope of present work is motivated by the need of novel and improved membrane materials and membranes which possess better chemical, thermal, and mechanical properties; showing improved permeability and selectivity characteristics with the reduction in the capital and operational costs. From the literature, it is evident that the polyarylsulfone polymers have been widely used as the membrane material. PPSU is one of the polyarylsulfone polymers and its application on fuel cells has been greatly explored. However, despite its extraordinary mechanical and chemical property, application of PPSU for water treatment has not gained much attention due to its poor hydrophilicity. Hence the fouling of membrane caused as a result of the hydrophobic nature of these materials ought to be overcome by alteration of membrane surface with suitable modification techniques to develop an efficient hydrophilic membrane. Keeping in view the application and scope of the work, following objectives were outlined.

1. To prepare pristine and modified flat sheet and hollow fiber membranes using polyarylsulfone polymers such as polysulfone and polyphenylsulfone.

2. To prepare organic and inorganic nanoparticles to be used as nanoadditives in the membrane preparation.

3. To characterize the prepared membranes and nanoparticles using TEM, SEM, AFM, powder-XRD, FTIR, ^{1}H-NMR, Zeta potential and particle size analyzer, contact angle measurement, and water uptake studies.

4. To study the membrane performance by permeation test, antifouling and antibiofouling studies, and solute rejection such as salt, heavy metal, dye, and proteins.

CHAPTER 2

PREPARATION AND CHARACTERIZATION OF POLYPHENYLSULFONE/POLYSULFONE ULTRAFILTRATION MEMBRANES CONTAINING GLYCINE BETAINE AS ADDITIVE FOR HEAVY METAL REJECTION

Abstract: *In this chapter, UF membranes were fabricated by blending PPSU and PSF with PEG-1000 as a pore former. Attempts were made to improve the membrane performance by using glycine betaine (GB) as a hydrophilic additive. The effect of the concentration of zwitterionic GB on blend membrane was also studied in this chapter. The membranes hence prepared were studied for their antifouling property and heavy metal rejection.*

2.1 INTRODUCTION

The UF membranes are widely used for the water purification. However, the efficiency of UF membranes reduces due to the membrane fouling. The foulant molecules present in the feed solution causes membrane fouling either by adsorption of the macromolecules on the hydrophobic surface or by blocking the pores of the membrane (Liu *et al.* 2013). Hence, the development of an ideal membrane with high permeability, low fouling, and excellent rejection has been a major challenge to date. Polyarylsulfone polymers like PPSU and PSF are often used as membrane materials for UF membrane due to its excellent properties such as chemical resistance, good mechanical strength, and hydrolytic stability (Jones *et al.* 2010, Peyravi *et al.* 2012). However, the major drawback of these polymers is their lower hydrophilic nature.

Hence, there is a need for increasing the surface hydrophilicity of the membranes which can be achieved by various modification techniques. Blending is considered as the simplest and cost-effective technique which results in the formation of a new type of materials for UF purpose. The property of the membranes can be further improved by the addition of additives such as organic molecules (eg. PEG, PVP) (Wongchitphimon *et al.* 2011, Pellegrin *et al.* 2015), inorganic salts (eg. LiCl, NH_4HCO_3) (Zhao *et al.* 2007), zwitterion molecules (Sun *et al.* 2006), and nanoparticles (Xu *et al.* 2013).

Applications of zwitterionic molecules in the membrane technology due to their unique property are trending. They are considered to have high protein adsorption resistance property (Shi *et al.* 2008) and ability to reject heavy metal ion by adsorption (Liu *et al.* 2010, Al Hamouz and Ali 2012). Phosphorylcholine,

sulfobetaine, and carboxybetaine are the common zwitterionic groups that have been widely used to improve the antifouling nature of membranes (Hasegawa *et al.* 2002).

GB is a zwitterionic molecule which contains a cationic quaternary ammonium group and an anionic carboxylate group. It is obtained both naturally and synthetically. It is also known to prevent protein aggregation and fouling interfaces as the trimethylglycine prevents the nonspecific protein adsorption (White and Jiang 2010). GB is also an osmolyte and can serve as an excellent additive to improve the hydrophilicity of the membrane due to its ability to retain water. It's nontoxic nature and abundant availability makes it an ideal additive.

Hasegawa *et al.* (2001) prepared membranes by blending PSF and (2-methacryloyloxyethyl phosphorylcholine) (MPC) polymer (Figure 2.1). The composition of MPC polymer in the blend was varied from 7-15 wt. %. The presence of phosphorylcholine in MPC polymer resulted in membranes with improved permeability and hydrophilicity. This also caused a reduction in the adsorption of proteins on its surface.
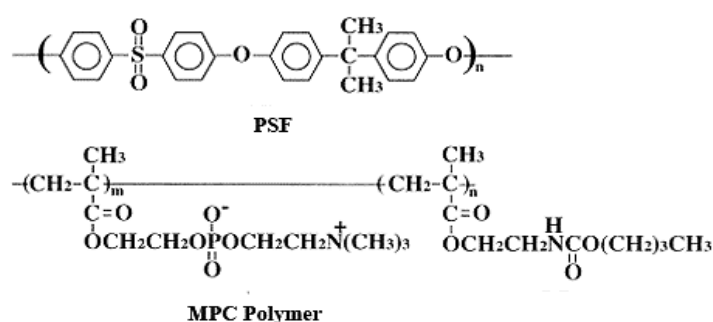
Figure 2.1 The chemical structure of the polymers (Hasegawa *et al.* 2001)

Sun *et al.* (2006) reported the fabrication of UF membrane by blending PAN with zwitterionic N,N-dimethyl-N-methacryloxyethyl-N-(3-Sulfopropyl) (DMMSA) groups. The zwitterionic blend membrane showed improvement in hydrophilicity and the antifouling property as the sulfobetaine groups in the membrane increased. The blend membranes could remarkably improve the irreversible fouling, as the protein adsorption sites are reduced. This could be due to the minimized conformational change of protein with the DMMSA molecules binding to protein via water molecule.

Zhang *et al.* (2011) prepared chitosan-betaine derivative and studied its antibacterial property against the strains of *E. coli* and *Bacillus sublis*. The incorporation of betaine to the chitosan could make the molecule highly hydrophilic as chitosan-betaine derivative was soluble in water. However, the derivative also showed lower antibacterial property when compared with that of chitosan.

Zhu *et al.* (2015) modified zwitterionic SiO_2 NPs using lysine to impart surface zwitterionic property of amino acid type (Figure 2.2). Then UF membrane was fabricated by blending the PVDF and zwitterionic SiO_2 NPs. The presence of zwitterionic group on NPs prevented its aggregation, hence resulted in the uniform dispersion of zwitterionic SiO_2 NPs in the membrane matrix. The membrane performance and antifouling property were found to improve with the increase in the amount of zwitterionic SiO_2 NPs content in the dope solution. The membranes showed a minimum of 95 % of FRR for the BSA and HA in the feed solution.
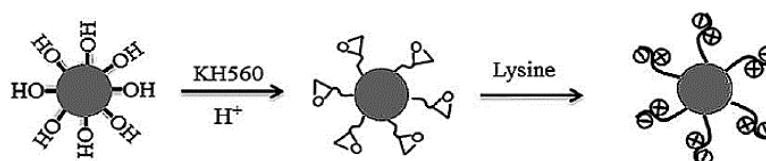
Figure 2.2 Modification of zwitterionic SiO_2 NPs (Zhu *et al.* 2015)

Kaner *et al.* (2017) synthesized the copolymers of methyl methacrylate (MMA) with two different zwitterionic copolymers sulfobetaine methacrylate (SBMA) and sulfobetaine-2-vinylpyridine (SB2VP), respectively. They studied the impact of zwitterion chemistry, zwitterionic/hydrophobic monomer ratio, and blend composition with PVDF on membrane performance and fouling resistance. They found that presence of low content of zwitterionic additive could bring about high permeance and good antifouling property, i.e., about 5 wt. % of zwitterionic additive in PVDF could result in doubling of the PWF and complete fouling resistance against both proteins and oil.

In the account of these observations, it was found that the use of zwitterionic GB has not been employed as a hydrophilic additive to improve the membrane performance. The PPSU/PSF UF membranes were prepared by blending PPSU, PSF,

and PEG-1000 using NIPS technique. The influence of GB on the blend membrane performance is studied and compared with the pristine membranes. The membranes were also tested for its antifouling property and heavy metal rejection.

2.2 EXPERIMENTAL

2.2.1 Materials

PSF (Mw ~ 35,000), PEG-1000, GB (Mw ~ 117.15) (Figure 2.3), cadmium nitrate tetrahydrate and lead nitrate were purchased from Sigma-Aldrich Co., India. PPSU (Radel R-5000) (average Mw ~ 50,000 g mol^{-1}) was provided by Solvay Advanced Polymer (Belgium). NMP was purchased from Merck India, Ltd. BSA (Mw ~ 69 kDa) were purchased from CDH Chemicals, India and PEI (Mn ~ 60,000) 50 wt. % aq. solution (branched) was purchased from Acros Organics, USA.
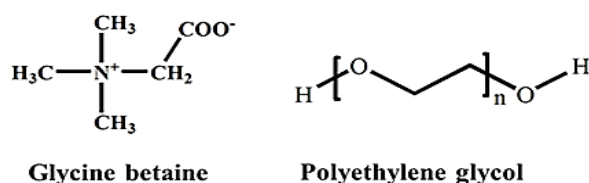
Figure 2.3 Structures of GB and PEG-1000

2.2.2 Preparation of blend membranes

PPSU/PSF blend UF membranes were prepared by wet phase inversion method based on the literature (Figure 2.4) (Kumar *et al.* 2013).
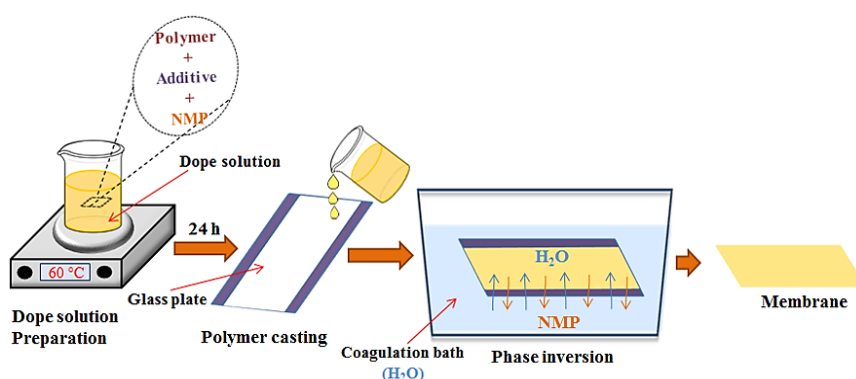
Figure 2.4 Schematic representation of membrane preparation

20 wt. % of polymer dope solution was prepared by dissolving the constituents as mentioned in Table 2.1. The solutions were subjected to constant mechanical stirring at 60 ^{o}C for 24 h to form a homogeneous mixture. The polymer solution was then filtered, degassed and cast onto a glass plate using casting blade. Later, it was immersed in a bath containing distilled water and the membranes formed were rinsed and stored in deionized (DI) water for the further analysis.

Table 2.1 Compositions of dope solution

Membrane code	Dope Solution compositions (20 wt. %) (Ratio of dope solution components)			NMP (wt. %)
	Polymer Blend (PPSU: PSF)	PEG-1000	GB	
P0-P	95 (0:100)	5	0	80
P75-P	95 (75:25)	5	0	80
P100-P	95 (100:0)	5	0	80
P75-G0.5	94.5 (75:25)	5	0.5	80
P75-G1	94 (75:25)	5	1.0	80
P75-G2	93 (75:25)	5	2.0	80

2.2.3 Morphological study

The membrane morphology was examined by SEM. The membranes were freeze-fractured to obtain the cross-sectional image, i.e., the membrane sample was frozen in liquid nitrogen and broken apart to obtain the internal structure of the membrane. The fractured surface of the sample was then sputter coated with gold to get the block face before the analysis. The cross-sectional images of the membranes were then captured using JEOL JSM-6380LA. The EDX spectrum was recorded to examine the retention of GB particles on the surface of the prepared membrane (Isloor *et al.* 2015).

2.2.4 Water contact angle measurement

The WCA was measured to analyze the surface hydrophilicity of the membranes. The WCA was recorded by placing water droplet on the membrane surface using a syringe. The WCA for at least three different sites was taken using FTA-200 dynamic contact angle analyzer by sessile droplet method (Pereira *et al.* 2016).

2.2.5 Water uptake, membrane porosity and mean pore radius study

The hydrophilicity and wettability of the membranes were determined by the water uptake capacity. Here the membrane samples were cut into pieces measuring 1 cm^2 and dipped in distilled water for 24 h. These swollen membranes were then taken out of the water and weighed after removing excess of water on its surface using a blotting paper. The wet membranes were dried in a vacuum oven for 24 h, and then the dry membrane samples were weighed (Shenvi *et al.* 2014). The water uptake capacity of the membranes was calculated using the following equation:

$$Water\ uptake = \left(\frac{W_w - W_d}{W_d}\right) \times 100 \quad (2.1)$$

Where, $'W_w'$ and $'W_d'$ are the wet and dry weight of membrane, respectively.

The porosity of membrane is calculated by the gravimetric method. The membrane porosity (ε) was calculated using the following equation.

$$\varepsilon = \left(\frac{W_w - W_d}{Al\rho}\right) \times 100 \quad (2.2)$$

Where, $'A'$ is the area of the membrane sample (cm^2), $'l'$ is the membrane thickness (cm) and $'\rho'$ is the density of water (0.998 gcm^{-3}).

The porosity of the membrane is utilized to determine the mean pore radius (r_m) of the membrane by the filtration velocity method using the Guerout–Elford–Ferry equation (Yuliwati *et al.* 2011, Yunos *et al.* 2014).

$$r_m = \sqrt{\frac{(2.9 - 1.75\varepsilon) \times 8\eta l Q}{\varepsilon \times A \times \Delta P}} \quad (2.3)$$

Where, $'\eta'$ is the water viscosity, $'Q'$ is the volume of permeate water per-unit time, and $'\Delta P'$ is the operational membrane pressure of 0.5 MPa.

2.2.6 Pure water flux study

The permeation property of the membranes was analyzed by PWF study using dead-end filtration set up (Figure 2.5) with an effective membrane area of 25 cm^2 (Hebbar *et al.* 2014). The membranes were immersed in water for 24 h before carrying out the permeation experiments. The wet membranes were placed in the membrane cell and pressure-dependent PWF of the different membranes was measured at 0.1-1.0 MPa transmembrane pressure (TMP) at room temperature (RT) by taking pure water in the feed tank. The membranes were subjected to compaction at 0.5 MPa TMP for 30 min before the study. The PWF of the membranes was calculated using the following equation:

$$J_w = \frac{Q}{\Delta t \times A} \quad (2.4)$$

Where, $'J_w'$ is the water flux expressed in Lm^{-2}h^{-1}, $'Q'$ is the amount of water passing through the membrane in litre (L), $'\Delta t'$ is the time in hours (h) and $'A'$ is the effective membrane area responsible for the filtration, expressed in (m^2).
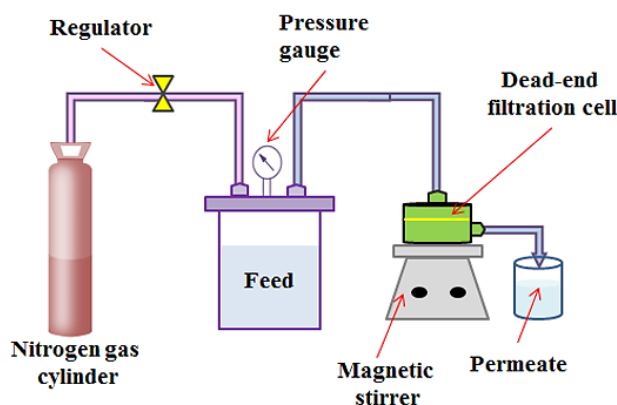
Figure 2.5 Schematic representation of dead-end filtration set up

2.2.7 Antifouling study

The BSA solution was used as a model foulant to study the antifouling property of the membrane. Initially, the PWF ($'J_{w1}'$) of the membrane was measured

at 0.5 MPa TMP for 1 h. Later, the membrane was subjected to the permeation of BSA solution prepared by dissolving 1.0 g of BSA in 1 L water to obtain 1000 ppm concentration. The flux for BSA solution is $('J_p')$ was measured for 1 h at 0.5 MPa pressure. After the BSA filtration, the membranes were washed with water for 20 min and then the PWF $('J_{w2}')$ was measured again. The antifouling property was evaluated by calculating FRR by the equation;

$$FRR = \frac{J_{w2}}{J_{w1}} \times 100 \quad (2.5)$$

The membrane fouling was further evaluated by calculating the reversible $'R_{rev}'$ and irreversible $'R_{irr}'$ fouling ratio by following equation (Vatanpour *et al.* 2011),

$$R_{rev} = \left(\frac{J_{w2} - J_p}{J_{w1}}\right) \times 100 \quad (2.6)$$

$$R_{irr} = \left(\frac{J_{w1} - J_{w2}}{J_{w1}}\right) \times 100 \quad (2.7)$$

The BSA passed through the membranes were simultaneously collected and the concentration of BSA in the feed and the permeate was measured using Ultraviolet-Visible (UV-Vis) spectrophotometer at a wavelength of 280 nm. The percentage of BSA rejected by the membranes was calculated using the following equation:

$$R = \left(1 - \frac{C_p}{C_f}\right) \times 100 \quad (2.8)$$

Where $'C_p'$ (mg.mL^{-1}) is the concentration of the solute in permeate and $'C_f'$ (mg.mL^{-1}) is the concentration of the solute in feed solution.

2.2.8 Heavy metal rejection study

PEUF technique for the heavy metal rejection was done based on the literature (Pereira *et al.* 2014). Here, the heavy metal ions were complexed using PEI. Aqueous solutions of Pb^{2+} and Cd^{2+} of 1000 ppm concentration were prepared by complexing them in a 1 wt. % solution of PEI in DI water. The pH of these aqueous solutions was

adjusted to 6±0.25 by the addition of a small amount of either 0.1 M NaOH or 0.1 M HCl. Solutions containing PEI and individual metal ions were thoroughly mixed and left standing for five days at RT to complete the complexation. The metal ion complexed PEI (Figure 2.6) solutions were filtered through the membranes at 0.5 MPa TMP and permeate was collected. The rejection of the metal ions by membrane was evaluated by measuring the concentration of the metal ions in the feed and permeates using atomic absorption spectrophotometer (AAS) (GBC 932 Plus) (Mbareck *et al.* 2009). Heavy metal ion rejected by the membranes was calculated using the equation (2.8).
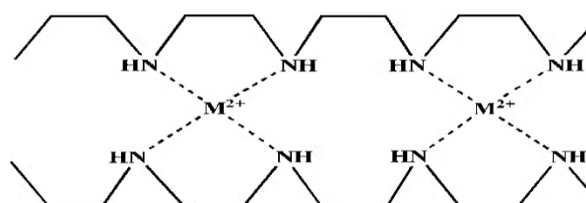
Figure 2.6 Complexation of PEI with the heavy metal ion ($M^{2+}= Pb^{2+}, Cd^{2+}$)

2.3. RESULTS AND DISCUSSIONS

2.3.1 Membrane morphology

The cross-sectional images of the prepared membranes displayed the typical asymmetric nature of membrane with dense top layer and thick porous sub-layer with finger-like projections (Figure 2.7) (Susanto and Ulbricht 2009). The finger-like structures were formed due to the instantaneous demixing of solvent and non-solvent during the phase inversion. Moreover, the addition of PEG-1000, a pore former into the casting solution increased the membrane's affinity to water as it leached out of the solution creating elongated and interconnected finger-like projection (Wongchitphimon *et al.* 2011). From the SEM images, it is clear that the blend membrane showed better morphology than that of pristine PPSU and PSF, which is due to the rise in the segmental gap (Sajitha *et al.* 2002).

The effect of hydrophilic additive GB, on the membrane morphology, was further observed with decrease in the thickness of dense top layer and formation of elongated pore interconnectivity. During the phase inversion, the hydrophilic carboxylic acid group present in the GB interacts with water molecules through

hydrogen bonding. The affinity of GB towards water causes it to diffuse through the membrane and increase the rate of demixing. There is a further enhancement in the pore connectivity as the concentration of GB is increased in the dope solution, which can be correlated to the superior interaction of GB with the polymer blend at higher concentration. However, the thickness of membrane increased with increase in the concentration of the GB. It can be observed from SEM images that the membrane with 2 wt. % of GB was found to be thickest out of all the membranes formed. This is due to the delayed demixing as the viscous polymeric dope overruled the instantaneous demixing offered by the hydrophilic GB additive.
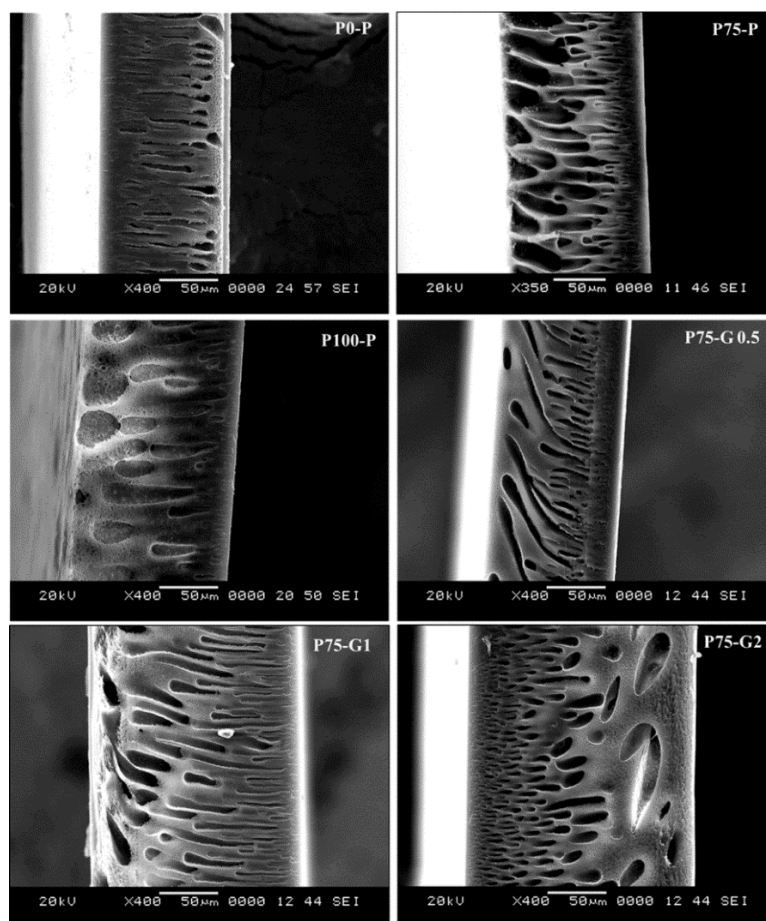
Figure 2.7 Cross-sectional images of prepared membranes

The EDX analysis confirms the retention of GB in the membrane. The retention of zwitterionic GB is due to the secondary force of interaction between the GB and polymer blend (Gao *et al.* 2017). The presence GB is indicated by the detection of

nitrogen in the membrane P75-G1 by the elemental mapping, which is due to the quaternary ammonium group present in GB (Figure 2.8).
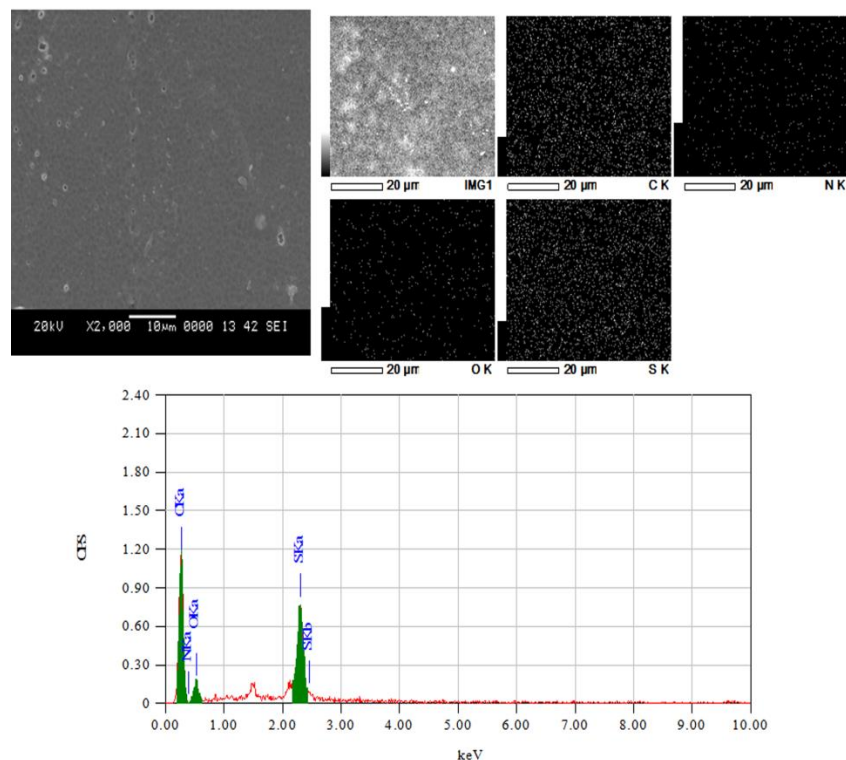
Figure 2.8 EDX spectrum and elemental mapping of the P75-G1 membrane surface

2.3.2 Membrane hydrophilicity

The surface hydrophilicity of the membrane was studied by measuring the WCA. The hydrophilic surface would display wettability to a greater extent as its affinity to water is higher, hence resulting in a lower contact angle for the hydrophilic surface. From the WCA results, it could be observed that the blend membrane showed lower contact angle than the pristine membrane which further decreases on the incorporation of GB (Figure 2.9). The incorporation of PEG-1000 into membranes is also responsible for better hydrophilicity as the PEG-1000 molecule could aid in the interaction of the water molecule with membrane surfaces as it diffuses through the membrane during phase inversion (Garcia-Ivars *et al.* 2014, Chan *et al.* 2015). The WCA of the prepared membranes decreased in the following order: P75-G0.5 > P75-G2 > P75-G1 as the composition of GB changed in the dope. This rise in the

hydrophilicity is due to the migration of GB to the membrane surface during phase inversion as a result of greater affinity of hydrophilic GB towards the water. Thus, the wettability of the membrane further increased as the concentration of the GB in dope solution increases. However, the P75-G2 showed slightly higher WCA than that of P75-G1 because, at higher concentration of GB, the increased number of alkyl group dominates the hydrophilic nature offered by the carboxylic acid group. Therefore, 1 wt. % of GB in dope solution is found to be the optimum composition.
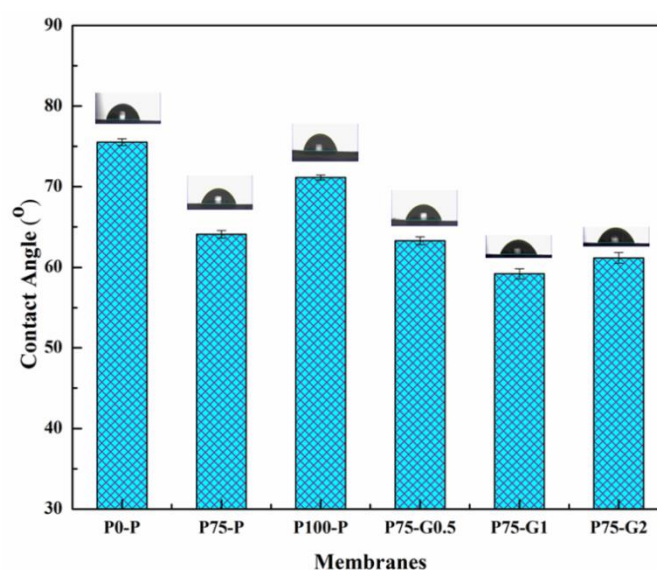
Figure 2.9 WCA of the membranes
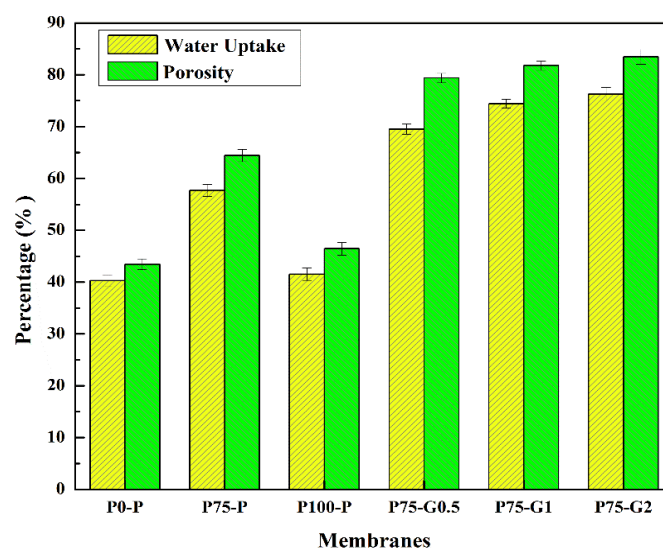
Figure 2.10 Water uptake and porosity of the membranes

The water uptake study is also performed to determine the bulk hydrophilicity of the membrane. The water uptake capacity ranged from 40-76 % (Figure 2.10). The water uptake of the blend membranes was found to be higher than the pristine membranes which can be attributed to the rise in the segmental gap due to blending. The high water uptake capacity of the membrane was also due to the addition of PEG-1000. The addition of GB to the polymer dope resulted in the increased affinity of the additives towards the water. The presence of hydrophilic group such as $-COOH$ in GB made the membranes more hydrophilic in turn increasing the water uptake capacity of membranes.

2.3.3 Membrane porosity and mean pore radius

Figure 2.10 also shows the porosity of the prepared membranes. It can be observed that the blending of PPSU and PSF resulted in higher porosity as compared to the pristine PPSU and PSF membranes, which may be due to the rise in the segmental gap between PPSU and PSF. The overall rise in the porosity is also contributed by the addition of PEG-1000, which improved pore interconnectivity due to the diffusion of PEG through the membrane during phase inversion (Malaisamy *et al.* 2002). The porosity of the prepared membranes was further increased with the addition of GB as an additive in the following order: P75-G0.5 > P75-G1 > P75-G2. The rise in porosity is evident from the SEM images due to the development of elongated pore as GB moved towards the membrane surface.

The mean pore radius was calculated by the filtration velocity method using the Guerout–Elford–Ferry equation (Yu *et al.* 2009). The PEG-1000 caused the development of pores as well as an overall rise in the pore radius by dissolution of entrapped PEG-1000 during the phase inversion process. The mean pore radius also increased on the incorporation of GB additive to the membranes. The r_m of the prepared membranes is in the order as follows: P0-P < P100-P < P75-P < P75-G1 < P75-G0.5 < P75-G2, with the pore radius range being 5 to 22 nm.

2.3.4 Pure water flux

The pressure-dependent PWF of the membranes were evaluated by subjecting the membranes from 0.2 to 1.0 MPa TMP. From the Figure 2.11, it can be observed

that the PWF of membranes increased linearly with a rise in pressure. The PWF of blend membranes is found to be higher than the pristine PSF and PPSU membrane, which is attributed to the rise in the membrane hydrophilicity, porosity and pore radius. Also, the presence of PEG-1000 gave rise to higher hydrophilicity and porosity that contributed to the rise in the PWF of prepared membranes.
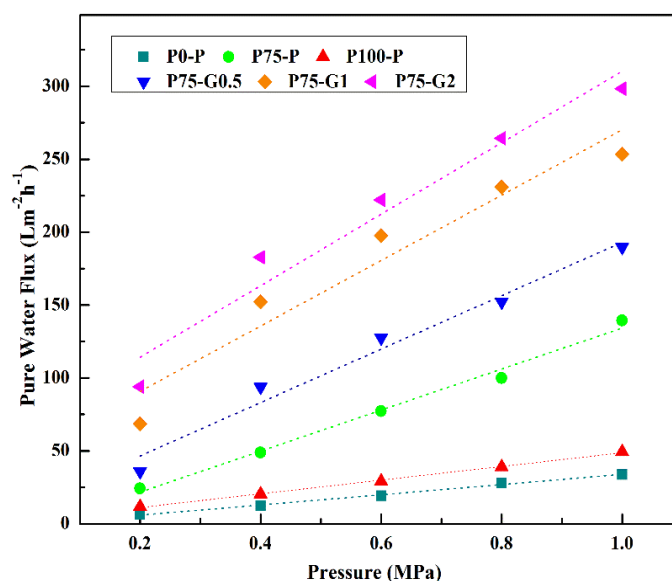
Figure 2.11 Pressure-dependent PWF of prepared membranes

The improved hydrophilicity and porosity on the addition of GB to the blend membranes aided in the improvement of PWF. Furthermore, PWF increased with the increase in GB concentration, in the following order: P75-G0.5 < P75-G1 < P75-G2. The P75-G2 exhibited highest PWF of 187.5 at 0.5 MPa TMP in spite of lower hydrophilicity due to higher porosity and larger pore size (Kumar *et al.* 2013).

2.3.5 Antifouling study

Figure 2.12 indicates the flux of membranes when pure water and BSA solution were passed alternately through the membranes for certain period at 0.5 MPa TMP. This experiment was performed to study the fouling of the membranes. The sharp decline in flux was observed when BSA solution was passed through the membranes as the BSA molecules got adsorbed on the membrane surface and caused clogging of the pores (Kumar *et al.* 2013). The membranes were then washed with water and PWF was measured. It was found that there was a decline in PWF after

subjecting it to BSA and the extent of decline on the flux depicted in the FRR of the membranes.
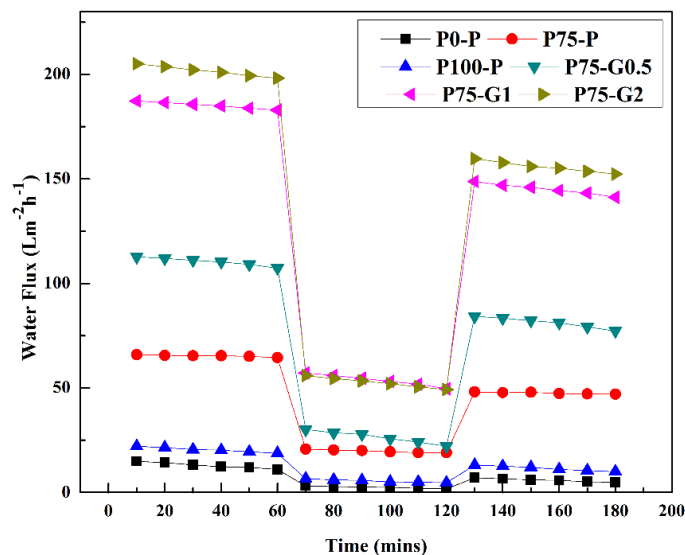
Figure 2.12 Flux vs. time for membranes before and after passing BSA feed at 0.5 MPa TMP
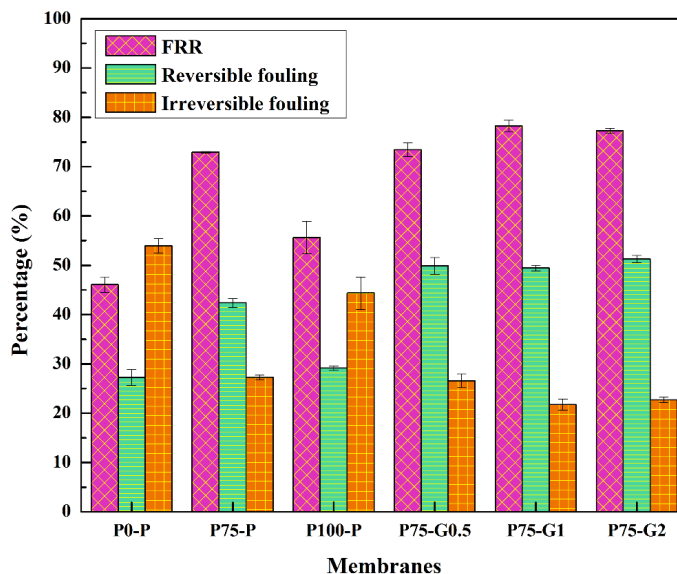
Figure 2.13 FRR and fouling resistance of the prepared membranes

The FRR of the prepared membranes showed the following trend: P0-P < P100-P < P75-P < P75-G0.5 < P75-G2< P75-G1 which exhibited the extent of fouling occurring on membranes. The membranes showed good FRR on the addition of GB were P75-G1 exhibited highest FRR of 78.1 % (Figure 2.13). In the aforementioned

study, the addition of PEG-1000 and GB result in an increase in the surface hydrophilicity, thereby creating a hydration layer over the membrane surface which could lower the interaction between the hydrophobic foulant and the membrane surface. Hence the adsorbed protein foulant could be easily removed from the hydrophilic surface of membranes by simple hydraulic cleaning (Teli *et al.* 2012).

The R_{rev} and R_{irr} was also calculated to understand the self-cleaning property of the membrane which in turn represents the membrane reusability. If the foulant adsorbed on membrane surface could be removed by simple hydraulic cleaning it is reversible fouling. Conversely, the irreversible fouling is when the foulant is strongly adhered to the membrane and can't be removed by hydraulic cleaning. Thus, lower value of R_{irr} indicates good fouling resistance offered by the GB containing membranes (Figure 2.13). This can be associated with the increase in the membrane hydrophilicity and electrostatic repulsion displayed between the $-COOH$ group present on the GB and the negatively charged BSA. As indicated in Figure 2.13, P75-G1 with 1 wt. % of GB showed the least fouling. This could be because of smaller pore size and increased hydrophilicity of the membrane. However, the antifouling performance declined on increasing the concentration of GB to 2 wt. % as the membrane showed lower hydrophilicity and FRR. This may be due to the increased pore size which caused irreversible fouling.

2.3.6 Rejection study

The prepared membranes were subjected to BSA and heavy metal rejection studies (Figure 2.14). The BSA rejection was conducted to study the UF property of the membranes. The membranes showed BSA rejection in the range 75-99 %, which is significant for a UF membrane. Also, the BSA rejection signifies the pore size of the membranes.

Heavy metals ions like Cd^{2+} and Pb^{2+} were filtered by PEUF and the filtrate was analyzed by AAS for rejection. Polymer enhanced heavy metal rejection was conducted by complexing the heavy metal ions like Pb^{2+} and Cd^{2+} with PEI, were the lone pair of electrons present in the nitrogen atom binds to the transition metal (Molinari *et al.* 2004). Both lead and cadmium being divalent in nature get easily

bound to the PEI ligand to form the PEI-Metal complex. However, the extent of binding and complex stability depends on the metal binding capacity. Therefore, the higher metal binding capacity of Pb^{2+} ions than Cd^{2+} ions resulted in stable PEI-Pb^{2+} complex than PEI-Cd^{2+}. The stability of the metal complex is also based on the strength of complexation which is correlated to the electronegativity of metal ions. Hence, the rejection of Pb^{+2} ions is observed to be higher than the Cd^{2+} ions. The PEUF of the heavy metal is based on the size exclusion principle where the rejection of heavy metal depends on the pore size and the size of the PEI-Metal complex. Hence the rejection is observed is in the following order: P0-P > P100-P > P75-P > P75-G1 > P75-G0.5 > P75-G2 where the rejection is reduced as the pore radius increased. However, the presence of the $-$COOH group in GB was also responsible for the rejection of uncomplexed metal ions due to the electrostatic interaction between the metal ions and GB.
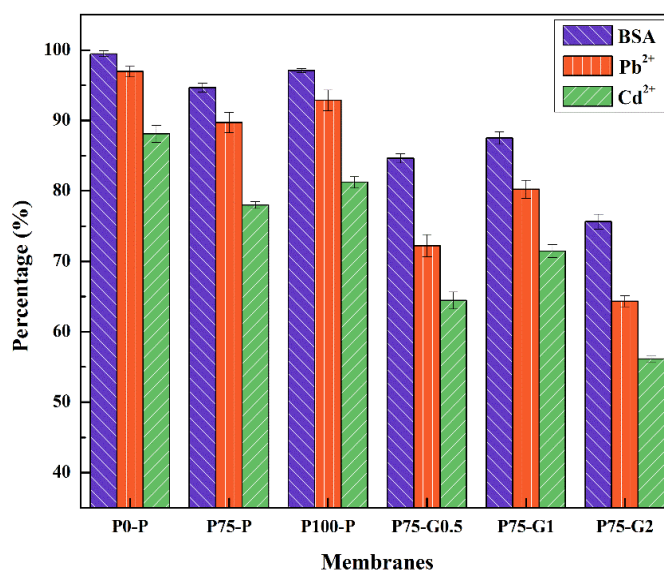
Figure 2.14 BSA and heavy metal rejection by membranes at 0.5 MPa TMP

2.4 CONCLUSIONS

A series of UF membranes were prepared by blending PPSU and PSF with PEG-1000 as an additive, and NMP as a solvent by NIPS technique. The blend membrane i.e. PPSU/PSF membranes with composition 75:25 showed better performance than pristine membrane due to the occurrence of the segmental gap. The addition of pore former PEG-1000 improved the membrane porosity. The effect of

hydrophilic additive GB, a zwitterion on blend membrane was further studied. The addition of GB into the casting solution increased the hydrophilicity of the membrane blend, in turn, increasing the flux and antifouling property. The P75-G1 membrane with 1 wt. % of GB showed better performance among the prepared membranes as it showed higher hydrophilicity, good porosity, and water uptake capacity. They also showed enhanced antifouling property with the rejection of 87.51 %, 80.23 % and 71.45 % for BSA, Pb^{2+}, and Cd^{2+}, respectively.

CHAPTER 3

EFFECTS OF BATH COMPOSITION ON SULFONATED POLYPHENYLSULFONE ULTRAFILTRATION MEMBRANES FOR ENHANCED REJECTION OF PROTEIN AND TOXIC HEAVY METAL

Abstract: *This chapter deals with the functionalization of the PPSU by chemical modification. The sPPSU was characterized and the effects of the concentration of sPPSU in the dope solution on the membranes were studied. The NIPS was conducted using different coagulation bath composition of aq. GB or aq. NMP or aq. NaCl solutions. Further, its effects on membrane performance were examined. The resultant membranes were checked for its ability to reject proteins like BSA, pepsin and trypsin, and toxic heavy metal ions such as Cd^{2+} and Pb^{2+}.*

3.1 INTRODUCTION

As discussed in previous chapters, the low hydrophilic nature of PPSU is a major drawback that has been researched. The functionalization of the aromatic structure of polymeric backbone with ionomeric groups, like sulfonic acid, carboxylic acid, amine etc. is reported to improve the hydrophilicity of the polymer (Di Vona *et al.* 2010). Moreover, the morphology and the membrane performance are influenced by elements like nature and concentrations of polymer, additives, solvents, and the non-solvents used (Han and Nam 2002, Madaeni and Rahimpour 2005, Wang *et al.* 2008). Hence membrane characteristics can be altered by the phase inversion technique as it is one of the commonly used methods for the preparation of UF membrane (Lalia *et al.* 2013). NIPS of the polymer takes place at a controlled rate, where the solvent and non-solvent interact to form the membrane with desired characteristics (Zhao *et al.* 2014). This (phase separation of the membrane) would result in asymmetric membranes with dense active layer and porous sub-layer. The porous sub-layer often consists of the large elongated finger-like structures. The coagulation bath composition can control the sub-layer formation of the membranes (Oh *et al.* 2009, Saljoughi *et al.* 2009).

Chun *et al.* (2000) investigated the effect of dimethylacetamide (DMAC) as a solvent in the coagulation bath on the pore-forming behavior in polyimide membranes. The pore-forming behavior was examined by coagulation value, phase diagram, the diffusion coefficient of non-solvent, and the solubility parameter. They observed that the increase in the concentration of DMAC resulted in the small difference between the solubility parameter of solvent and non-solvent, hence caused

a delay in liquid-liquid demixing during phase inversion, which in turn reduced the porosity and the pore size in the skin layers.

Yang and Liu (2003) reported the use of water, aq. NaCl, and aq. Na_2CO_3, as coagulation bath to fabricated PAN UF membrane with $CaCl_2$ as an additive. The increase in NaCl concentration (5-20 wt. %) in the coagulation bath showed low permeability as the rate of dimixing reduced because of decline in the chemical potential of the water due to salt effect. Whereas, the coagulation bath with aq. Na_2CO_3 showed increased permeability, as Na_2CO_3 in the coagulation bath reacts with the $CaCl_2$ present in the casting solution to precipitate $CaCO_3$. The decrease in gelation time with an increase in the concentration of Na_2CO_3 in coagulation bath depicts the high rate of solvent and non-solvent diffusion.

Madaeni and Rahimpour (2005) prepared PES and PSF UF membranes using different solvents and non-solvents. The effect of coagulation bath composition containing water, 2-butanol, and a mixture of water and solvents such as 1-butanol, 2-butanol, and 2-propanol on the membrane morphology and performance were studied. The membrane morphology changed from dense to porous as the coagulation bath composition varied from 2-butanol to pure water, a mixture of isopropyl alcohol (IPA) and water, and a mixture of 2-butanol and water. The change in membrane morphology was observed, which in turn affected the flux and rejection. They claimed the main factor affecting the change in membrane morphology was the change in the solubility parameters between solvents and non-solvents.
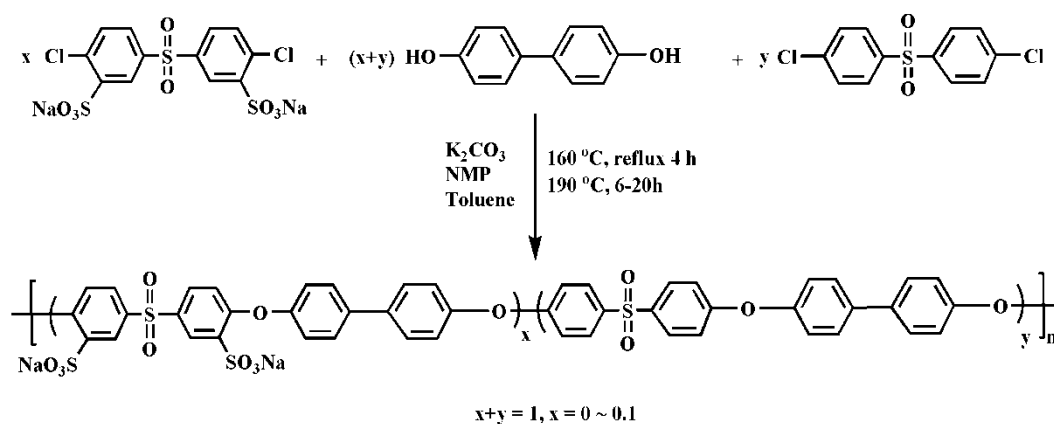
Scheme 3.1 Sulfonation of PPSU by copolymerization method (Liu *et al.* 2012)

Liu *et al.* (2012) demonstrated controlled sulfonation of sulfonated monomer to synthesize a series of sPPSU random copolymers by direct copolymerization method (Scheme 3.1). The sPPSU UF membranes were fabricated via phase inversion technique with the superior antifouling property as the R_{irr} reduced significantly. They reportedly increased the permeability of pure water and protein solution membranes with the increased degree of sulfonation (DS). This was due to improved hydrophilicity and presence of negative charge on the sulfonated polymer.

Xu *et al.* (2014) studied the effect of coagulation bath composition on the membranes prepared by blending PSF with capsaicin-mimic groups by phase inversion technique. Various coagulation bath compositions such as water, aq. ethanol, and aq. acetic acid (AA) was used to study its effect on the membrane morphology and performance. The shrinkage of pores on the membrane surface and improvement in its hydrophilicity was observed with the increase in the concentration of ethanol or aq. AA in the coagulation bath. Here instantaneous demixing was observed when the concentration of ethanol was below 10 % while the slow rate of demixing dominated with an increase in the concentration of ethanol (10-25 %). However, AA showed a similar effect at the very low dosage of 0-2 %. They also reported that the presence of ethanol in coagulation bath lead to better permeability and antifouling property while the AA resulted in good HA rejection.

Yam-Cervantes *et al.* (2017) fabricated asymmetric sPPSU membrane using sPPSU of different DS and coagulation bath composition such as acetone/IPA, and AA-NaHCO$_3$/IPA. The DS was determined by titration. They found that the membrane hydrophilicity increased with an increase in the DS. It also showed lower antifouling property for sPPSU membrane than pristine PPSU membrane due to the presence of the HSO$_3$ groups in sPPSU asymmetric membranes. The AA-NaHCO$_3$/IPA bath showed better morphology with spongy asymmetric structure due to a lower isoelectric point of the solvents when compared with AC/IPA coagulation bath, where the finger-like structures are observed. NMP functioned as retardant when added to the coagulation bath as it avoids macrovoid formation.

In this work, the PPSU was chemically modified by sulfonation to incorporate negative charge and to improve the hydrophilicity of PPSU. The lower mechanical

stability of sPPSU was addressed by blending it with PSF. The effect of coagulation bath composition on the membrane properties and performance were also examined. As the non-solvent phase inversion of the membranes is influenced by the mass transfer and the rate of liquid-liquid demixing, the phase inversion was conducted using different coagulation bath composition of aq. GB or aq. NMP or aq. NaCl solutions. The morphology, hydrophilicity, hydraulic permeability, and anti-fouling property of the prepared membranes were analyzed by SEM, WCA measurement, and dead-end filtration experiments.

3.2 EXPERIMENTAL

3.2.1 Materials

PSF (Mw ~ 35,000), GB (Mw ~ 117.15), Cadmium nitrate tetrahydrate and lead nitrate were procured from Sigma-Aldrich Co., India. PPSU (Radel R-5000) (average Mw ~ 50,000 g mol^{-1}) was purchased from Solvay Advanced Polymer (Belgium). NMP and Sulfuric acid were from Merck India, Ltd. BSA (Mw ~ 67 kDa), Pepsin (Mw ~ 35 kDa) and Trypsin (Mw ~ 23 kDa) were procured from CDH Chemicals, India. NaCl was acquired from Nice chemical (P), Ltd.
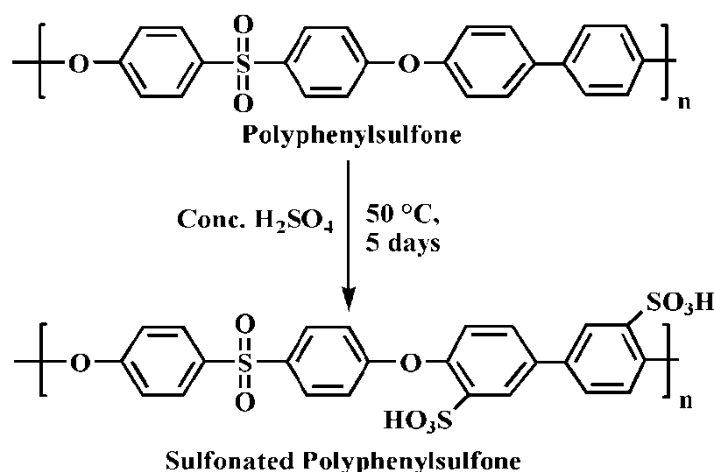
Scheme 3.2 Scheme for the sulfonation of PPSU

3.2.2 Synthesis of sPPSU

PPSU (5 g) was dissolved in Conc. H_2SO_4 (500 mL) at 50 $^\circ$C for 5 days under a nitrogen atmosphere (Scheme 3.2). The reaction mixture was then precipitated using a

large volume of distilled ice-cold water with constant stirring. The white precipitate obtained was left overnight. It was then filtered and washed with distilled ice-cold water to attain neutral pH. The sPPSU was then dried under vacuum for 4–6 h at RT (Di Vona *et al.* 2010).

3.2.3 Degree of sulfonation of sPPSU

The DS of the prepared polymer was determined by titration as revealed in the literature (Shenvi *et al.* 2014). The 0.5 g of dry sPPSU was stirred for complete dissolution in 10 ml of DMF. The solution was titrated with 0.1 N NaOH solution using phenolphthalein as an indicator to find the amount of H^+ ions liberated. The DS was calculated as follows:

$$DS = \frac{0.388 \times C_{NaOH} \times V_{NaOH}}{W - 0.081 (C_{NaOH} \times V_{NaOH})} \quad (3.1)$$

Where $'W'$ is the weight of the sample, $'C_{NaOH}'$ is the concentration of the standard NaOH solution, $'V_{NaOH}'$ is the amount of NaOH solution consumed, 388 is the molecular weight of the repeating unit of PPSU, and 81 is the molecular weight of the $-SO_3H$ segment.

3.2.4 Characterization of polymer

The synthesized sPPSU polymer was characterized by recording ATR-FTIR spectra using Shimadzu IR Prestige 21 (Japan) spectrophotometer. The spectra of dried samples were recorded in the range of 4000 – 600 cm^{-1} (Shenvi *et al.* 2013). The sulfonation of PPSU polymer was confirmed by recording a proton nuclear magnetic resonance (^{1}H-NMR) spectrum using Bruker 400 MHz NMR spectrometer. DMSO-d$_6$ was used to dissolve the sample and spectra were taken with a relaxation delay time of 1s and 64 numbers of scans using H^1 probe (Padaki *et al.* 2012).

3.2.5 Preparation of membranes

The casting solutions were formulated by blending different compositions of sPPSU polymer with PSF in NMP as solvent (Table 3.1). The homogeneous solutions were obtained by mechanical stirring at 60°C for 24 h. The polymer solution was filtered and sonicated for 15 min at 40 kHz to remove the trapped air bubbles. The

dope solution was cast onto a glass plate with a doctor blade and it was further dipped into a coagulation bath (Kumar *et al.* 2013). The coagulation medium containing distilled water, aq. GB, aq. NMP, and aq. NaCl was used to prepare membranes by wet phase inversion method (Xu *et al.* 2014).

Table 3.1 Compositions of the dope solution and coagulation bath

Membrane code	Casting solution Compositions (20 wt. %)		NMP (wt. %)	Coagulation bath composition
	PSF	**sPPSU**		
W 5	95	5	80	Distilled Water
W 10	90	10	80	Distilled Water
W 15	85	15	80	Distilled Water
G 15	85	15	80	5 % aq. GB
N 15	85	15	80	5 % aq. NMP
S 15	85	15	80	5 % aq. NaCl

3.2.6 Membrane characterization and performance

The cross-sectional images were captured to study the morphology of membranes using SEM (JEOL JSM-6380L). The membrane surface topography was analyzed using atomic force microscopy (AFM). The AFM device used was Innova SPM Atomic Force Microscope with antimony doped silicon cantilever having a force constant in the range of 20-80 N/m. AFM analysis was conducted by placing dry membrane samples on a substrate where the surfaces image was taken by tapping mode. The surface roughness parameters of the membranes were calculated including, average roughness (R_a) and root mean square roughness (R_q) (Pereira *et al.* 2015).

The hydrophilicity of the membrane surface was analyzed by measuring the WCA of the membranes using FTA-200 dynamic contact angle analyzer by sessile droplet method. The water uptake capacity, porosity, and mean pore radius of the membranes were calculated as mentioned in Chapter 2, Section 2.2.5.

The membrane performance studies were conducted by measuring PWF and FRR. The equation (2.4) and (2.5) in Chapter 2 were used to determine the PWF and FRR. In addition to the FRR, the antifouling property of the membranes was assessed by R_{rev} and R_{irr} fouling values using the equation (2.6) and (2.7), respectively in Chapter 2.

The protein rejection study was performed using in-house designed dead-end filtration set up. The protein solution of 1000 ppm containing BSA, Pepsin and trypsin were separately passed into membranes and flux of the permeate (J_p) was quantified at 0.3 MPa TMP using the equation (2.4). The protein rejection was also analyzed by measuring the absorbance of permeate using a UV-Vis spectrophotometer at a wavelength of 280 nm. The percentage of protein rejection was estimated using the equation 2.8 in Chapter 2. The PEUF of heavy metal ions were also conducted as mentioned in Chapter 2, Section 2.2.8 and the percentage of metal ion rejection was calculated using the equation (2.8).

3.3 RESULTS AND DISCUSSIONS

3.3.1 Characterization of polymer

The functionalization of PPSU by the sulfonation was identified by the ATR-FTIR spectroscopy and confirmed by the ^{1}H-NMR spectroscopy. The Fourier transformed infrared (FTIR) spectra showed the formation of additional peaks for sPPSU when it was compared with PPSU (Figure. 3.1). The presence of peak around 3400 cm^{-1} and 1640 cm^{-1} indicates the vibration of O-H from sulfonic acid groups interacting with molecular water. The absorption bands at 1089 cm^{-1} are assigned to SO_3H vibration while vibration peaks at 1233 cm^{-1} and 1016 cm^{-1} indicates SO_3^- group in sPPSU (Kim *et al.* 2013).

The ^{1}H-NMR spectrum of sPPSU in Figure 3.2 shows all the characteristic peaks observed at chemical shift between 7-8.5 ppm. The existence of sulfonic acid was validated by the peak at 8.08 ppm for acidic proton (Di Vona *et al.* 2010). Moreover, the DS was determined by titration using equation (3.1), which is found to be 37.2 ± 2.3 % (Shenvi *et al.* 2014).
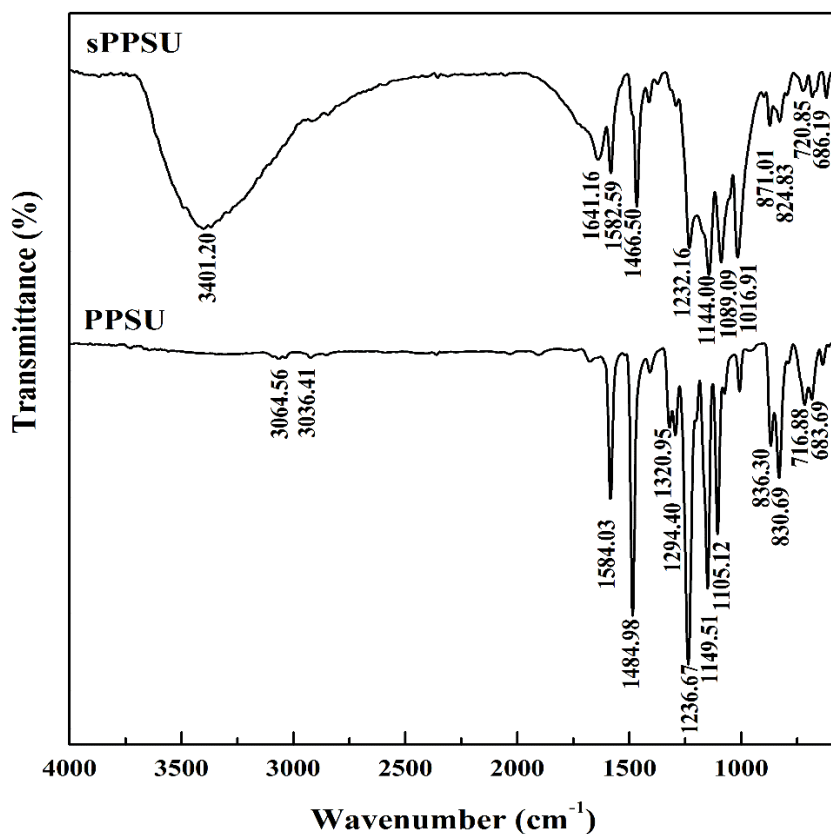
Figure 3.1 FTIR spectra of sPPSU and PPSU
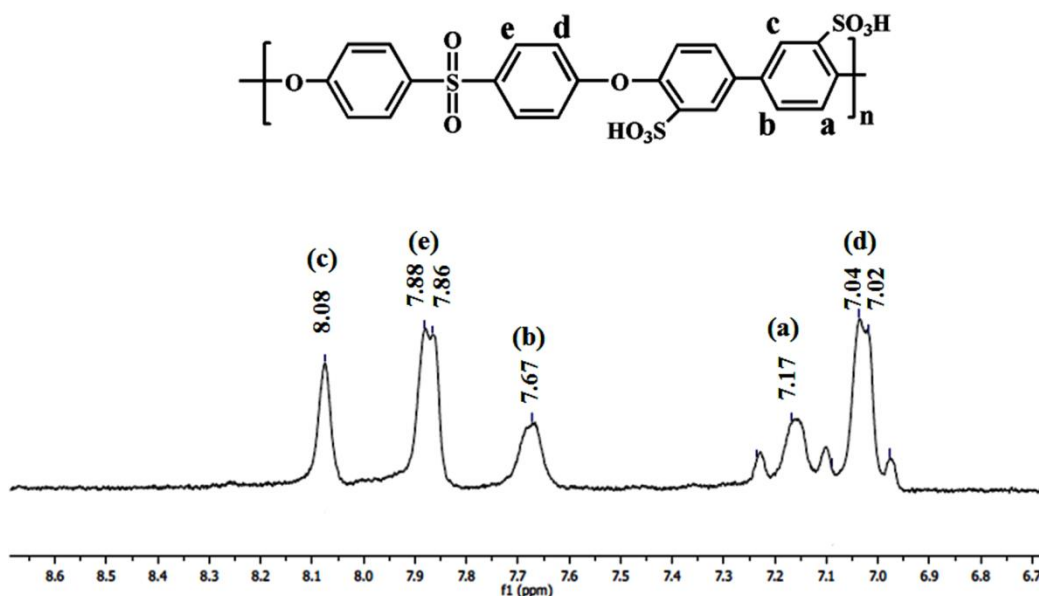
Figure 3.2 ^{1}H NMR spectrum of sPPSU

3.3.2 Membrane morphological study

3.3.2.1 Scanning electron microscopy

The cross-sectional SEM images were taken to study the membrane morphology. The membranes displayed asymmetric nature with top dense layer and porous sub-layer with finger-like projections (Figure 3.3). The membranes displayed elongated finger-like projections when the concentration of sPPSU in the dope solution was increased. This is due to the strong H-bond interaction of the hydrophilic sulfonic group present in the sPPSU with water resulting in the instantaneous demixing of solvent and non-solvent to give rise to elongated finger-like pores (Arumugham *et al.* 2015). The variation in membrane thickness with gelation time i.e. the time gap between the dipping of the casted plate into the coagulation bath and the emergence of opaque membrane film is shown in Table 3.2. It was observed that the gelation time for the membrane increased with the increase in sPPSU ratio indicating the formation of thicker membranes. However, the concentration of sPPSU was limited to 5-15 wt. % as the membrane showed the poor film forming ability at higher concentration of sPPSU due to inhomogeneity in the blend above the 15 wt. %.
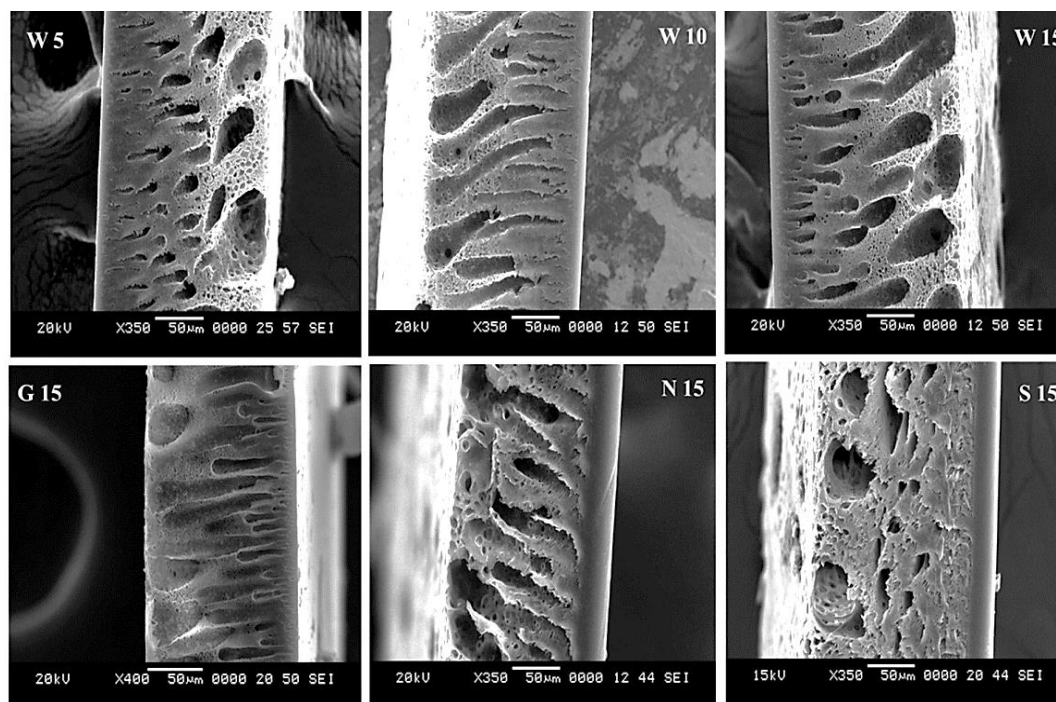
Figure 3.3 Cross-sectional images of prepared membranes

The membrane with casting composition of 85:15 PSF/sPPSU was further studied for the effect of coagulation bath composition as the membrane morphology is expected to change with the coagulation bath condition and composition. The addition of NMP to the coagulation bath suppressed the formation of macrovoid due to delayed liquid-liquid demixing (Strathmann and Kock 1977). Therefore, the presence of NMP in coagulation bath resulted in the thick and dense membrane with low pore interconnectivity. The addition of inorganic salt i.e. NaCl in coagulation bath also reduced macrovoid formation due to the diminished rate of demixing.

Table 3.2 Gelation time, membrane thickness, and mean pore radius

Membrane code	Gelation time (s)	Thickness of membrane (µm)	Mean Pore Radius (nm)
W 5	7	158	6.43
W 10	9	173	9.66
W 15	11	177	11.20
G 15	10	149	12.16
N 15	14	194	14.32
S 15	18	197	15.42

Moreover, the decrease in the chemical potential of bath due to the salt effect was the reason for the decline in the driving force during the film precipitation. Hence, the mass transfer of the solvent was observed to be slower for coagulation bath containing NaCl and NMP than the water as a coagulant. There is an increase in thickness of the dense top layer observed due to the lower diffusion rate. However, the addition of GB to the coagulation bath displayed an inverse effect due to its high dipole moment and chemical potential (Lutchmiah *et al.* 2014). The GB in coagulation bath caused instantaneous mixing of the polymer-rich phase and polymer lean phase resulting in the thin top layer and elongated finger-like projection (Liu *et al.* 2012). The variation of gelation time and membrane thickness with the change in coagulation bath composition is in the order: G15 < W15 < N15 < S15, which is in

accordance with the rate of demixing (Li *et al.* 2011). The variation in the pore size with the change in coagulation bath composition is in the order: G15 < W15 < N15 < S15, which is in accordance with the rate of demixing.

3.3.2.2 Atomic force microscopy

The surface topographical analysis of membrane was performed using AFM. It also gives surface roughness parameter of the membrane such as R_a and R_q, which can be related to the antifouling nature of the membranes, as the membranes with rough surface get fouled easily due to deposition of foulant over the depressions on the surface (Razmjou *et al.* 2011). The 3D scan AFM image over an area of 5×5 µm^2 under tapping mode displayed peaks (bright region) and valleys (dark region) (Figure 3.4) (Cao *et al.* 2006). The membrane showed fewer peaks and valleys when the concentration of sPPSU in the membranes increased, which attributed to the smoother surface. The roughness of the membranes given in Table 3.3 further supports the observation. The roughness parameters varied with the concentration of sPPSU in the order as follows: W 5 > W 10 > W 15 (Daraei *et al.* 2012). This decrease in surface roughness value is due to the development of smoother surface that can felicitate the low fouling due to reduced adsorption of foulant over the surface of the membrane.
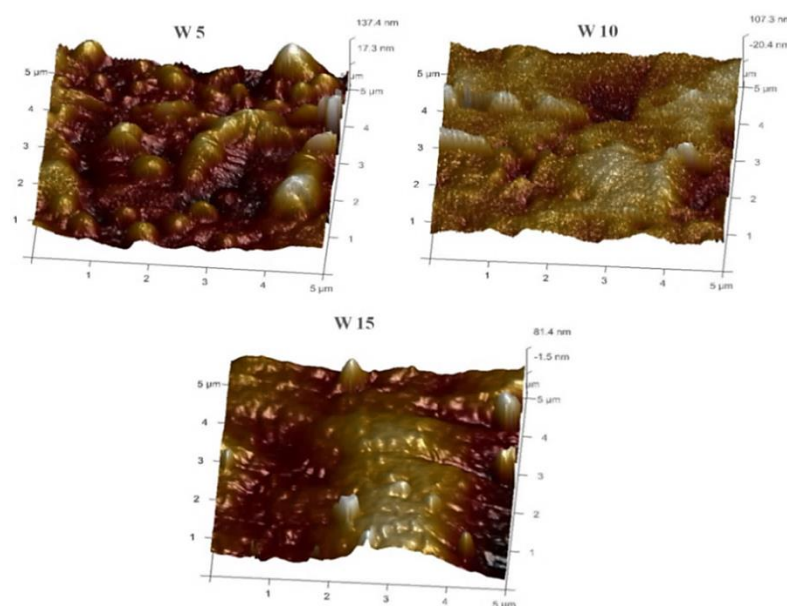
Figure 3.4 3D AFM images of prepared membranes

Table 3.3 Surface roughness parameters of membranes

Membrane code	Roughness Parameters	
	R_a (nm)	R_q (nm)
W 5	26.8	34.1
W 10	23.8	32.7
W 15	18.9	23.6

3.3.3 Membrane hydrophilicity and porosity

The hydrophilicity and wettability of the membrane were evaluated by the WCA and water uptake capacity measurement. The decrease in WCA can be observed as the concentration of sPPSU increased, i.e. smaller the contact angle more hydrophilic is the membrane surface (Kumar *et al.* 2013). This trend was observed due to the migration of hydrophilic group to the surface of the membranes during the phase inversion, i.e., the hydroxyl group present in sulfonic acid has a strong affinity to water and form H-bond with the water molecule resulting in the increase in surface wettability and hydrophilicity of the membranes. The hydrophilicity of the membranes was further increased with the increase in the concentration of sPPSU in the blend as the number of the sulfonic groups present on membrane surface increases. Figure 3.5 shows the WCA of the prepared blend membranes which range from 65° to 55°. However, the coagulation bath did not bring any significant change in the WCA.

The water uptake capacity of the membrane also increases with the increase in the concentration of sPPSU in the blend membranes. This is due to the increasing number of sulfonic group on the membrane surface, which forms strong H-bonding with water molecules. The change in water uptake capacity is well in agreement with the WCA results. However, the change in coagulation bath condition also brought changes in the water uptake capacity (Figure 3.6).

. The presence of GB in the coagulation bath improved the rate of demixing, thereby resulting in the membranes with elongated pores. Evaluating the water uptake

capacity of the membranes prepared in the coagulation bath containing NaCl and NMP, it is observed that their lower porosity and the dense structure was responsible for lower water uptake capacity.
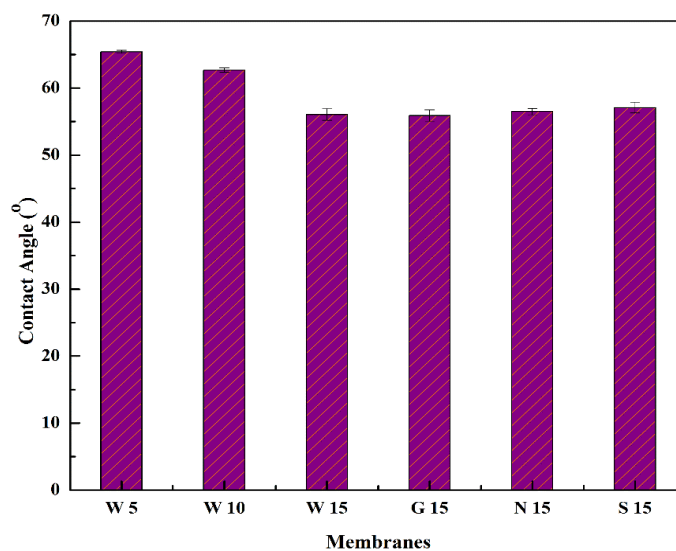
Figure 3.5 WCA of the membranes
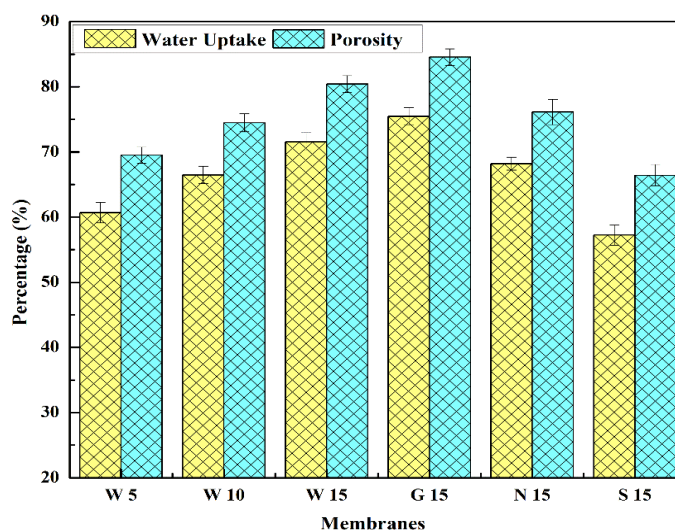
Figure 3.6 Water uptake and porosity of the membranes

Figure 3.6 displays the porosity of the membrane which is observed to increase with the increase in the concentration of sPPSU. This can be related to the formation of elongated pore structure due to the migration of hydrophilic sulfonic group toward the membrane surface. On the other hand, the effect of coagulation bath condition on the porosity is related to the morphological changes taken place in the

membrane during the phase inversion. Thus, the porosity of the membrane increased as S 15 < N 15 < W 15 < G 15. The coagulation bath containing GB resulted in the membrane with the highest porosity, as spongy membranes with many interconnected finger-like structures were formed because of faster demixing. The lower diffusion rate of the membrane in the presence of NaCl and NMP in the coagulation bath causes a decline in porosity with the formation of the dense membrane due to delayed liquid-liquid demixing (Buonomenna *et al.* 2007).

3.3.4 Pure water flux

The permeation property of the membranes was estimated by the PWF. The PWF of membranes increased with the increase in sPPSU concentration. This could be associated with the increase in the hydrophilicity, pore size, and porosity of the membranes. As mentioned earlier, the polar sulfonic acid group present in sPPSU makes the surface of the membrane more hydrophilic and its strong affinity towards water results in larger flux. The PWF of the membranes prepared with different coagulation composition was also assessed. From Figure 3.7, the pressure-dependent PWF of the membranes can be viewed, which is as S 15 < N 15< W 15 < G 15. The highest permeability of G 15 is observed due to highest porosity and water uptake capacity of the membrane, while the S 15 and N 15 membrane showed lower flux due to the dense morphology of the membrane along with lower porosity.
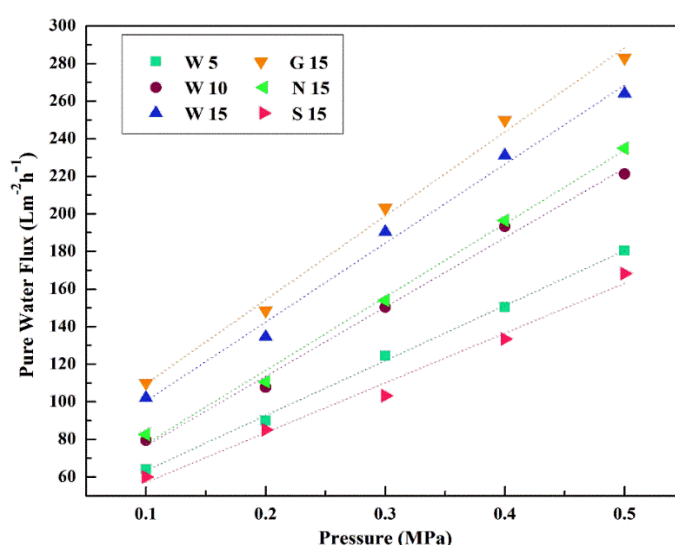
Figure 3.7 Pressure-dependent PWF of prepared membranes

3.3.5 Antifouling study

The antifouling behavior of the membranes was assessed by passing BSA solution through the prepared membranes. There is a decline in the flux of BSA observed from Figure 3.8, which is due to the adsorption of BSA and blocking of the pores by BSA in the membrane. The order of fouling in the prepared blend membranes is W 15 < W 10 < W 5, which is in accordance with the surface hydrophilicity and roughness of the membranes. The PWF was measured after the BSA flux (J_{w2}) and the FRR was calculated to study the extent of membrane fouling and reusability. The increased FRR of the membrane is witnessed with the increase in the ratio of sPPSU in the polymer (Figure 3.9). It can be explained by the increase in the number of sulfonic groups present on the membrane surface as the concentration of sPPSU in the blend increased. The large FRR proposes that the protein deposited on the surface of the membrane could be easily removed by washing. The weak interaction between the foulant and the membrane surface due to the formation of hydration layer make it easier to wash away the foulant. The fouling resistance was also determined by measuring the R_{rev} and R_{irr} fouling value as seen in Figure 3.9. The membrane with the blend ratio of 85:15 of PSF/sPPSU showed least R_{irr} and R_{rev} of 13.43 % and 54.67 %, respectively. The presence of negatively charged $-SO_3H$ group on the surface caused the electrostatic repulsion of the negatively charged protein foulant, hence lower adsorption of foulant on the membrane surface is observed (Zhu *et al.* 2007). The trend in membrane fouling agrees with the AFM results, where the surface roughness decreases with the increase in the sPPSU concentration.

The effect of coagulation bath on the FRR was also studied, where the G 15 membrane showed slightly higher FRR than the S 15 and N 15. This trend could be related to the hydrophilicity and the pore size of the membranes. The G 15, membranes with the highest hydrophilicity and lower pore size showed least R_{irr} as the membrane fouling due to clogging of the pore is reduced. The pore clogging is a major reason for increased R_{irr} as the foulant gets adhered to the membrane pore. The removal of these foulant becomes difficult as the membrane hydrophilicity decreases. Hence, S 15 and N 15 membranes, which possess lower hydrophilicity and higher

pore size shows lower FRR and increased R_{irr}. Therefore, lower pore radius and higher hydrophilicity of the G 15 membranes resulted in membranes with better FRR.
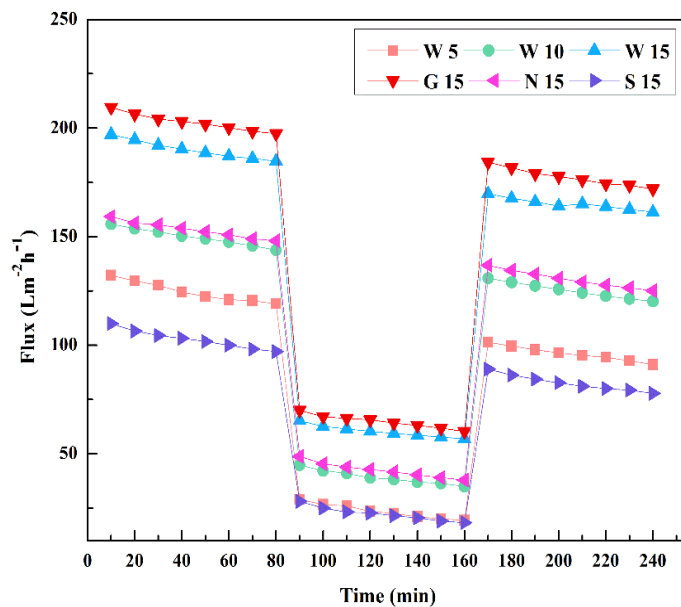
Figure 3.8 PWF vs. time for the membranes before and after passing BSA at 0.3 MPa TMP
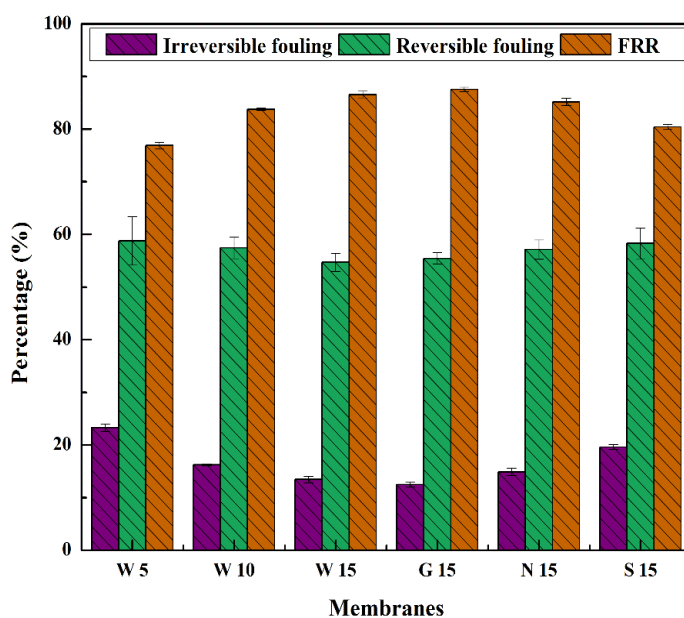
Figure 3.9 FRR and fouling resistance of the prepared membranes

3.3.6 Rejection study

3.3.6.1 Protein rejection

The protein solutions such as BSA (Mw ~ 66.5 kDa), pepsin (Mw ~ 34.5 kD) and trypsin (Mw ~ 23.3 kDa) were passed separately through the membranes to study their protein flux and rejection (Figure 3.10 & 3.11).
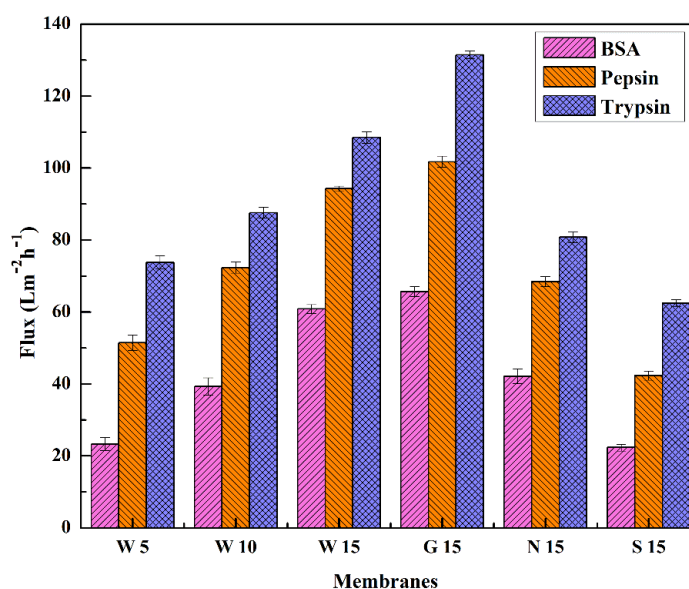
Figure 3.10 Protein flux of the prepared membranes at 0.3 MPa TMP
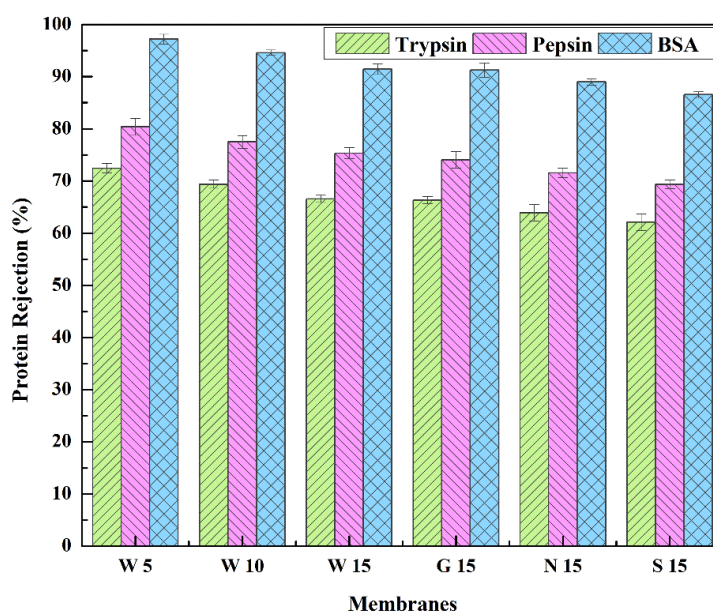
Figure 3.11 Protein rejection by prepared membranes at 0.3 MPa TMP

The results reveal that the increased hydrophilicity and the enlarged pore size lead to the higher PWF, which is also relevant for the protein flux. The protein flux showed a similar trend to that of the PWF. Moreover, the rejection of the protein and high flux could be attributed to the electrostatic repulsion of protein by the membrane surface, causing the reduced pore blockage (Liu *et al.* 2015). Therefore, the percent of protein rejection increases with the increase in the sPPSU concentration as the number of sulfonic acid group which is responsible for the negative charge in membrane increases. The BSA demonstrated the least flux with the highest rejection while trypsin showed the highest flux with least rejection. This trend is based on the molecular weight of the protein, where the movement of the bulkier proteins is restricted through the membranes. Therefore, trypsin with least molecular weight showed the highest flux with least rejection while BSA which has largest molecular weight showed the highest rejection and low flux. The sequence of protein flux and rejection of the blend membranes with the change in coagulation bath is in the following the order: G 15 > W 15 > N 15 > S 15. During the protein rejection test, the elongated interconnected pores and smaller pore size of the G 15 membranes cause easy passage of water through the membrane while rejecting the protein. Hence, this result in highest flux for all the three protein samples with maximum rejection reported to be 66.3 %, 74.0 % and 91.2 % for trypsin, pepsin, and BSA, respectively.

3.3.6.2 Heavy metal rejection

The PEUF was carried out by complexation of heavy metal ions with PEI (Aroua *et al.* 2007). The PEI-metal complex is formed as metal interacts with the lone pairs of electrons present in the PEI giving rise to macromolecules which are larger than the metal ions. The PEUF of Pb^{2+} and Cd^{2+} were conducted and the percentage of rejection is displayed in Figure 3.12.

In the PEUF studies, the rejection of Pb^{2+} is greater than Cd^{2+}. This is because of the stronger binding of Pb^{2+} over Cd^{2+} in the PEI-metal complex that can be related to the electronegativity of metal ions (Takagishi *et al.* 1985, Vijayalakshmi *et al.* 2008). It was further observed that, the amount of heavy metal rejection with a change

in the ratio of PSF:sPPSU in the dope solution is as follows: W 5 > W 15 > W 10. The initial decline in the rejection by the membranes with an increase in the sPPSU composition from 5 wt. % to 10 wt. % is due to the enlargement in pore size. The percentage rejection eventually increased due to the increase in the number of the negatively charged sulfonic group present on the membrane surface that dominated the increase in pore size. The larger pore size of the membrane prepared in a coagulation bath containing NMP and NaCl lead to the lower rejection. The elemental mapping was carried out to demonstrate the adsorption of Pb^{2+} and Cd^{2+} on the membrane surface (Figure 3.13).
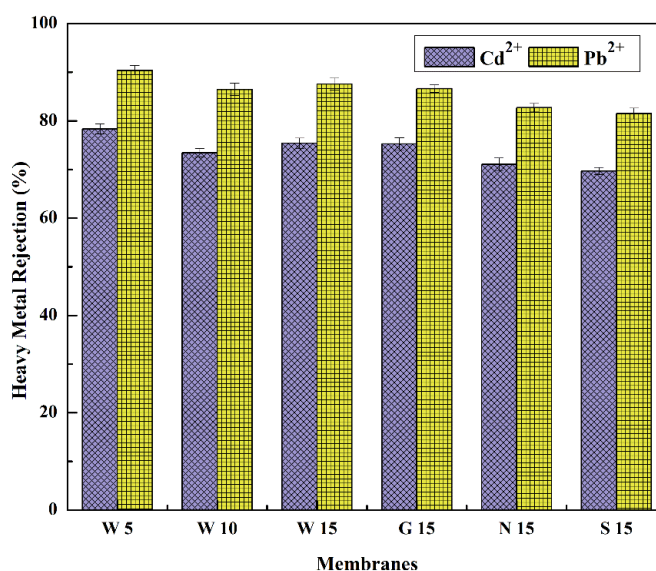
Figure 3.12 Heavy metal rejection by prepared membranes at 0.3 MPa TMP
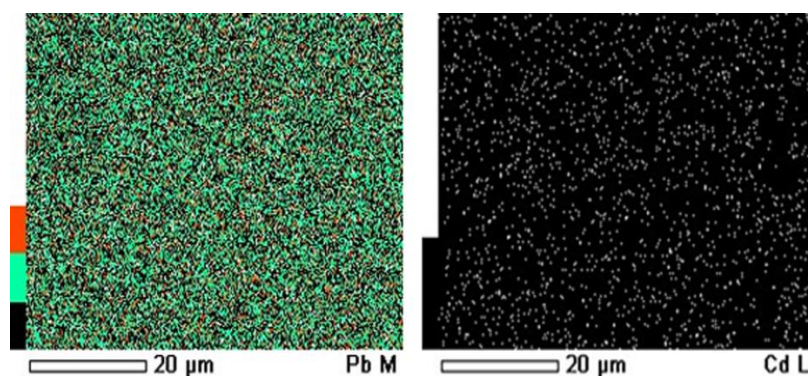
Figure 3.13 Adsorption of Pb^{2+} and Cd^{2+} on the G 15 membrane

3.4. CONCLUSIONS

The UF membranes fabricated by blending PSF and sPPSU with different concentration of sPPSU exhibited enhanced hydrophilicity, permeability and fouling resistance. The presence of sulfonic acid group on the surface of the membrane leads to superior membrane performance. The blend membrane with 15 wt. % concentration of sPPSU presented good permeation, hydrophilicity, fouling resistance, and rejection. The lower fouling resistance of W 15 membrane demonstrated the membrane reusability with R_{irr} and R_{rev} values of 13.43 % and 54.67 %, respectively. Among the series of prepared membranes, the well-performed membrane, i.e. W 15 was formulated at different coagulation bath composition namely, an aqueous solution of GB or NaCl or NMP. The membrane morphology and performance were also studied for the membranes with different composition of coagulation bath. The addition of GB to the coagulation bath resulted in the thinner membrane with higher porosity. The G 15 membrane showed the highest protein flux of 65.65 $Lm^{-2}h^{-1}$, 101.73 $Lm^{-2}h^{-1}$, 131.48 $Lm^{-2}h^{-1}$ and protein rejection of 66.3 %, 74.0 % and 91.2 % for trypsin, pepsin and BSA, respectively. However, there was a decline in the membrane performance on the addition of NMP or NaCl to the coagulation bath due to the formation of dense membranes. The PEUF for Pb^{2+} and Cd^{2+} metal ions were carried out where the rejection of Pb^{2+} and Cd^{2+} range between 76-90 % and 65-79 %, respectively.

CHAPTER 4

FABRICATION OF ANTIFOULING HOLLOW FIBER MEMBRANES EMBEDDED WITH CHITOSAN AND SILVER-LOADED CHITOSAN NANOPARTICLES FOR DYE REJECTION

Abstract: *This chapter deals with fabrication of HF membrane embedded with chitosan nanoparticles (CNPs) and silver loaded chitosan nanoparticles (Ag-CNPs). The effect of concentration of CNPs and Ag-CNPs on the membrane property was analyzed by filtration and antifouling studies. The synthesized HF membranes were used for the dye removal, with the maximum rejection of 89.1 % and 86.04 % for RB 5 and RO 16, respectively. Hence, the HF membranes with Ag-CNPs are pertinent in developing antibiofouling membranes for the treatment of industrial dye effluents.*

4.1 INTRODUCTION

The HF membranes are considered to be the advanced membranes due to its unique properties such as the large surface area to volume ratio, energy efficiency, and self-supporting structure (Qin and Chung 1999). Conversely, there are certain limitations such as inherent fouling, chlorine resistance, and disagreement between water flux and rejection, which hinder its application in industrial wastewater treatment (Wei *et al.* 2014). Efforts have been made to alleviate the extent of fouling by various methods like, the design of antifouling membranes, pre-treatment of feed water, and adjusting operational conditions (Jin *et al.* 2009, Mi and Elimelech 2010). However, the present-day filtration membranes lack antibacterial property, in turn, causes membrane biofouling, which compels repeated backwashing, chemical treatment, and replacement of the membranes.

The unique properties of NPs have been employed to improve the membrane properties due to their small size, large surface area, higher stability, and activity. The NPs are capable of increasing membrane hydrophilicity, flux, antifouling nature, selectivity, hydrophilicity, conductivity, mechanical strength, and antiviral and antibacterial properties of the polymeric membranes (Kim and Van der Bruggen 2010). The enhancement in membrane performance with the addition of NPs is due to the synergistic properties between the surface of the NP and the polymer chain. The increased permeability has been ascribed to the increased free volume in the polymer matrix caused by the NPs disrupting the packing of the polymer chains.

Chitosan is a semi-crystalline, non-toxic biopolymer with high metal complexation. Chitosan is considered a good adsorbent as it contains amino and

hydroxyl functional groups as active sites which can serve to remove heavy metals (Wu *et al.* 2010) and dyes (Stefancich *et al.* 1994, Ngah *et al.* 2011) by chelation. It also exhibits a broad range of antimicrobial activity, which depends on the molecular weight (Jia and Xu 2001), pH (Li *et al.* 2002), and the solvent. Chitosan NP (CNP) has been synthesized to foster superior activity due to the effect of the small size of NPs (Qi *et al.* 2004). Moreover, the adsorption capacity improved with the reduction of particle size. The bioactivity of chitosan is further enhanced by the inclusion of Ag^+ ions (Ma *et al.* 2008), which is non-toxic for human cells, and has proved to be a disinfectant and effective in eliminating bacterial colonies (Zhang *et al.* 2003). Ag NPs were reported to exhibit bactericidal trait against *E. coli* (Silver 2003)*, Pseudomonas aeruginosa* (Liau *et al.* 1997)*, Staphylococcus epidermidis,* and *Staphylococcus aureus (S. aureus)* (Cao *et al.* 2010).

Du *et al.*(2009) reported the synthesis CNP and metal loaded CNPs by the ionotropic gelation of chitosan with sodium tripolyphosphate (TPP). The CNPs were loaded individually with different metal ions like Ag^+, Cu^{2+}, Zn^{2+}, Mn^{2+}, or Fe^{2+}. The particle size and the ZP of the NPs were analyzed and found that the size and ZP increased with the addition of metal ions. These NPs inhibited the microbial growth and showed appreciable enhancement of antimicrobial property by loading metal ions, especially for Cu^{2+} loaded CNP, with the minimum inhibitory concentration being 21–42 times lesser than Cu^{2+} alone.

Later Ali *et al.* (2011) compared the antibacterial property of the CNPs and silver loaded CNP (Ag-CNP). The CNP was synthesized by ionic gelation with TPP and subsequently, Ag is loaded using silver nitrate to produce Ag-CNPs. The CNPs and Ag-CNPs were characterized by X-ray diffraction (XRD), FTIR, differential scanning calorimetry (DSC), thermogravimetric analysis (TGA), and transmission electron microscopy (TEM). The crosslinking of TTP with chitosan was revealed by FTIR while the amorphous nature of CNPs was confirmed by the XRD result. They stated that loading of Ag to the CNPs could enhance the antimicrobial activity against *S. aureus* due to the synergistic effect.

Feng *et al.* (2014) grafted chitosan onto bromomethylated poly(phenylene oxide) (BPPO) (Scheme 4.1) UF membrane. The membrane showed improved surface hydrophilicity due to the presence of polar groups of chitosan on membranes surface. These polar groups could reduce the interaction between the foulant and the surface as there is a decrease in interfacial free energy of the surface. These membranes also showed good FRR since it was easy to desorb the adsorbed foulant. The antibacterial nature of chitosan leads to 70 % hike in antibacterial activity of chitosan-grafted BPPO membranes.
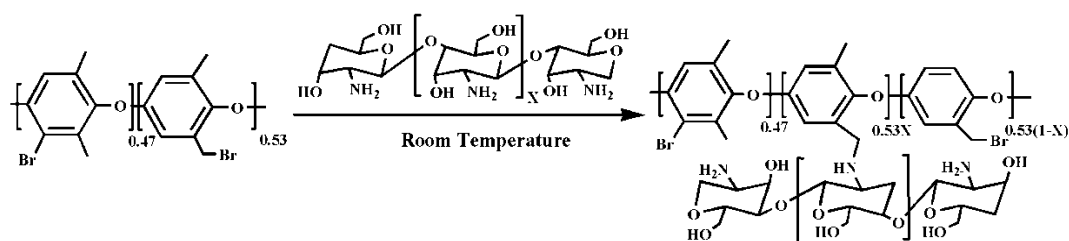
Scheme 4.1 Scheme for grafting chitosan onto BPPO (Feng *et al.* 2014)

Zinadini *et al.* (2014) fabricated NF membranes by blending O-carboxymethyl chitosan/Fe_3O_4 NPs (CC–Fe_3O_4 NPs) (Figure 4.1) with PES. The surface of modified membrane displayed higher affinity towards water than the pristine PES membrane. The presence of high content of CC–Fe_3O_4 NPs, i.e. 0.5 % in the casting solution caused agglomeration of NPs in the polymer matrix which reduced the membrane performance. Hence, a small amount of CC–Fe_3O_4 NPs could bring about high FRR of 91 %. The negative charge created by the modification led to the higher rejection of Direct Red 16 dye.
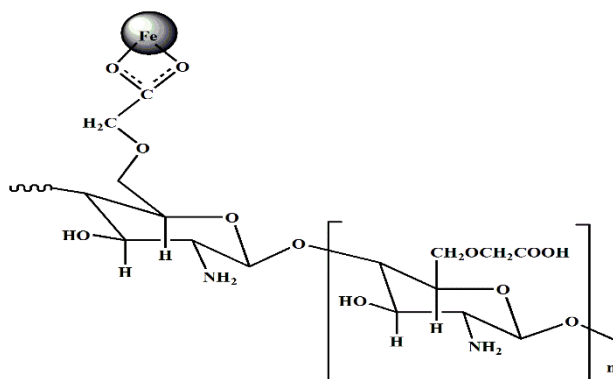
Figure 4.1 Illustration of CC–Fe_3O_4 NPs (Zinadini *et al.* 2014)

Ramalingam *et al.* (2015) demonstrated synthesis of the magnetite-chitosan microsphere (MCSM) decorated with Ag NPs of size 3.63 μm and 16 ± 2.5 nm, respectively (Scheme 4.2). The dye adsorption and anti-microbial property of the Ag NPs loaded MCSM were analyzed, and studies showed that 99.5 % of dyes and microbial contaminants were removed from water bodies efficiently. The magnetic behavior of the MCSM made it easy to remove and reuse, while the Ag NPs inhibited the growth of the microorganism.
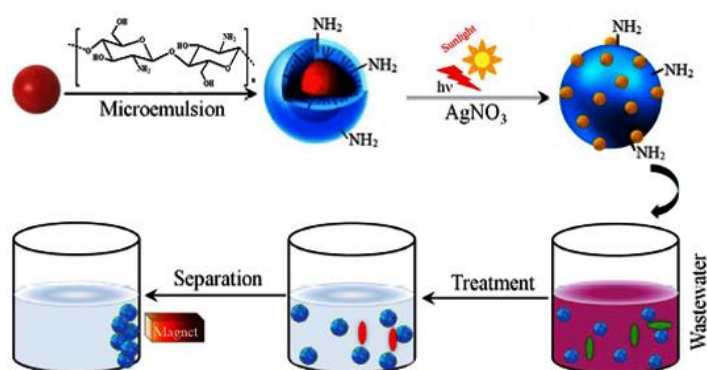
Scheme 4.2 Synthesis and separation of MCSM (Ramalingam *et al.* 2015)

Zhu *et al.* (2015) prepared the composite NF membranes by incorporating Chitosan–Montmorillonite (CS–MMT) nanosheets into the PES matrix. The PWF increased with increase in CS–MMT nanosheets content in the membranes. The composite membranes showed good antifouling property with high FRR of 92 % and low flux decline ratio (FDR) of 26 % on addition of 1.0 wt. % of CS–MMT nanosheets. They also reported the excellent dye rejection of RB 5 and Reactive Red 49.

Venkatesan *et al.* (2017) developed a porous composite with antimicrobial property using chitosan, alginate, and Ag NPs, wherein the pore forming ability was due to chitosan and alginate. The porous composites of chitosan-alginate-Ag NPs were characterized using SEM, FTIR, XRD, and UV-Vis spectroscopy. The antimicrobial activity of the composites was tested against *E. coli* and *S. aureus*, were the addition of Ag NPs to the chitosan-alginate composite improved the antimicrobial property with an inhibition zone of 11±1 mm and 10±1 mm for *E. coli* and *S. aureus*,

respectively. Moreover, the chitosan-alginate-Ag NPs composites displayed 1.5 times higher bacterial filtration ability than the chitosan-alginate composites.

It can be observed that suitable property of chitosan, such as its abundant availability, cost-effectiveness, non-toxic nature, antibacterial, and adsorptive property, makes it as an effective candidate for the treatment of industrial effluents. The usage of chitosan in membrane technology is limited due to its poor mechanical property, which constrains the use of chitosan in membrane research. Moreover, the use of CNPs and Ag-CNPs as additives to fabricate nanocomposite membranes is not been studied. Hence, the nanocomposite HF membranes were fabricated by incorporating CNPs and Ag-CNPs into PPSU polymer matrix. These HF membranes were then tested for its hydrophilicity, permeability, antibiofouling property, and dye rejection capability.

4.2 EXPERIMENTAL

4.2.1 Materials

Chitosan (Mw ~ 440 kDa and deacetylation degree of 82 %), TPP, PEG-1000, BSA (Mw~66.5 kDa), RB 5, and RO 16 were provided by Sigma–Aldrich and used without further purification. PPSU (Radel R-5000) (average Mw ~ 50,000 g mol−1) was procured from Solvay Advanced Polymer (Belgium). NMP was supplied by QREC, Malaysia. AgNO$_3$, glacial AA, and NaOH were purchased from Merck, India. The nutrient agar that was used to perform the antimicrobial testing was bought from Sisco Research Laboratories (SRL) Pvt. Ltd. India.

4.2.2 Preparation of nanoparticles

The CNPs were prepared by ionic gelation method as shown in scheme 4.3 (Qi *et al.* 2004). Chitosan solution of 0.5 % (w/v) was obtained by dissolving chitosan in 1 % (v/v) AA. The pH of the chitosan solution was maintained between 4.6-4.8 using 10 N NaOH. 0.25 % (w/v) TPP solution was dissolved in the DI water and drop by drop addition of the aq. TPP solution to chitosan solution at 1:3 ratio was carried out. The suspension was stirred at RT for 12 h using a magnetic stirrer and then centrifuged at 7000 rpm. The NPs attained by centrifugation were washed with DI

water and dried before further analysis. Ag-CNPs were prepared by the addition of the AgNO$_3$ solution to attain the concentration of 120 µg.mL^{-1} followed by stirring for another 12 h. This is then added to the chitosan solution during synthesis of NPs prior to centrifugation (Ali *et al.* 2011).
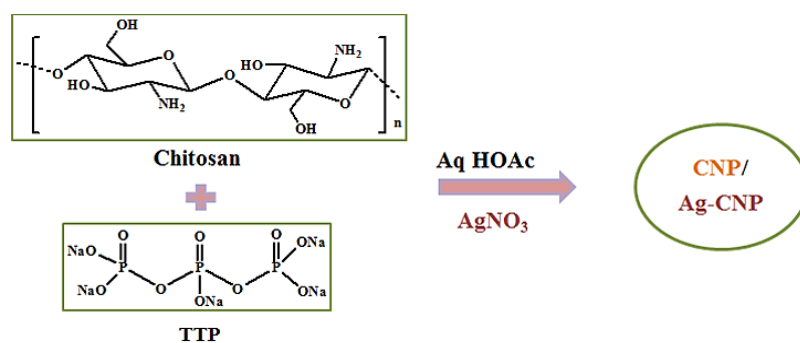
Scheme 4.3 Synthesis of CNP and Ag-CNP

4.2.3 Characterization of nanoparticles

The prepared NPs were characterized by XRD, TEM, ZP and particle analyzer, and FTIR spectroscopy. The XRD of the NPs was performed using Rigaku Miniflex 600. The samples were scanned at a rate of 2 ^{o}/min with CuKα radiation as an X-ray source. ZP and hydrodynamic size of the NPs were analyzed using a nanoparticle analyzer (Horiba SZ 100). The sample was analyzed by dispersing the NPs in milliQ water at 25 ^{o}C and recording the intensity of 532 nm laser scattered at an angle of 90°. The morphology of synthesized NPs was assessed by means of TEM (JEOL JEM-2100). The NPs were dispersed in ethanol and placed on the carbon-coated copper grid and dried before TEM analysis. FTIR spectra were obtained by KBr pellet method using Alfa FTIR Spectrometer (Bruker). The KBr pellets containing NPs were scanned for the range of 4000-500 cm^{-1}.

4.2.4 Preparation of hollow fiber membranes

4.2.4.1 Preparation of dope solution

PPSU pellets were dried in an oven at 50 ^{o}C for 24 h. The synthesized NPs were sonicated using probe sonicator at 40 kHz for 15 min to obtain a uniform dispersion of NPs in NMP. The dope solutions were formulated by the addition of PEG-1000

and PPSU to this dispersion and then stirred at 500 rpm in 50 $^{\circ}$C for complete dissolution of the polymer (Yuliwati *et al.* 2011). The dope solutions were then degassed in an ultrasonic bath to get rid of any trapped air bubbles. The compositions of the dope solution are as described in Table 4.1 below. The dope solution for neat PPSU was prepared in the same way as above, without the addition of NPs. The viscosity of the dope solutions was recorded using a viscometer (Model: EW-98965-40, COLE PARMER, 20-2 million centipoises).

Table 4.1 Compositions of dope solution

Membrane code	PPSU (wt. %)	CNP (wt. %)	Ag-CNP (wt. %)	PEG-1000 (wt. %)	NMP (wt. %)
HF 0	20	-	-	5	75
HF 0.05	20	0.05	-	5	74.95
HF 0.15	20	0.15	-	5	74.85
HF 0.30	20	0.30	-	5	74.70
Ag-HF 0.05	20	-	0.05	5	74.95
Ag-HF 0.15	20	-	0.15	5	74.85
Ag-HF 0.30	20	-	0.30	5	74.70

4.2.4.2 Fabrication of hollow fiber membrane

The HF membranes were fabricated by dry-wet spinning technique (Razmjou *et al.* 2012). Figure 4.2 gives the pictorial representation of the HF spinning setup. The spinning parameter given in Table 4.2 was used for the spinning of HF membranes. The dope emerging from the spinneret positioned at an air gap of 5 cm to the coagulation bath containing water resulted in the HF. The HF collected by the collecting drum was soaked in coagulation bath for one day to remove the residual solvent. They were then treated with 10 % glycerol solutions for 24 h to prevent

contraction and collapsing of the pores, and then air dried for two days at 27 $^\circ$C before further characterization.

Table 4.2 Hollow fiber spinning parameters

Dope composition	PPSU/PEG/ CNP/NMP PPSU/PEG/ Ag-CNP/NMP PPSU/PEG/NMP (For Neat)
Dope extrusion rate (DER)	6 mLmin^{-1}
Bore fluid	Distilled water
Bore extrusion rate (BER)	3 mLmin^{-1}
Air gap	5 cm
Spinneret dimension (o.d/i.d)	1.7 /0.55 (mm)
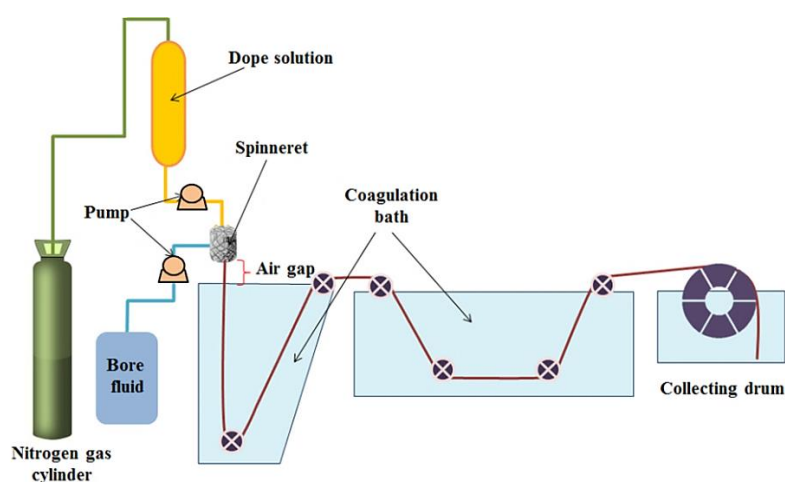
Figure 4.2 Pictorial representation of the HF spinning set up

4.2.5 Membrane characterization

The HF membrane morphology was examined using SEM (JEOL JSM-6380L) were the cross-sectional image of HF membranes was inspected at 20 kV (Kumar *et al.* 2013). AFM was used to study the membrane surface topography and surface roughness by calculating the roughness parameters such as R_a and R_q (Pereira *et al.*

2015). The HF membranes were investigated for surface hydrophilicity by using contact angle goniometer (Model: OCA 15EC, Dataphysics), which measure the dynamic contact angle of the membrane by the sessile drop method (Kajekar *et al.* 2015).

The water uptake and porosity studies were carried out by measuring the dry and wet weight of membrane obtained by immersing dry HF membrane samples of length 5 cm in DI water for 24 h. The water uptake and porosity of HF membranes were calculated by the equation (2.1) and (2.2), respectively. The Guerout–Elford–Ferry equation was used to find out the mean pore radius using porosity of the HF membrane by employing filtration velocity method as given in equation (2.3).

4.2.6 Filtration study

The filtration experiments such as permeate flux and the dye rejection study were conducted using a cross-flow filtration set up (Figure 4.3). The lab scale modules of HF membranes were compiled using five HF membranes of length 15 cm potted into a holder using an epoxy resin and hardener (Zulhairun *et al.* 2014). The permeation study was performed using pure water in the feed tank. The HF membranes were initially compacted at 0.3 MPa for 30 min and the PWF were estimated at 0.2 MPa TMP. The Permeate flux $'J_w'$ was evaluated using the following equation:

$$J_w = \frac{Q}{n \times \Delta t \times A} \quad (4.1)$$

Where, $'Q'$ is the filtrate volume (L) within the operation time, $'\Delta t\,'$ (h), $'A'$ is the area of the membrane (m^2) and $'n'$ is the number of HFs.

The water-soluble dyes such as RB 5 and RO 16 of 10 ppm concentration were taken in feed tank to conduct the rejection experiment. The rejection experiments were carried out at a steady pressure of 0.2 MPa. The amount of dye rejected by HF was verified using a UV–Vis spectrophotometer (HACH/ Model: DR5000) at a wavelength of 597 nm and 494 nm for RB 5 and RO 16, respectively. The percentage rejection (R) was evaluated using the equation (2.8) in Chapter 2, Section 2.2.7.
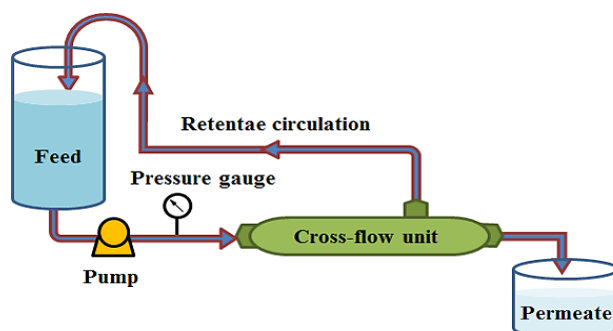
Figure 4.3 Diagram of cross-flow filtration unit

4.2.7 Antifouling studies

4.2.7.1 Antifouling test

The antifouling nature of HF membranes was studied using BSA solution (1 mgmL^{-1}) as the foulant, where the extent of fouling and reusability is estimated based on FRR and FDR (Zha *et al.* 2015) given in equation (2.5) and (4.2), respectively. The fouling behavior was studied by passing BSA feed solution through the pre-filtered HF membranes at 0.2 MPa TMP for 80 min. The HF membranes were then backwashed with water for 30 min and the PWF for the membranes were estimated (Shenvi *et al.* 2014).

$$FDR = \left(\frac{J_{w1} - J_p}{J_{w1}}\right) \times 100 \quad (4.2)$$

Where, $'J_{w1}'$ is the pure water flux of membranes, $'J_p'$ is the flux of the protein solution.

4.2.7.2 Zone of inhibition experiment

The conventional disc diffusion method was performed to investigate the antibacterial property of the CNP, Ag-CNP, and the HF membranes. The standard cultures of three bacteria *Mycobacterium smegmatis (M. smegmatis)*, *S. aureus,* and *E. coli* of 100 µL (0.5 Mac Farland) was inoculated on the nutrient agar media (28.0 g.L^{-1}). The aqueous suspensions of NPs (1 µL and 2 µL concentration) and HF membrane samples of 1 cm length were incubated on nutrient agar containing microbial culture for 12 h at 30 °C. The zone of inhibition was then measured and compared with that of Streptomycin as the reference (Yu *et al.* 2015).

4.2.7.3 Antibiofouling study

Antibiofouling property of the membranes was studied by incubation method where the HF membrane samples of a length of 3 cm were incubated in the vial containing microbial cultures for 12 h. After the incubation, all the HF membranes were removed from the vials and set onto the nutrient agar plates. The nutrient agar plates were then monitored for the bacterial growth over the HF membrane samples and the results were recorded (Hebbar *et al.* 2016). The sterilized Whatman filter paper strip of comparable size was used as a control.

4.3. RESULTS AND DISCUSSIONS

4.3.1 Characterization of nanoparticles

4.3.1.1 Hydrodynamic size and zeta potential

The characteristic features of NPs such as size (including size distribution) and charge were analyzed by using nanoparticle analyzer (Müller *et al.* 2001).
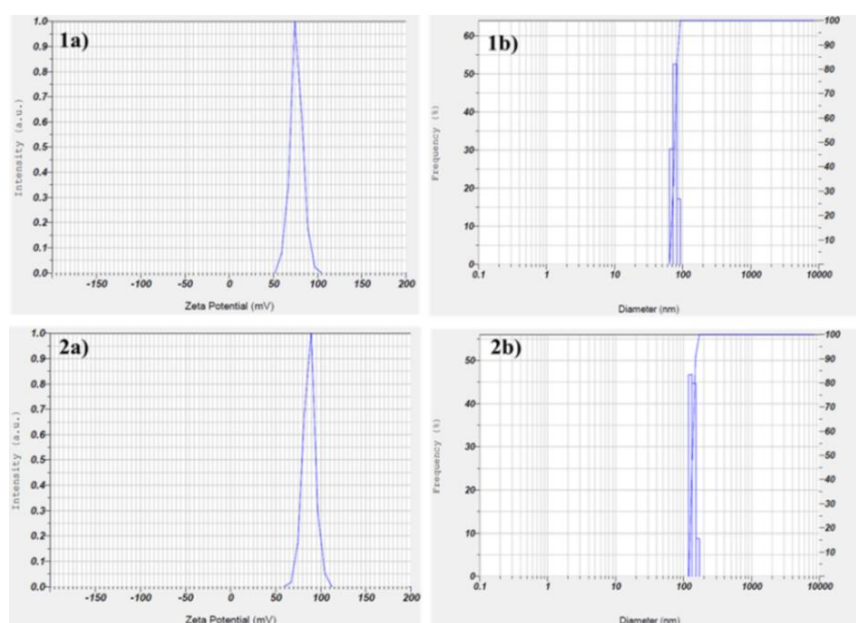
Figure 4.4 ZP of 1a) CNP and 2a) Ag-CNP, and Particle size distribution of 1b) CNP and 2b) Ag-CNP

The hydrodynamic size of CNP and Ag-CNP verifies the formation of NPs along with the size of NPs when dispersed in an aqueous medium. Figure 4.4 (1b)

shows a constricted size distribution of CNPs with the mean diameter of 76.5 ($\pm$6.9) nm. The inclusion of silver ions onto CNP increased the mean diameter to 136.6 ($\pm$10.9) nm and the wide size distribution due to surface chelation of Ag^+ ions with CNPs (Figure 4.4(2b)).

The ZP of the NPs was measured to understand the charge and stability of the synthesized NPs in an aqueous medium (Du *et al.* 2009). From Figure 4.4 (1a and 2a), the ZP of +74.9 mV and +92.05 mV were observed for CNPs and Ag-CNPs, respectively. The considerable rise in ZP displayed by Ag-CNPs on loading silver ions to CNPs is due to the positive charge borne by silver ions. It is reported that a minimum ZP value of $\pm$30 mV is essential for the stability of NPs in the suspension (Müller *et al.* 2001). Hence, the prepared NPs are stable with positive net charge.

4.3.1.2 Morphological study

Morphology of CNPs and Ag-CNPs, along with their average size and crystallinity were observed from TEM images given in Figure 4.5. The TEM micrograph of CNPs showed spherical shape with a size range of 5-10 nm while Ag-CNPs displayed the aggregated and multi-shaped structure with a size range of 25-50 nm. The increased size of Ag-CNPs can be associated to the chelation of silver ions with chitosan. The electron diffraction pattern of NPs obtained from the TEM reveal the amorphous and crystalline state of CNP and Ag-CNP, respectively.

The average particle size for CNPs and Ag-CNPs obtained from TEM micrographs were observed to be lower than the values obtained by particle size analyzer. This variation in the average particle size was due to the difference in the method employed for measurement. The particle analyzer measured the hydrodynamic diameter of NPs in swollen form as it is dispersed in aqueous media, while the TEM images provided the particle size of dry NPs.

The EDX analysis of Ag-CNP was carried out to confirm the loading of silver ions onto the CNP. Figure 4.6 shows EDX spectrum, where the elemental peaks for C, P, O, and Ag, verifies the formation of Ag-CNP.
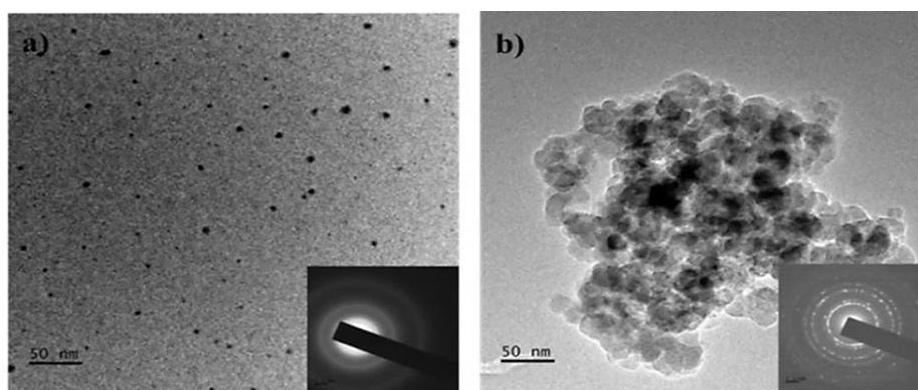
Figure 4.5 TEM images of a) CNP and b) Ag-CNP
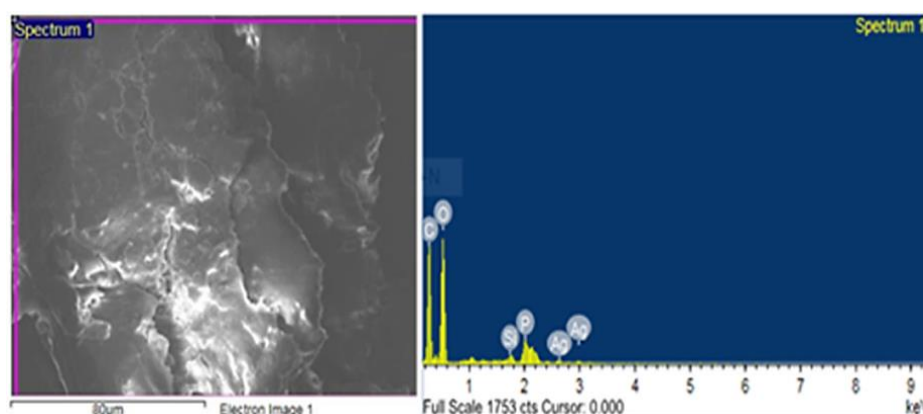
Figure 4.6 Electron micrograph and EDX spectrum of Ag-CNP powder

4.3.1.3 Fourier transform infrared analysis

The chemical structure of the NPs synthesized by cross-linking of chitosan and TPP were characterized using FTIR spectroscopy and the spectra are given in Figure 4.7. A combined peak at 3452 cm^{-1} is observed for the stretching vibration frequency of -NH$_2$ and -OH group present in CNP. A sharp peak at 1637.16 cm^{-1} due to NH$_2$ bending observed in CNP, splits on loading with Ag to produce two peaks at 1634.16 cm^{-1} and 1545.94 cm^{-1} as Ag binds with O and N, respectively. A peak at 1255.90 cm^{-1} is observed for P=O stretching due to crosslinking of chitosan with TPP. The peaks were observed at ~1000 cm^{-1} and 1350 cm^{-1} for C–N stretching and bending, respectively (Wu *et al.* 2005).
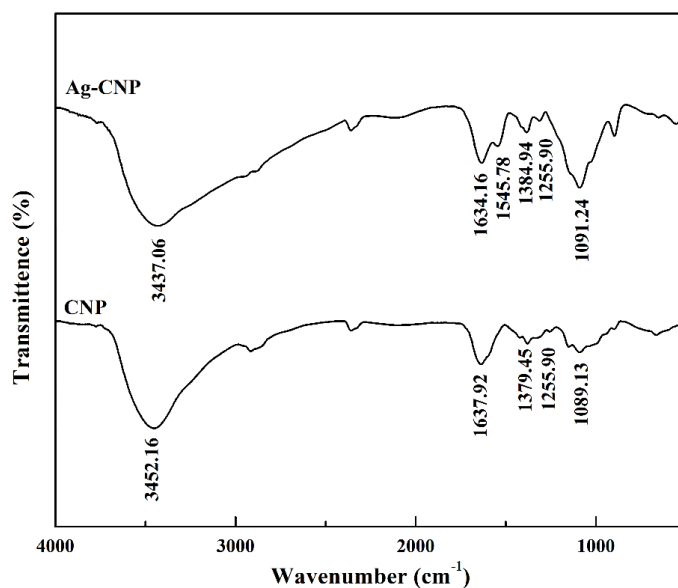
Figure 4.7 FTIR spectra of a) Ag-CNP and b) CNP

4.3.1.4 X-ray diffraction

Figure 4.8 shows the XRD spectra representing the crystallographic structure of chitosan, CNP, and Ag-CNP.
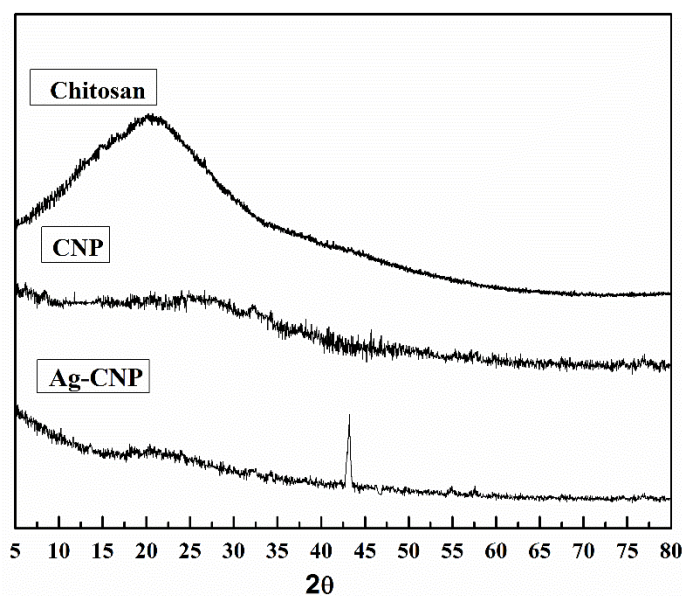
Figure 4.8 XRD pattern of chitosan, CNP, and Ag-CNP

The broad peak obtained at $2\theta = 21.8°$ depicts the semi-crystalline structure of chitosan with their crystal lattice constant α corresponding to 4.075. The CNPs

showed no diffraction pattern indicating the amorphous nature of the CNPs due to the dense network produced by the crosslinking of chitosan with TPP resulting in large disarray in the chain orientation (Tang *et al.* 2003). The XRD pattern for Ag-CNPs displayed a sharp peak at $2\theta = 44.3°$, which is due to the crystalline structure of Ag at (2 0 0) plane of the face-centered cubic crystal lattice (Ali *et al.* 2011).

4.3.2 Morphological study of hollow fiber membranes

4.3.2.1 Scanning electron microscopy

The asymmetric morphology of PPSU/CNP and PPSU/Ag-CNP HF membranes were examined using cross-sectional SEM images, presented in Figure 4.9. A spongy and porous sub-layer sandwiched between the finger-like structures extending from the inner and outer wall was observed due to the liquid-liquid demixing of polymer dope solution with the bore fluid and the non-solvent bath. Moreover, in the dry-wet spinning technique, the polymer dope solution undergoes coagulation within the air gap region and coagulation bath. Thus, the non-convective and delayed demixing takes place in the air gap region as the humid air comes in contact with the outer surface of the membranes, followed by a rapid phase inversion as the dope solution from the spinneret enters the coagulation bath. Hence the small air gap of 5 cm (Table 4.2) overthrows the delayed demixing and leads to the formation of extended finger-like structures (Pereira *et al.* 2016).

The addition of CNP and Ag-CNP to the dope solution improves the membrane morphology by the formation of elongated finger-like projection, thereby decreasing the thickness of porous sub-layer. This is because of faster demixing of the solvent from polymer rich phase and non-solvent from polymer lean phase caused by high affinity of NPs towards water (Dzinun *et al.* 2015). The migration of these NPs hence results in the formation of pore interconnectivity. However, the membranes showed wider spongy layer with shorter finger-like structure when the concentration of NPs raised from 0.15 wt. % to 0.3 wt. %. This is due to the delayed demixing occurring due to increase in viscosity which dominates the effect of hydrophilicity of NPs. The agglomeration of Ag-CNPs at higher concentration, i.e. at 0.3 wt. % was

also observed (Figure 4.10 a). The EDX spectrum verifies the retention of Ag-CNPs on membranes by the presence of an elemental peak corresponding to Ag (Figure 4.10 b).
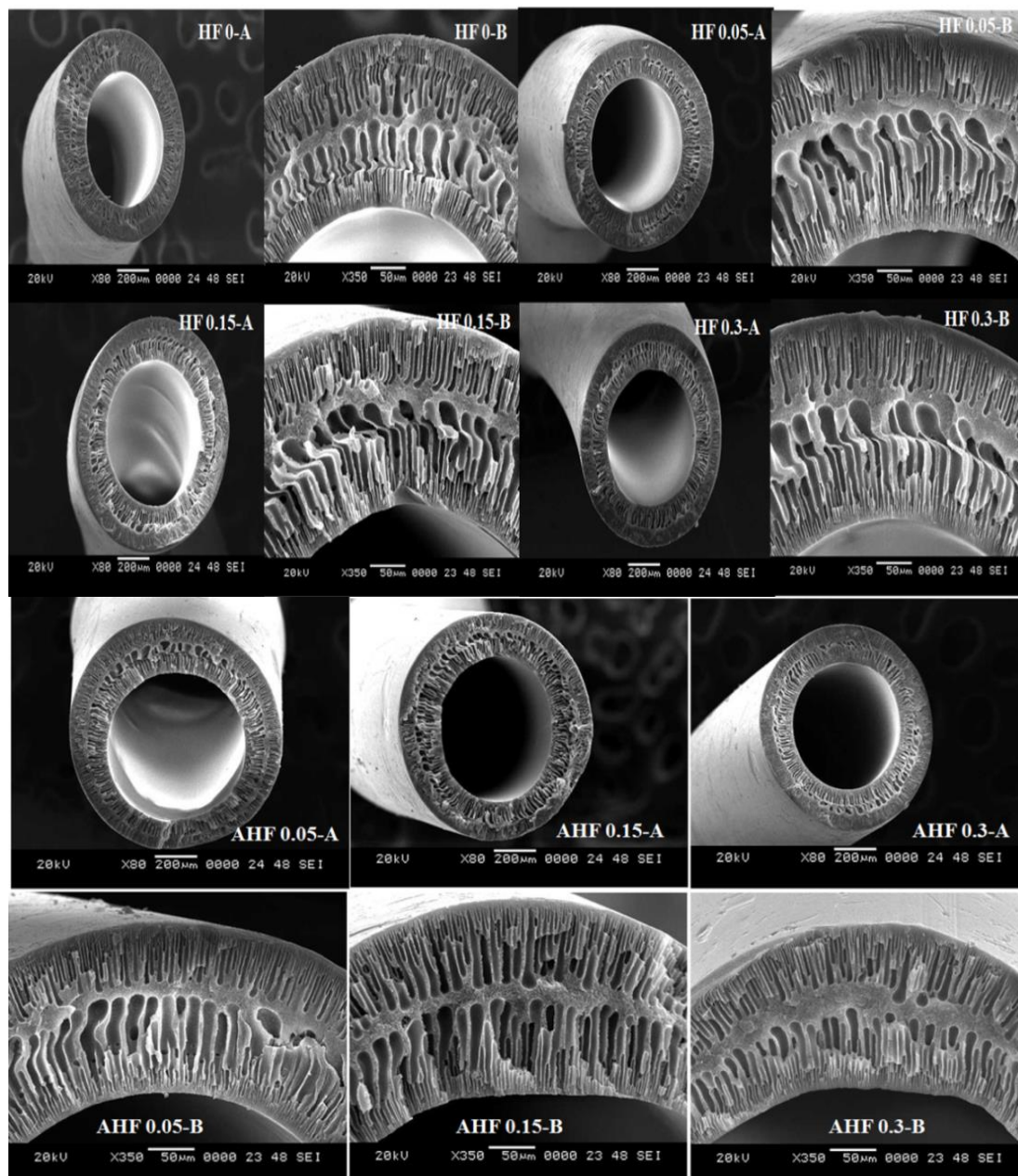
Figure 4.9 Cross-sectional images of HF membranes at A) ×80 magnification and B) ×350 magnification
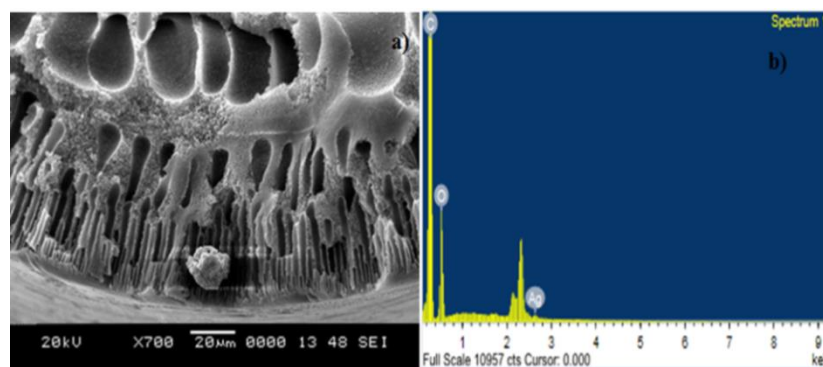
Figure 4.10 a) Cross-Sectional image with agglomeration and b) EDX spectrum of AHF 0.3

4.3.2.2 Atomic force microscopy

The surface topography and roughness of HF membranes were evaluated using AFM analysis. The 3D images of the HF membrane surface in Figure 4.11 revealed the peaks and valleys in the form of bright and dark regions, respectively. The presence of numerous peaks and valleys indicated the roughness of the surface.
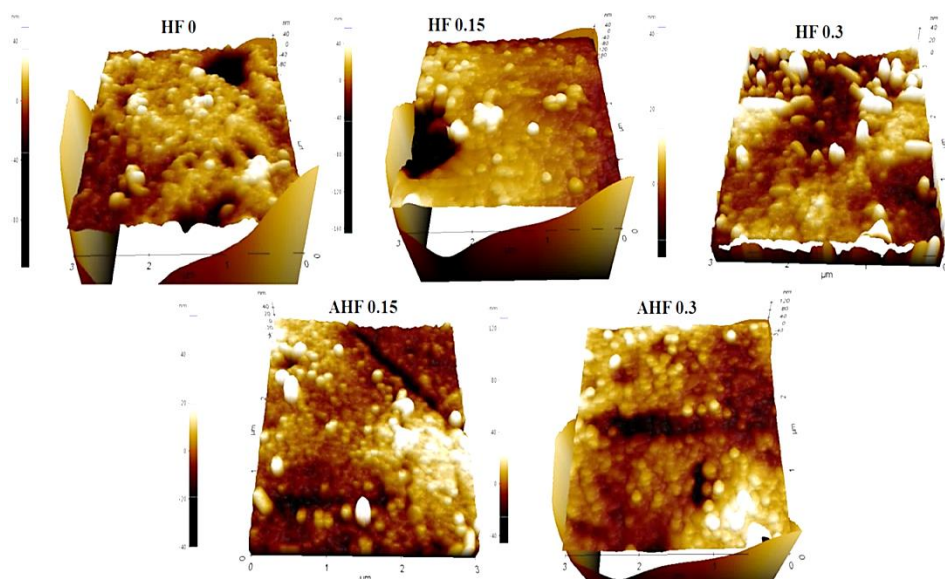
Figure 4.11 3D AFM images of HF membranes

The roughness parameters are calculated to verify the surface roughness (Table 4.3). It was observed that the roughness parameter of the membranes decreased by the incorporation of NPs such as CNPs and Ag-CNPs, where R_a decreased from

11.74 nm to 3.54 nm and 7.56 on the addition of 0.15 wt. % of CNP and Ag-CNP, respectively. The results obtained was in agreement with the literature, where the nanocomposite HF membrane showed lower surface roughness than its pristine form (Zhu *et al.* 2011). This is because the movement of the hydrophilic nanofillers towards the membrane surface during phase inversion leads to the filling the valleys on the membrane surfaces with the nanofillers to deliver to a smooth surface. However, a further increase in the concentration of NPs to 0.3 wt. % caused a slight increase in the R_a value as the NPs agglomerated at higher concentration. Moreover, the addition of CNPs showed lower roughness than Ag-CNP, which is due to the smaller size of CNP than Ag-CNP.

Table 4.3 Surface roughness parameters of membranes

Membrane code	Roughness parameter	
	R_a (nm)	R_q (nm)
HF 0	11.74	17.73
HF 0.15	3.54	4.45
HF 0.3	5.97	7.58
AHF 0.15	7.56	9.86
AHF 0.3	8.34	13.04

4.3.3 Membrane hydrophilicity

Membrane hydrophilicity is analyzed through the WCA measurement and water uptake capacity of membranes. The WCA measurement reflects the surface hydrophilicity of HF membranes. In general, smaller the WCA, higher is the hydrophilicity. The addition of hydrophilic NPs enhanced the hydrophilicity due to the decrease in interface energy as the NPs migrated to the surface of membranes during the phase inversion. The HF membranes showed decreased WCA with the increase in CNP and Ag-CNP loading as the number of hydrophilic sites on the membrane surface increase. The AHF 0.3 membrane with 0.3 % of Ag-CNP

composition showed the least contact angle of 50.52° (Figure 4.12). The possible explanation for the improvement of the membranes hydrophilicity on the incorporation of Ag-CNP could be due to the release of Ag^+ ions from Ag-CNPs in the aqueous phase by oxidation. The hydrated Ag^+ ions hence released can adsorb onto the surface of the NPs, in turn, contributing to the membrane hydrophilicity (Liu and Hurt 2010). Hence, higher hydrophilicity was observed for Ag-CNP loaded HF membranes than CNP loaded HF membranes, due to the combined effect of both hydrophilic chitosan and Ag^+ ion in Ag-CNP.
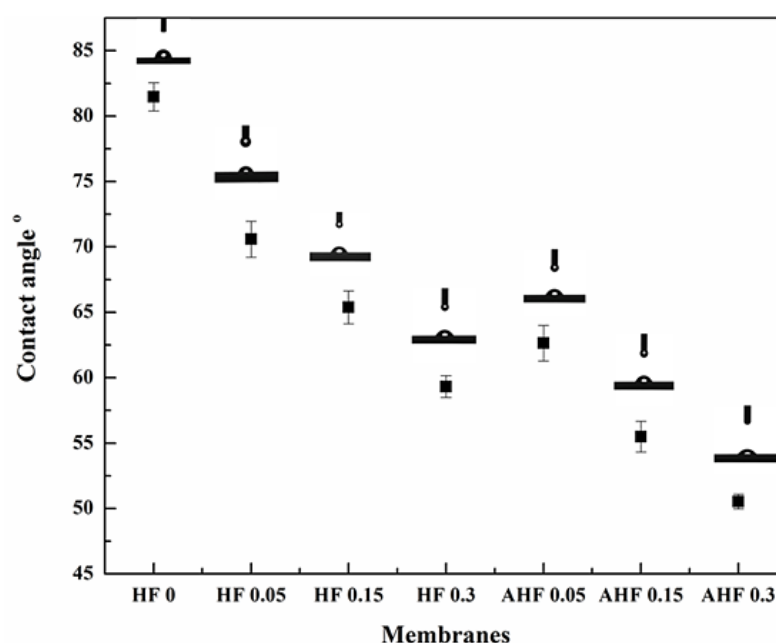
Figure 4.12 WCA of HF membranes

The membrane morphology and hydrophilic group present on the surface influence the water uptake capacity of the membrane (Table 4.4) (Kumar *et al.* 2014). The pristine HF membranes showed the water uptake capacity of 43.5 % and it increased on the incorporation of CNPs and Ag-CNPs into the membrane matrix. This is due to the rise in the number of hydrophilic groups, such as amine and hydroxyl groups on the membrane surface and due to increased pore interconnectivity of the membrane. The higher affinity of Ag-CNP to water caused by the combined effect of CNP and Ag attracted more water flow into the membrane, leading to higher water uptake capacity than the membranes containing CNPs.

Table 4.4 Water uptake, porosity, and mean pore radius of HF membranes

Membrane code	Water Uptake (%)	Porosity (%)	Mean pore radius (nm)	Viscosity (mPa.s)
HF 0	43.5	40.3	6.3	1563
HF 0.05	54.2	49.5	6.9	1624
HF 0.15	67.9	59.9	7.1	1863
HF 0.30	70.2	57.7	7.9	2008
AHF 0.05	57.76	54.6	8.3	1716
AHF 0.15	69.43	66.9	9.1	1932
AHF 0.30	74.12	63.4	9.2	2160

4.3.4 Membrane porosity and mean pore radius

The porosity and mean pore radius of the HF membranes containing CNPs and Ag-CNPs are shown in Table 4.4. The porosity and mean pore radius of the membranes increased by increasing the CNP and Ag-CNP concentration in the dope solution. This is due to the migration of NPs to the membrane surface during phase inversion which results in the formation of interconnected pores. The presence of pore former PEG-1000 in polymer dope solution caused an overall increase in the membrane porosity (Ma *et al.* 2011). However, the decline in membrane porosity was observed for HF 0.3 and AHF 0.3 as the agglomeration of NPs takes place at a higher concentration, which causes pore blockage (Dzinun *et al.* 2015). Moreover, higher porosity and mean pore radius were observed for HF membrane with Ag-CNPs than CNPs as an additive, due to the larger size of Ag-CNP than CNP.

4.3.5 Pure water flux

The permeability of the HF membranes was estimated by the time-dependent PWF as displayed in Figure 4.13. The HF membranes showed higher PWF than the pristine HF membrane as the addition of hydrophilic NPs to the membrane matrix

contributed to the rise in hydrophilicity and porosity of the HF membranes. A substantial rise in the PWF of HF membranes was observed with the increased CNP and Ag-CNP concentration, as the hydrophilic additives could draw water molecules within the membrane matrix and stimulate the movement of water across the membrane. The improved permeability of the Ag-CNP incorporated HF membranes are observed when compared to HF membranes with CNP as PWF of 96.84 $Lm^{-2}h^{-1}$ and 113.74 $Lm^{-2}h^{-1}$ was exhibited for HF 0.15 and AHF 0.15, respectively. This could be correlated with an increase in the hydrophilicity and pore size of the HF membranes which is a product of combined effect of silver ions and CNP in Ag-CNP. However, a decline in PWF was observed in addition of 0.3 wt. % of CNP and Ag-CNP, which may be due to the pore blockage by the agglomerated NPs.
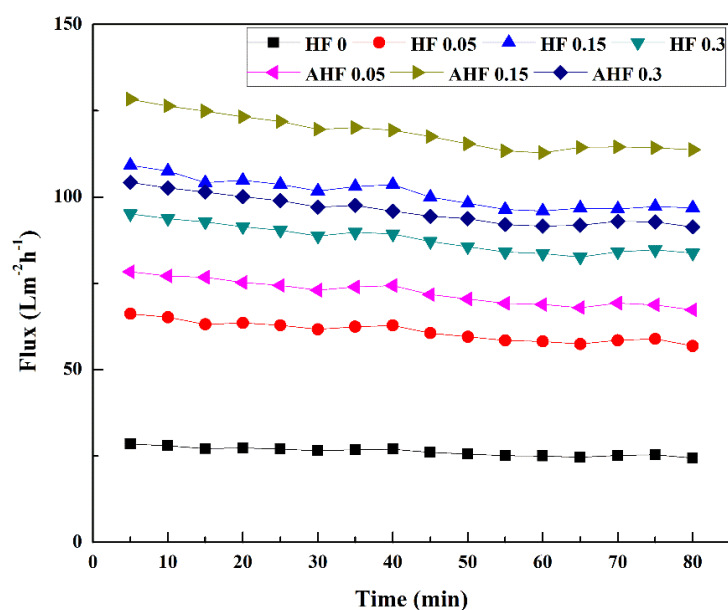
Figure 4.13 PWF for HF membranes at 0.2 MPa TMP

4.3.6 Antifouling study

The antifouling study was determined by measuring FRR and FDR of the HF membranes. Figure 4.14 displays a drop in the permeation flux for the HF membranes when pure water was substituted with the BSA solution. The pristine PPSU membrane demonstrated greater flux decline as acute fouling occurred due to the lower hydrophilic nature of PPSU polymer. However, the addition of CNPs and Ag-

CNPs to membrane matrix could reduce the decline in flux than pristine PPSU membrane due to its higher hydrophilicity. Hence, the nanocomposite HF membranes displayed smooth surface with enhanced permeability while mitigating the membrane fouling simultaneously (Martín *et al.* 2015).
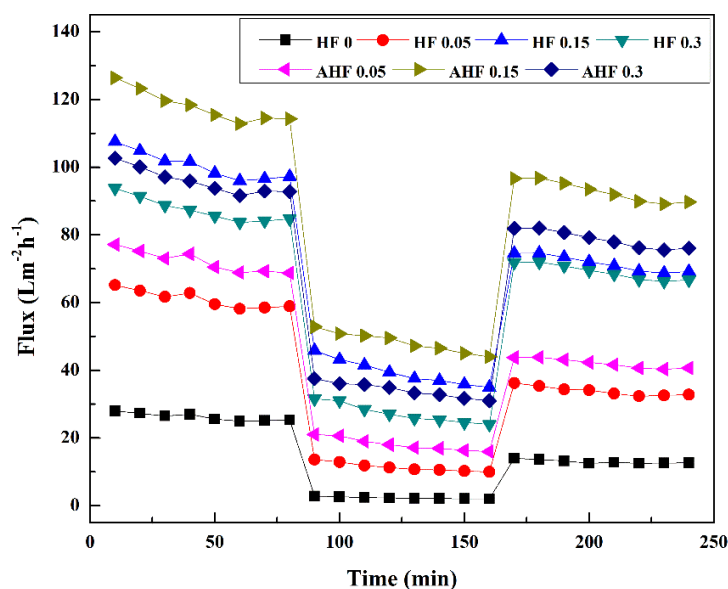
Figure 4.14 Flux vs. time for HF membranes before and after passing BSA at 0.2 MPa TMP
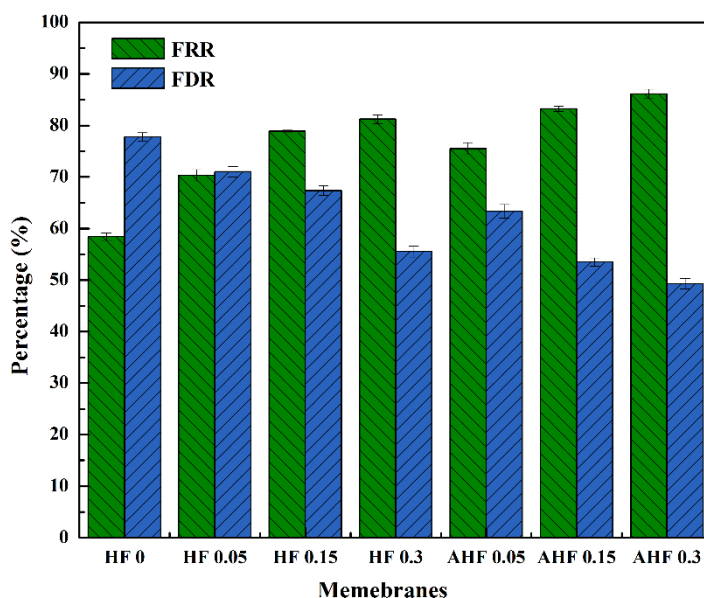
Figure 4.15 FDR and FRR of HF membranes

The FRR of HF membranes were calculated by conducting pure water permeation study for HF membranes before and after passing BSA solution as feed (Figure 4.15). The FRR of 81.21 % and 86.13 % were displayed by the membrane with 0.3 wt. % CNP and Ag-CNP, respectively. The superior FRR for the HF membranes signifies the ease of desorption of the adsorbed BSA molecules from the hydrophilic membrane surface with simple hydraulic washing. The incorporation of CNPs to the dope solution caused an increase in the FRR value as the surface hydrophilicity of membrane is increased by the hydrophilic functionality such as -OH and $-NH_2$ groups present in CNP. The hydrophilic surface of membranes hence creates a layer of water molecules as a shield to oppose the adhesion of hydrophobic protein molecules. Consequently, the weak interaction between the foulant and surface of HF membrane result in the better antifouling property. From the FRR values, it was also evident that the HF membranes with Ag-CNP showed superior antifouling performance, which may be ascribed to the combined effect of hydrophilicity of silver ions and CNPs.

4.3.7 Dye rejection study

Figure 4.16 represents the rejection of RB 5 and RO 16 by the HF membranes, where, nanocomposite HF showed higher rejection than the pristine membrane. This is because of the addition of CNPs and Ag-CNPs to HF imparted $-NH_3^+$ to the membrane surface which encourages the rejection of dye molecules due to the electrostatic interaction between positively charged chitosan and the anionic dye. The anionic dyes such as RB 5 and RO 16 dissociates in aqueous solution to give sulfonic acid groups that got adsorbed on the positively charged membranes (Figure 4.17). The rejection of dyes by the HF membranes, increased with the increase in CNP and Ag-CNP content, as the number of sites for adsorption increased on the surface of the membrane. It was also observed that Ag-CNP loaded HF membranes showed higher rejection than the CNP loaded HF membranes. This is because of the combined effect of silver ions and chitosan in the Ag-CNP.
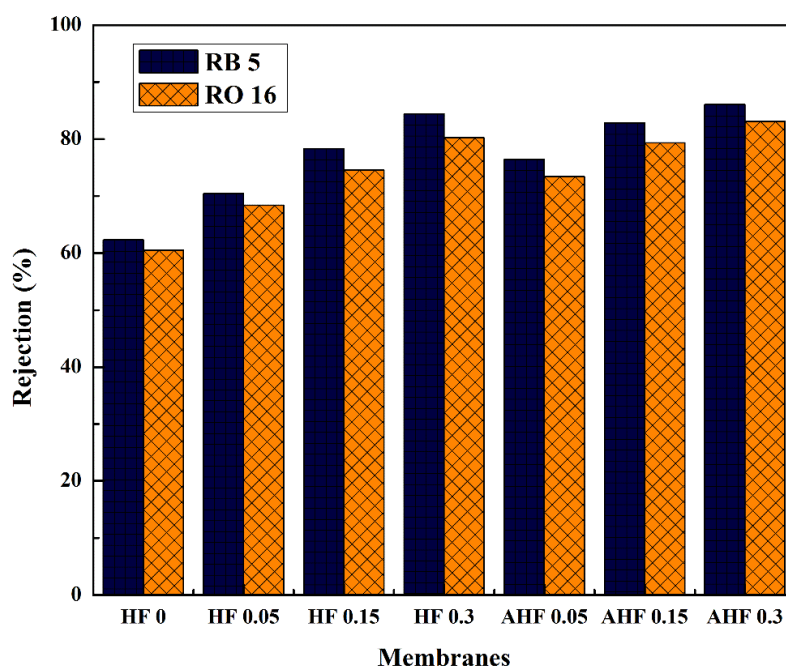
Figure 4.16 Dye rejection by HF membranes at 0.2 MPa TMP
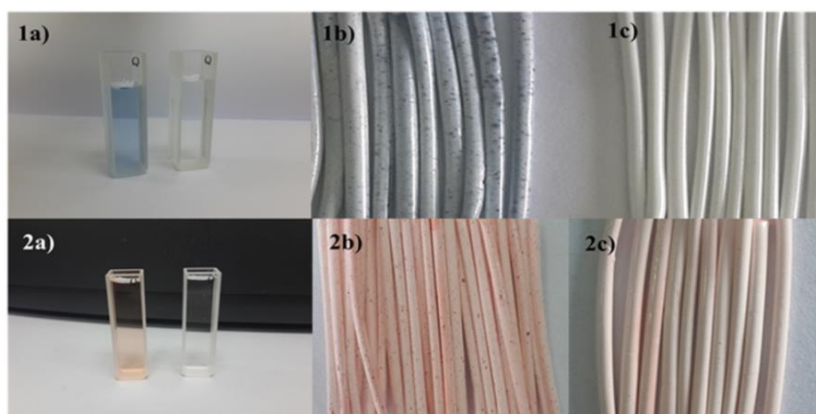
Figure 4.17 Digital image of feed and permeate for 1a) RB 5 and 2a) RO 16; AHF 0.3 and HF 0 dye rejection of 1b) RB 5, 2b) RO 16, and 1c) RB 5, 2c) RO 16, respectively.

4.3.8 Antibiofouling study

The antibiofouling property of the HF membranes was studied by a zone of inhibition and incubation method, where the model strains of bacteria such as *M. smegmatis, S. aureus,* and *E. coli* were used. The CNPs and Ag-CNPs dispersed in water were dropped over the microbial inoculum to investigate the zone of inhibition.

The zone of inhibition exhibited by CNP and Ag-CNP powder samples were significant in Gram-positive bacteria *S. aureus* and less significant for Gram-negative bacteria, *M. smegmatis* and *E. coli* (Table 4.5)*.* The antibacterial property of the CNP and Ag-CNP incorporated HF membranes were also tested by placing the HF membranes on the microbial culture and observed for the microbial growth around and underneath the membranes. The HF membranes could inhibit the growth of microbes underneath the membranes (Figure 4.18 b and c). However, unlike NPs, no zone of inhibition was displayed by the HF membranes (Figure 4.18 a).

Table 4.5 Zone of inhibition

	S. aureus	*M. smegmatis*	*E. coli*
Control	-	-	-
CNP (2μl)	16.6 mm	7 mm	4 mm
(1 μl)	15 mm	-	-
Ag-CNP (2μl)	18 mm	12.3 mm	9 mm
(1 μl)	15 mm	9.6 mm	5 mm
Streptomycin	38.6 mm	35.6 mm	36.33 mm

The inhibition of the growth of bacterial colonies by the CNPs is due to the antibacterial property possessed by chitosan, which is further enhanced by the reduction of particle size to the nanoscale. The higher surface area of CNPs resulted in the availability of a large number of free –NH$_2$ groups to interact with the bacterial cell wall. Moreover, the CNP being positively charged could inhibit bacterial cell growth due to the electrostatic interaction between the negatively charged bacterial cell wall and positively charged CNP. In Figure 4.18 (a), the larger zone of inhibition is observed for Ag-CNP due to the combined effect of Ag and CNP, i.e. the silver in Ag-CNP alters the cell wall permeability as negatively charged cell wall binds with silver ions (Hamouda and Baker 2000, Sondi and Salopek-Sondi 2004). Moreover, it is reported that the treatment with Ag can inactivate the cellular proteins (Feng *et al.*

2000) and alter DNA replication by bringing aberrations in the cytoplasmic contents, size, cell membrane, and outer cell wall of bacterial cells (Chernousova and Epple 2013).
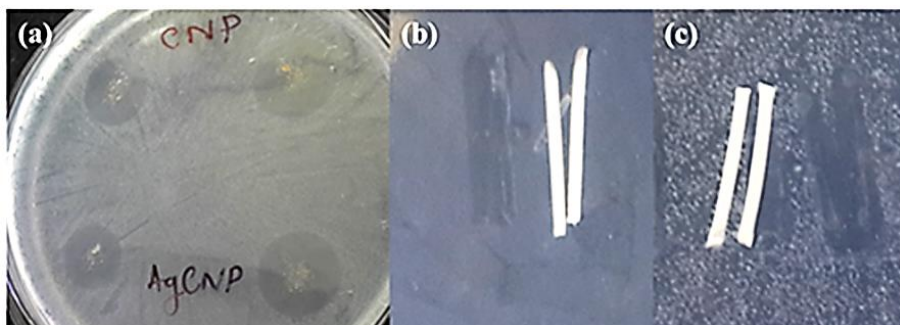
Figure 4.18 Zone of inhibition by a) CNP and Ag-CNP in *S. aureus,* b) HF 0.3 in *E. coli*, and c) AHF 0.3 in *M. smegmatis*

The HF membranes were tested for biofilm inhibition property by incubating it in microbial culture and subsequently placing it over the nutrient agar medium. Figure 4.19 shows the antibiofouling performance of the HF membranes, where the nanocomposite HF membranes showed no microbial growth, whereas pristine HF membranes supported the growth of few microbial colonies. The antibiofouling results showed that the nanocomposite HF membranes are capable of restricting microbial growth over them. Moreover, its antibacterial nature of the material has proven to be potent in inhibiting the growth of microorganisms on their surface.
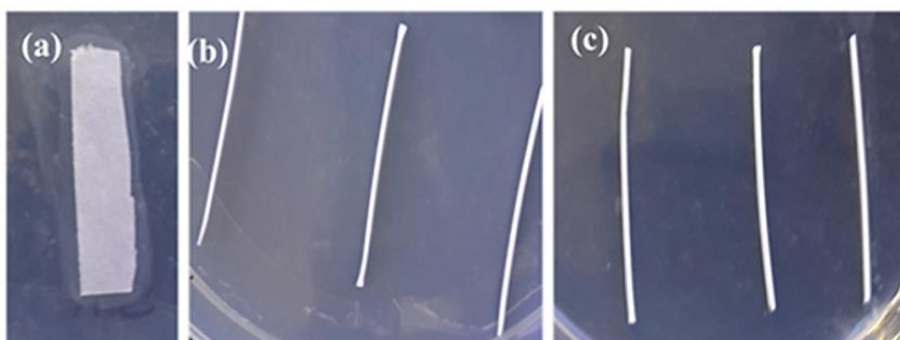
Figure 4.19 Antibiofouling study for a) Control (Whatman paper), b) AHF 0.3, and c) HF 0 dipped in *S. aureus*

4.4 CONCLUSIONS

The CNPs and Ag-CNPs were prepared by gel ionotropic method and used as an additive in the PPSU HF membranes. The HF membranes with different composition of CNP or Ag-CNP were fabricated and their effects on membranes were studied for membrane filtration, hydrophilicity, and antibiofouling property. The addition of CNPs and Ag-CNPs could effectively improve the permeability and hydrophilicity of the HF membrane, with PWF of 96.84 $Lm^{-2}h^{-1}$ and 113.74 $Lm^{-2}h^{-1}$ on the addition of 0.15 wt. % of CNPs and Ag-CNPs, respectively. Moreover, the HF membranes with Ag-CNPs as additive showed better results than the CNPs because of the combined effect of both silver ions and CNPs. The addition of 0.3 wt. % Ag-CNP resulted in effective dye rejection of 89.01 % and 86.04 % for RB 5 and RO 16, respectively. The antibiofouling experiment illustrated that the Ag-CNP containing HF membranes had remarkable antibiofouling property. Moreover, the antibacterial test indicated that the AHF 0.3 showed a good antibacterial activity against *S. aureus, M. smegmatis,* and *E. coli*. Hence, the modified membrane has proven to be potent material to inhibit the growth of microorganisms on their surface. These novel membranes could be applied for the treatment of the industrial dye effluents with high flux and antibiofouling property.

CHAPTER 5

FABRICATION OF NOVEL HOLLOW FIBER MEMBRANES CONTAINING MOLYBDENUM TRIOXIDE NANOPARTICLES FOR THE EFFICIENT REMOVAL OF DYE AND HEAVY METAL

Abstract: *The Molybdenum trioxide (MoO$_3$) NPs were prepared by a hydrothermal technique and further used in the fabrication of HF membranes. The effect of the different concentration of MoO$_3$ NPs as nanofillers on the performance of PPSU HF membranes was investigated in this chapter. The ability of HF membrane in the removal of the methylene blue (MB) dye and rejection of heavy metal ion was studied. The HF membrane displayed adsorption and photodegradation of MB dye under ultraviolet radiation. The membranes also showed rejection to toxic heavy metal ions such as lead and cadmium ions.*

5.1 INTRODUCTION

As mentioned in chapter 4, the HF membranes can be tailored by incorporation of nanoadditives in order to attain desired membrane morphology and properties (Chen *et al.* 2015). Incorporation of inorganic NPs into the polymer dope solution to prepare HF membranes has been an interesting and simple approach that improves the separation properties, having advantages of both NPs and organic membranes. Transition metal oxides NPs like oxides of iron, manganese, aluminum, and titanium have been widely used for the water treatment applications such as heavy metal and dye removal (Chen *et al.* 2002, Cao *et al.* 2012, Pereira *et al.* 2015, Bashir *et al.* 2016). Moreover, sorption of heavy metal ions by the transition metal oxide is reported to be an effective method for the profound removal of toxic heavy metals, so as to fulfill increasingly strict rules.

MoO$_3$ NPs has become an attractive material due to its photocatalytic and adsorptive property. The photocatalytic degradation of the dye presented by the MoO$_3$ NPs is due to the large band gap of 2.8-3.0 eV, which lie in the visible light region (Julien *et al.* 1995, Allogho and Ashrit 2012). Its wide range of application such as oxidative catalyst, gas sensors, photochromic coatings, and as additives in paint make it well-known (Sunu *et al.* 2004, Paraguay-Delgado *et al.* 2007, Cheng *et al.* 2009). MoO$_3$ can act as a source of molybdenum which is one of the essential trace elements of primary importance to biological systems as it is non-toxic and cost-effective (Hussain *et al.* 2005).

MoO$_3$ NPs has been synthesized by various methods including hydrothermal

(Phuruangrat *et al.* 2012, Zeng *et al.* 2013), solvothermal (Michailovski *et al.* 2005, Kim *et al.* 2010), sol-gel (Ganguly and George 2007) method. Lou and Zeng (2002) reported the synthesis of the MoO$_3$ NPs by hydrothermal method, wherein acidification of ammonium heptamolybdate tetrahydrate (AHM) (NH4)$_6$Mo$_7$O$_{24}$.4H$_2$O at 140-200 °C resulted in nanoribbons or nanorods of orthorhombic MoO$_3$ (α-MoO$_3$), whose crystal structure was controlled by nitrate salts of Na, K, Mg and Al.

Chen *et al.* (2010) studied the photocatalytic degradation of MB dye using MoO$_3$ nanobelts prepared using hydrothermal techniques. The nanobelts obtained were of 200-300 nm in width and several tens of micrometers in length. The ZP result shows that the nanobelts are negatively charged, which serve as the site for the adsorption of positively charged MB dye. The photocatalytic studies demonstrated the activity and stability of MoO$_3$ nanobelts during the degradation of dye. They also demonstrated the self-sensitized photocatalytic degradation of MB dye under visible light (Figure 5.1).
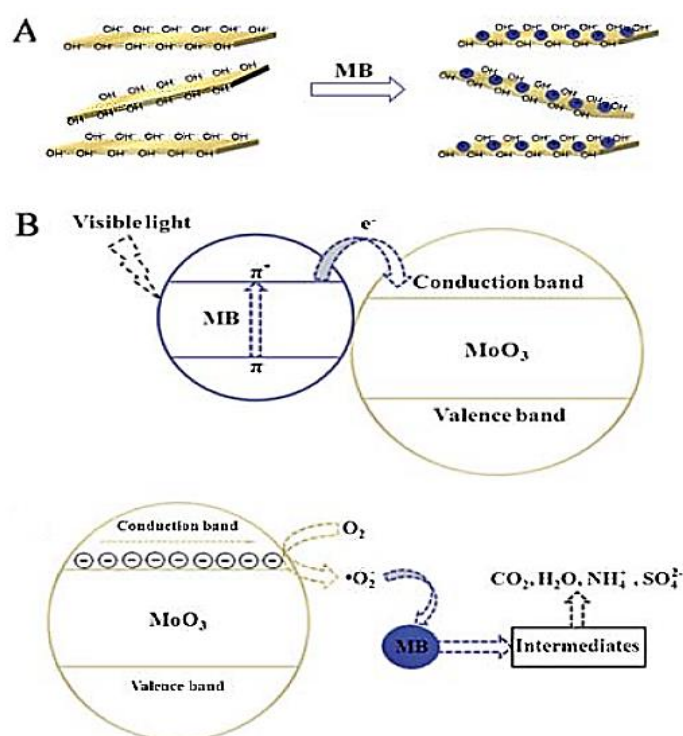
Figure 5.1 Representation of MB dye (A) adsorption and (B) degradation (Chen *et al.* 2010)

Zollfrank *et al.* (2012) modified the surface of PU hollow tube and Ti rods using MoO$_3$ particles, so as to develop the materials with antimicrobial activity. The modified material was tested for antimicrobial activity against *S. aureus and Pseudomonas aeruginosa*. They observed that the material could inhibit the microbial growth 6 h after contracting with the pathogens. The antimicrobial activity displayed is as the acidic nature of the surface weakens the growth of the bacterial cell without harming host cell.

Reports on the synthesis of nanostructured MoO$_3$ using AHM and conc. HNO$_3$ was presented by Chithambararaj *et al.* (2013). The MoO$_3$ NPs showed good photocatalytic degradation of MB dye under visible light radiation, wherein the rate of degradation improved with an increase in the intensity of light, operating temperature and the amount of NPs, while it decreased with an increase in the initial concentration of dye.

Manivel *et al.* (2015) prepared the MoO$_3$ NPs in three distinct methods which include thermal, microwave, and sonochemical techniques. The physiochemical properties were analyzed by SEM, TEM, XRD and surface analyzer. The MoO$_3$ NPs prepared by different methods are hexagonal rod-shaped and displayed azo dye degradation in aqueous condition. It was found that MoO$_3$ NPs synthesized by sonochemical method displayed the superior degradation by total removal of dye in 20 minutes, due to the greater surface area of NPs with a large number of active sites for effective dye interaction.

Fakhri and Nejad (2016) synthesized MoO$_3$ NPs by hydrothermal method and studied its photocatalytic property under visible light, ultraviolet (UV) light and sunlight for ketamine degradation. A high efficiency for the photocatalytic reaction was observed as the MoO$_3$ NPs showed good optical property with a band gap of 2.78 eV. The MoO$_3$ NPs also showed antifungal activity against *Candida albicans* and *Aspergillus niger*, and high resistance to Gram-negative and positive bacteria.

Molybdenum materials are also reported to possess great importance for the sorption of heavy metal (Chehbouni and Apblett 2005, Perkins *et al.* 2014). Kapnisti *et al.* (2016) demonstrated the extensive and selective effects of the AHM derived MoO$_3$ (Scheme 5.1) for removal of lead and uranium ions. The chemisorption of Pb

and U resulted in insoluble molybdates such as wulfenite ($PbMoO_4$) and umohoite ($UMoO_6.2H_2O$), respectively. They also showed the ability to remove the radionuclides such as Ba, Cs, Eu with good stability during desorption.

$$(NH_4)_6Mo_7O_{24} \cdot H_2O \xrightarrow{\text{300 °C}} 7MoO_3 + 6NH_3 + 7H_2O$$
$$\text{(s)} \qquad\qquad\qquad \text{(s)} \quad\ \text{(g)} \qquad \text{(g)}$$
$$\text{(AHM)}$$
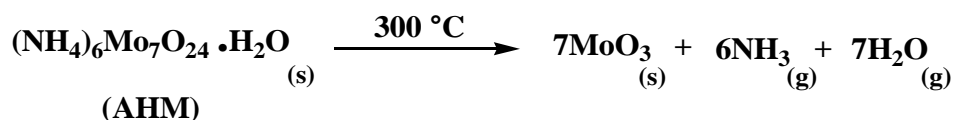
Scheme 5.1 Synthesis of MoO_3 from AHM (Kapnisti *et al.* 2016)

Shafaei *et al.* (2017) developed the CA-based composite by embedding MoO_3 and studied the antibacterial activity of the composite against *S. aureus*, *E. coli,* and *Pseudomonas aeruginosa*. The composite membranes exhibited good antibacterial property due to the high intrinsic proton release rate and a large surface area. The composite showed lasting durability for the MoO_3 particles in the polymer with improved tensile strength.

Therefore, MoO_3 NPs can be chosen as a potential candidate to improve the membrane performance. However, the extensive usage of NPs for wastewater treatment can lead to the inclusion of these NPs into water bodies. Hence, the polymer membranes embedded with the NPs for water treatment is a sensible approach. Moreover, the study on MoO_3 NPs as an additive in membrane fabrication is not reported among transition metals. In this chapter, HF membranes were fabricated by incorporation of MoO_3 NPs to the dope solution. The effect of the MoO_3 NPs on the HF membrane performance such as hydrophilicity, permeability, and antibiofouling properties was studied. The membranes were also tested for the rejection of Pb^{2+} and Cd^{2+} ions, and degradation of MB dye.

5.2. EXPERIMENTAL

5.2.1 Materials

PPSU (Radel R-5000) (average Mw ~ 50,000 g mol−1) was supplied by Solvay Advanced Polymer (Belgium). AHM, Cadmium nitrate tetrahydrate, lead nitrate, MB (Mw~373.9 g/mol), BSA, PEG-1000, were procured from Sigma−Aldrich and used without further purification. NMP was provided by QREC, Malaysia. HNO_3 (69 %)

was purchased from Merck. The nutrient agar used to carry out the antibiofouling testing was bought from Sisco Research Laboratories (SRL) Pvt. Ltd. India.

5.2.2 Synthesis of MoO₃ nanoparticles

The MoO₃ NPs were prepared by hydrothermal method (Chithambararaj *et al.* 2013) (Scheme 5.2). 0.2 M AHM was prepared by dissolving 2.3 g of AHM in 10 mL of DI water and further stirred at RT for 15 min. The AHM solution was acidified by slowly adding 5 mL of 1.5 M HNO₃. It was then transferred to a Teflon-lined stainless steel autoclave, where the reaction mixture was kept for 12 h at 120 °C. The precipitate hence obtained were centrifuged, washed with DI water and then dried in at 70 °C for 6 h.
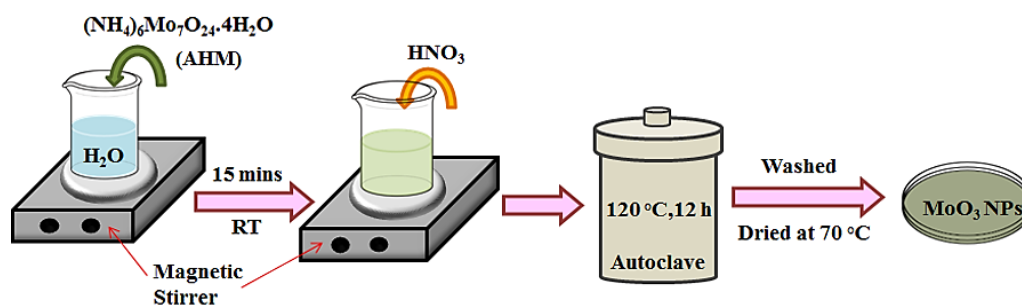
Scheme 5.2 Synthesis of MoO₃ NPs

5.2.3 Preparation of hollow fiber membranes

Series of HF membranes were fabricated by the incorporation of different concentration MoO₃ NPs into PPSU polymer dope solution as mentioned in Table 5.1. The dope solution was prepared by dispersing MoO₃ NPs in NMP with probe sonicator at 40 kHz for 15 min, with subsequent addition of PPSU and PEG-1000 (Yuliwati *et al.* 2011). The Basic viscometer (Model: EW-98965-40, COLE PARMER, 20-2 million centipoises) was used to record the viscosity of the prepared polymer dope solutions. The HF membranes were then fabricated by dry-wet spinning technique as mention in Chapter 4, Section 4.2.4.2, with the spinning parameters exercised as given in Table 5.2.

Table 5.1 Compositions of dope solution

Membrane code	PPSU (wt. %)	MoO$_3$ NPs (wt. %)	PEG-1000 (wt. %)	NMP (wt. %)
M 0	20	0	5	75
M 1	20	1	5	74.0
M 2	20	2	5	73.0
M 3	20	3	5	72.0

Table 5.2 HF spinning parameters

Dope composition	PPSU/PEG/ MoO$_3$NP/NMP PPSU/PEG/NMP (For Neat)
DER	3 mL/min
Bore fluid	Distilled water
BER	1.5 mL/min
Air gap	5 cm
Spinneret Dimension (o.d/i.d)	1.15/0.55 (mm)

5.2.4 Characterization of MoO$_3$ nanoparticles

The XRD, FTIR, ZP, and particle size of the prepared MoO$_3$ NPs were analyzed as mentioned in Chapter 4, Section 4.2.3. The SEM analysis was performed to demonstrate the morphology and size of the MoO$_3$ NPs. Here, the powder MoO$_3$ NPs sample was placed on the carbon tape and sputtered with gold to obtain the SEM images taken by JEOL JSM-6380L at 20 kV.

5.2.5 Membrane characterization

The morphology of the HF membranes was studied by taking the SEM images of the cross-section. The membrane wettability and hydrophilicity were measured by

WCA and water uptake capacity of the HF membranes as mentioned in Chapter 4, Section 4.2.5. The Guerout–Elford–Ferry equation was used to find out the mean pore radius using porosity of the HF membrane employing filtration velocity method as mentioned in equation (2.3). The permeability of membranes was conducted by calculating the PWF using equation (4.1). The membrane fouling performance is analyzed as mentioned in Chapter 4, Section 4.2.7.1 where FRR and FDR are calculated using the equation (2.5), and (4.2), respectively. The membranes were also examined for antibiofouling studied as mentioned in Section 4.7.2.3, in Chapter 4.

5.2.6 Heavy metal rejection study

The removal of toxic heavy metal ions from the feed solution was performed by filtration experiment. The aqueous solutions of heavy metal ions were prepared by dissolving 1 g of heavy metal salts such as lead nitrate and cadmium nitrate in 1000 mL of water to obtain a concentration of 1000 ppm. The heavy metal ion solution was taken in the feed tank were filtered individually through the membrane. Permeate collected was examined for heavy metal ion rejection by measuring the concentration of metal ions in the feed and permeate using AAS and the percentage rejection was calculated using equation (2.8).

5.2.7 Dye removal study

The MB dye removal efficiency of HF membranes was conducted at both dark and UV light radiation. The HF membranes were cut into pieces and were put in aqueous dye solutions of 10 ppm concentration. The solutions were agitated constantly at 200 rpm in an orbital shaker (ORBITEK LT) for 12 h under UV (11 W Philips), and dark conditions (Chithambararaj *et al.* 2013). The small portion of the solution was collected and the concentration of dye is detected by measuring the absorbance at 665 nm using UV-Vis spectrophotometer (SPECORD S 600). The degree of dye removal was then calculated using the equation (2.8).

5.3 RESULTS AND DISCUSSIONS

5.3.1 Characterization of MoO₃ nanoparticles

5.3.1.1 Hydrodynamic size and zeta potential

The hydrodynamic diameter and surface charge of MoO_3 NPs dispersed in aqueous media was measured using particle size and ZP analyzer. The ZP of MoO_3 NPs was found to be -62.2 mV at neutral pH (Figure 5.2 (a)). The negative ZP for MoO_3 NPs is due to the presence of $-OH$ adsorbed on the surface of MoO_3 NPs giving it a negative surface charge (Chen *et al.* 2010). Large ZP encourages the repulsion between the like-charged particles in the suspension, hence resulting in fewer agglomerations and greater stability of MoO_3 NPs. Figure 5.2 (b) shows the broad range of size distribution of MoO_3 NPs with the mean diameter value of 266.0 ±86.7 nm. The particle size obtained by this method is expected to be higher than that of the actual size due to the formation of hydration sphere over the MoO_3 NPs when in contact with water.
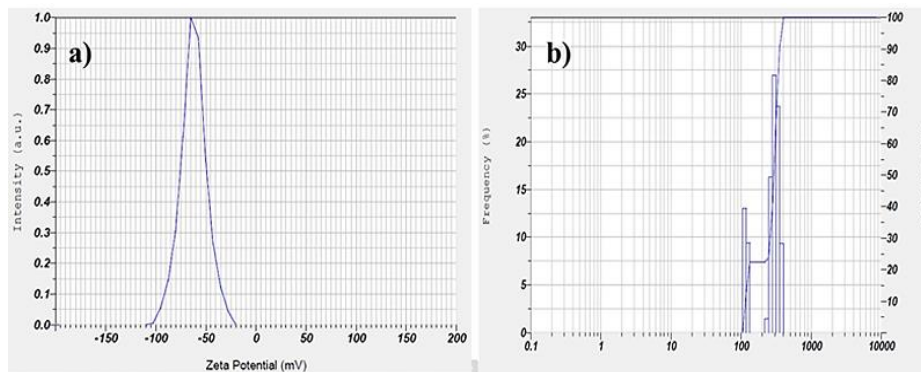
Figure 5.2 (a) ZP and (b) Particle size of MoO_3 NPs

5.3.1.2 Scanning electron microscopy and X-Ray diffraction spectroscopy

The SEM image shows the morphology of MoO_3 NPs taken at 1 μm scale (Figure 5.3 (a)). The SEM image of MoO_3 NPs displayed the rod-shaped particles with a wide range of particle size, which is in correlation with the results obtained from particle size analyzer. The EDX of MoO_3 NPs confirmed the purity and elemental composition of MoO_3 NPs (Figure 5.3 (b)).
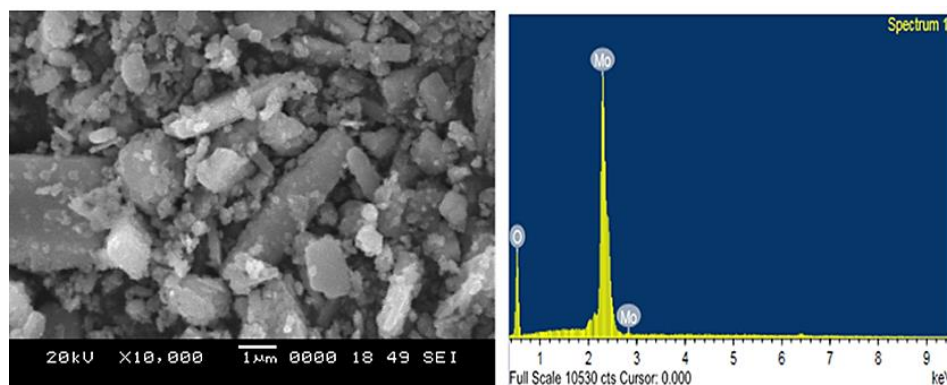
Figure 5.3 (a) SEM image and (b) EDX spectrum of MoO_3 NPs

Powder XRD was carried out to study the crystallinity of the synthesized the MoO_3 NPs, wherein the Figure 5.4 shows the peaks corresponding to the orthorhombic phase of α-MoO_3 NPs. The peak at 2θ of 12.6° indicates the presence of the orthorhombic crystal symmetry of the plane (020). Further, the appearance of the peak corresponding to planes (110), (040), (021), (111), and (060) reveal the orthorhombic phase.
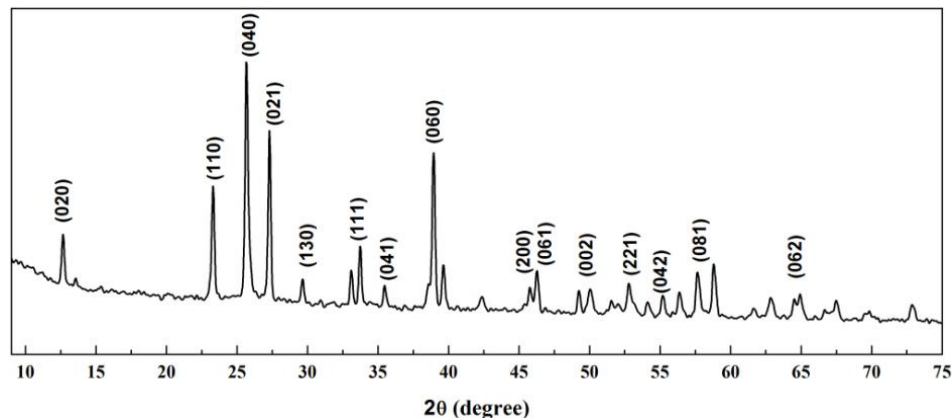
Figure 5.4 XRD spectrum of MoO_3 NPs

5.3.1.3 Fourier transform infrared analysis

Figure 5.5 shows the FTIR spectrum of MoO_3 NP scanned in the range of 4000–400 cm^{-1}. The presence of major absorption bands at 571 cm^{-1}, 865 cm^{-1}, 988 cm^{-1}, and 1629 cm^{-1} confirms the formation of MoO_3 NPs (Nazri and Julien 1992, Chen *et al.* 2010).
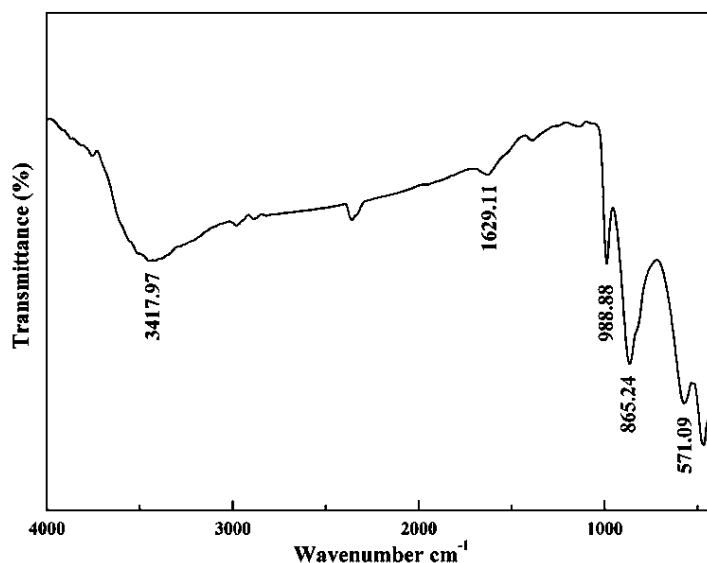
Figure 5.5 FTIR spectrum of MoO$_3$ NPs

The bending vibration of the Mo-O-Mo, where each O^{2-} ion is shared by three Mo^{6+} ions was displayed by the presence of a band at 571 cm^{-1}. The absorption band at 865 cm^{-1} and 988 cm^{-1} is ascribed to the Mo-O-Mo vibration of Mo^{6+} and terminal Mo=O stretching vibration mode, respectively (Dong and Dunn 1998). A broad band at 3417 cm^{-1} was spotted due to −OH stretching vibration associated with water adsorbed on MoO$_3$ NPs. The bending vibration of OH group of water adsorbed in the MoO$_3$ NP was displayed by a weak peak at 1629 cm^{-1}.

5.3.2 Morphological study

5.3.2.1 Scanning electron microscopy

The cross-sectional images of HF membranes fabricated by incorporation of MoO$_3$ NPs are shown in Figure 5.6. The HF membranes showed an asymmetric structure with spongy sublayer sandwiched between the finger-like projections extending from inner and outer surface during phase inversion (Xu and Qusay 2004). The incorporation of MoO$_3$ NPs caused the formation of more elongated finger-like projection with thinner spongy layer when compared to that of pristine HF membranes. The viscosity of the dope solution as found to increase with an increase in the concentration of MoO$_3$ NPs (Table 5.4). This is because the greater affinity of MoO$_3$ NPs towards water increases the diffusion velocity of non-solvent during phase

inversion. However, the addition of 3 wt. % of MoO_3 NPs to the dope solution resulted in a wider spongy layer with shorter finger-like structures as the effect of viscosity overrules the increase in diffusion velocity offered by the MoO_3 NPs. The viscosity of the dope solution affects the rheological property during liquid-liquid demixing, were the decrease in mass transfer rate prevents the formation of elongated finger-like projection (Dzinun *et al.* 2015). The retention of MoO_3 NPs in HF membranes was verified by the EDX spectra, were elemental peaks for Mo is observed (Figure 5.7).
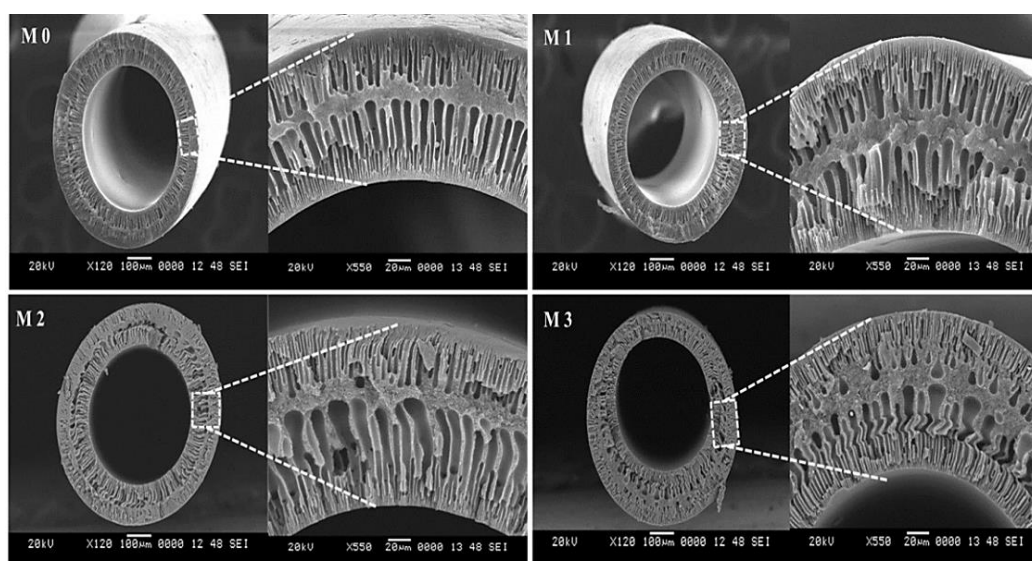
Figure 5.6 SEM cross-sectional images of M 0, M 1, M 2, and M 3
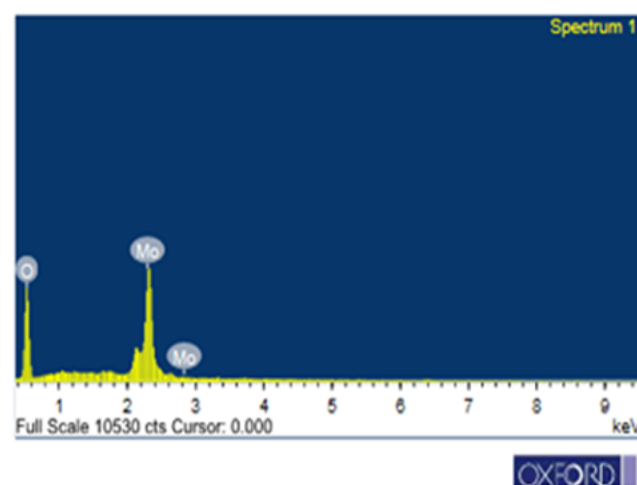
Figure 5.7 EDX spectrum of M 2

5.3.2.2 Atomic force microscopy

The surface topography of HF membrane was studied using AFM. The 3D scan images of M 0, M 2, M 3 is shown in Figure 5.8, where bright and dark region displays the peaks and valleys on the membrane surface. The roughness parameters were also calculated wherein the roughness parameters for HF membrane increased with the rise in addition of MoO_3 NPs (Table 5.3). This might be due to the increased pore size formed with higher content of MoO_3 NPs in the polymer matrix. The agglomeration of MoO_3 NPs at higher concentrations was also responsible for the hike in surface roughness as nodules or lumps were formed on the surface of HF membranes.
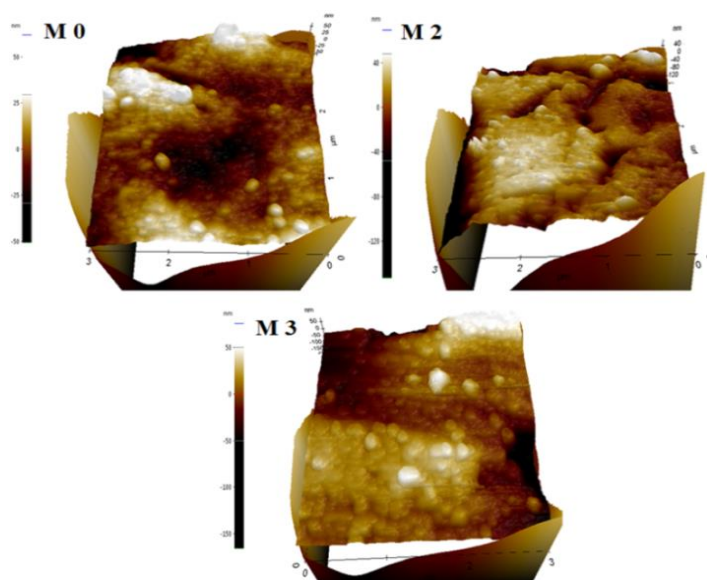
Figure 5.8 3D AFM images of HF membranes

Table 5.3 Surface roughness parameters of membranes.

Membrane code	Roughness Parameter	
	R_a (nm)	R_q (nm)
M 0	11.74	17.73
M 2	17.88	24.45
M 3	24.6	28.2

5.3.3 Hydrophilicity

The hydrophilicity of membrane surface is a crucial factor which influences the membrane performance such as permeability and antifouling nature. The surface hydrophilicity is normally analyzed by WCA and wettability. Figure 5.9 demonstrates the trend of the WCA with the addition of MoO_3 NPs, where the WCA declined with increase in concentration MoO_3 NPs. This is due to the migration of hydrophilic MoO_3 NPs towards the membrane surface during the phase inversion. Hence, the interaction of water with the membranes increased, thereby enhancing the surface hydrophilicity of membrane. However, there is an increase in WCA observed for M 3 is due to the agglomeration of MoO_3 NPs at higher concentration.
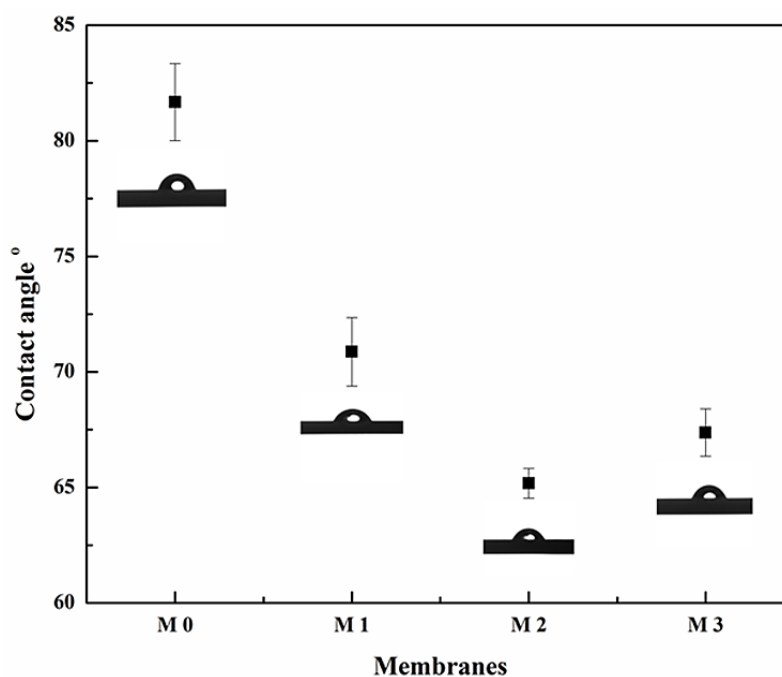
Figure 5.9 WCA of the HF membranes

The membrane hydrophilicity can be further evaluated by calculating the water uptake capacity (Table 5.4). The water uptake capacity for the HF membrane increased with the incorporation of MoO_3 NPs in the dope solution. This is because of the higher affinity of MoO_3 NPs towards the water. The oxygen moieties present in the MoO_3 NPs contribute to its hydrophilic property, which in turn enhances the affinity of HF membrane towards the water. However, there is a slight decline in

water uptake observed when MoO_3 NPs concentration increased from 2 wt. % to 3 wt. %, which is due to the pore blockage caused by agglomeration of MoO_3 NPs.

Table 5.4 Swelling, porosity, and mean pore radius of HF membranes

Membrane code	Water uptake capacity (%)	Porosity (%)	Mean pore radius (nm)	Viscosity (mPa.s)
M 0	40.4	39.5	6.1	1563
M 1	52.9	46.2	9.8	2208
M 2	66.9	55.5	12.1	2420
M 3	65.3	53.5	11.0	2763

5.3.4 Porosity and mean pore radius

The porosity and pore size of the HF membrane increased with the inclusion of MoO_3 NPs (Table 5.4). The increase in porosity is due to the formation of the interconnected pore as the MoO_3 NPs migrated to the surface during phase inversion membranes. Moreover, the presence of higher amount of MoO_3 NPs would attract more water flow into the membrane, leading to higher porosity (Dzinun *et al.* 2015). The seepage of pore former, i.e. PEG-1000 out of the dope solution during the demixing, contributed to the overall porosity of HF membrane. However, the addition of 3 wt. % of MoO_3 NPs decreased the porosity due to agglomeration of MoO_3 NPs. Also, increased viscosity caused the delayed demixing which leads to decrease in the pore interconnectivity (Sengur *et al.* 2015).

5.3.5 Pure water flux

Figure 5.10 displays the PWF values of the HF membranes carried out at 0.2 MPa TMP. It can be observed that the PWF of HF membranes increased from 23 $Lm^{-2}h^{-1}$ to 89 $Lm^{-2}h^{-1}$ on the addition of 2 wt. % of MoO_3 NPs to the polymer dope. The addition of MoO_3 NPs increased the surface hydrophilicity of membranes due to the migration of NPs to the membrane surface. The increased PWF is the product of combined effect of large pore size, enhanced surface hydrophilicity, and porosity.

However, the PWF declined on increase in the concentration of MoO_3 NPs from 2 wt. % to 3 wt. %, as the membrane hydrophilicity and pore size decreased. This is because of the high viscosity of dope solution which leads to the formation of spongy sub-layer with shorter interconnected pores as a result of slow demixing. Moreover, the clogging of the pore in membrane due to agglomeration of MoO_3 NPs also contributed to the lower PWF.
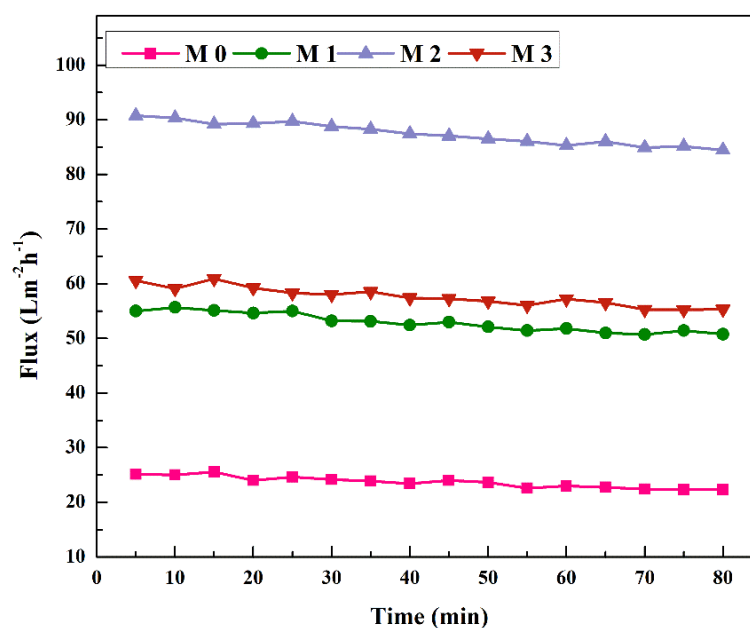
Figure 5.10 PWF of the HF membranes at 0.2 MPa TMP

5.3.6 Antifouling and antibiofouling study

The antifouling nature of the HF membranes was evaluated by passing the BSA solution, a model foulant through the membranes at 0.2 MPa TMP. The HF membranes showed a sudden decline in the flux when BSA is taken as feed solution (Figure 5.11). The decline in PWF during BSA ultrafiltration may be attributed to the adsorption of BSA on the membrane surface and pores. The flux of the pure water was again estimated after subjecting the HF membranes to hydraulic washing. Comparison of the prepared nanocomposite membranes with selected nanocomposite membranes reported in the literature is given in Table 5.5.
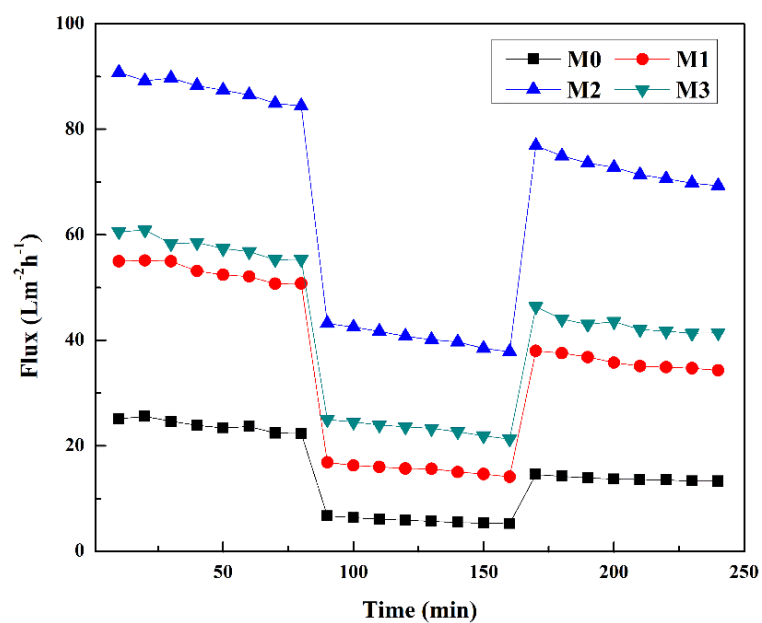
Figure 5.11 Flux vs. time graph for HF membranes before and after passing BSA at
0.2 MPa TMP
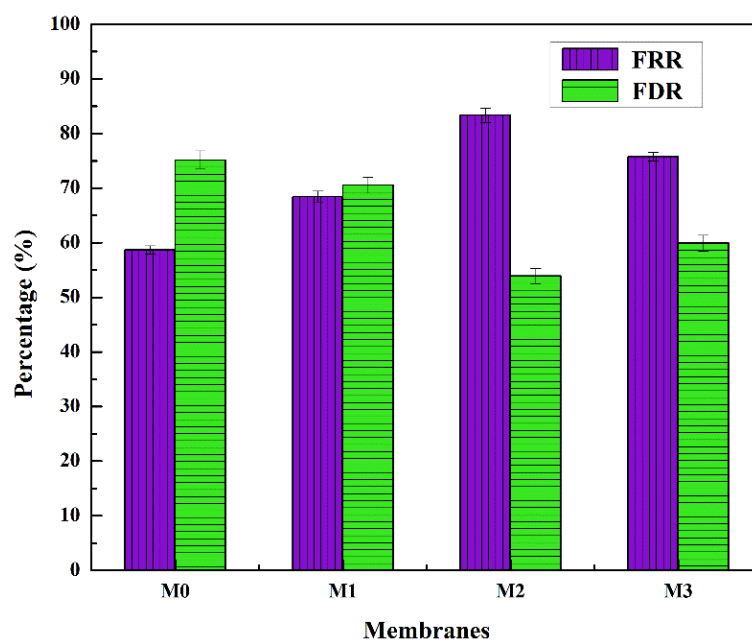
Figure 5.12 FRR and FDR of HF membranes

Table 5.5 Comparison of selected nanocomposite HF membrane performance with the prepared membrane

Nanoparticles	Operational pressure (MPa)	Flux $(Lm^{-2}h^{-1})$	FRR (%)	References
APTES-TiO$_2$	0.1	~55	61.54	(Razmjou *et al.* 2012)
PVP-g-MMT	0.1	74.64	81.09	(Wang *et al.* 2012)
PANI	0.2	~57	~68	(Kajekar *et al.* 2015)
Carboxylated Fe$_2$O$_3$	0.25	124.00	91.2	(Hebbar *et al.* 2017)
MoO$_3$	0.2	89.71	83.34	Present Study

The antifouling ability and membrane reusability of HF membranes were also evaluated by calculating the FDR and FRR (Figure 5.12). The HF membranes displayed a decrease in FDR and increase in FRR on the addition of MoO$_3$ NPs, where M 2 showed the highest FRR of 83.34 %. MoO$_3$ NPs present on the membrane surface leads to the formation of hydration layer that weakened the adsorption of BSA on the membrane surface. This improves the antifouling nature of the HF membrane. Moreover, the negative charge developed on the membrane surface by the incorporation of MoO$_3$ NPs inhibits the adhering of negatively charge BSA on its surface due to electrostatic repulsion. Therefore, the removal of loosely adhered BSA molecules from the membrane surface could be done by simple hydraulic cleaning. The high FRR and low FDR value indicate the improved antifouling behavior for nanocomposite HF membranes. However, there is a decline in FRR displayed by M 3 which is due to the increased fouling taking place at rougher surface formed by the agglomeration MoO$_3$ NPs on the membrane surface.

The antibiofouling study was conducted against *M. smegmatis*, *S. aureus* and *E. Coli* by incubation method. Figure 5.13 shows the images of the control (Whatman filter paper) and membranes incubated in agar medium after dipping it into the microbial culture. The HF membrane M 2 showed inhibition to the bacterial growth

while the control supported the development of the microbial colony. The antibiofouling nature of these HF membranes was due to the antibacterial activity of the MoO_3 NPs. The bacterial cell fatality was due to the raised reactive oxygen levels when in contact with the NPs (Akhavan and Ghaderi 2010, Krishnamoorthy *et al.* 2012) along with the electrostatic repulsive force between negatively charged HF membranes and bacterial surface.
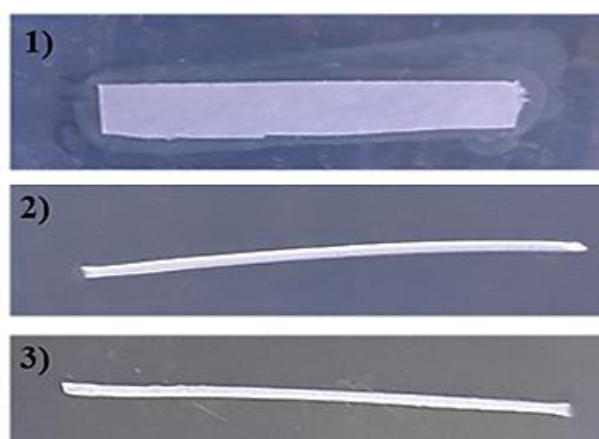
Figure 5.13 (1) Colonies of *S. aureus* around the control strip, while (2) M 2 and (3) M 3 is membrane strip with no colonies

5.3.7 Heavy metal rejection study

The rejection of the heavy metal ions such as Pb^{2+} and Cd^{2+} were shown in the Figure 5.14. The rejection of metal ions was observed due to adsorption of positively charged heavy metal ions on negatively charged membranes. That is, the negatively charged MoO_3 NPs imparted a negative charge onto the surface of HF membranes which function as active sites for the adsorption of Pb^{2+} and Cd^{2+} ions. The HF membranes with 3 wt. % of MoO_3 NPs showed lower rejection for heavy metal ions than with 2 wt. %. This is due to the aggregation of NPs at a higher concentration that causes lower surface area for adsorption. The Pb^{2+} exhibited higher removal capacity due to the strong electrostatic interaction with the MoO_3 NPs (Kapnisti *et al.* 2016). Although, the larger size of Pb^{2+} to that of Cd^{2+} ions caused the higher rejection of Pb^{2+} ions.
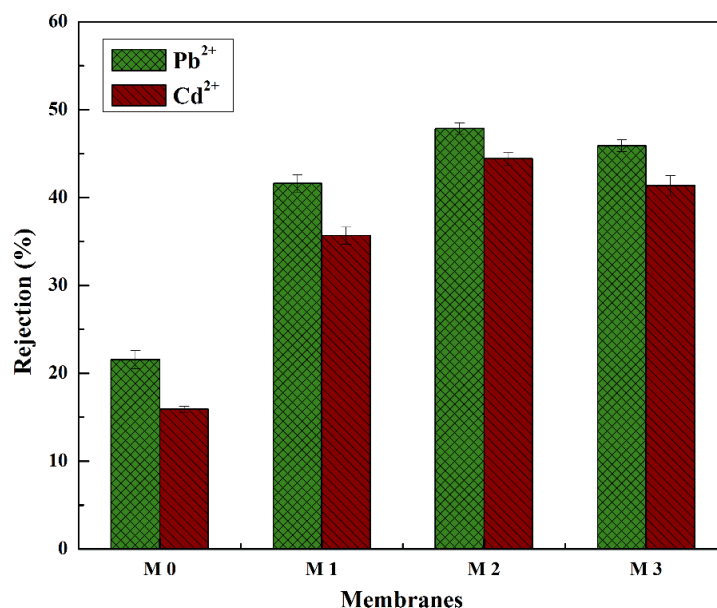
Figure 5.14 Heavy metal ion rejection by HF membranes at 0.2 MPa TMP

5.3.8 Dye removal study

The HF membranes, M 0 and M 2, were studied for dye removal by placing the HF membrane samples in MB solution under the dark condition and UV radiation. It was observed that M 2 membranes could remove the MB dye from the solution as the color of membranes transformed from white to blue when dipped in MB solution (Figure 5.15). This is due to the adsorption of dye onto the negatively charged HF membranes. Since MB is a cationic dye, it gets adsorbed onto the surface of HF membrane surface containing negatively charged MoO_3 NPs due to electrostatic interactions (Li *et al.* 2011).

The MB solution was also tested by UV-Vis spectroscopy, where the MB dye solution presented a strong absorption band at 665 nm for monomeric (0–0 band) and a weak band at 605 nm for dimeric (0–1 band) forms of MB (Figure 5.16 (1)). The percentage of dye removal by M 0 and M 2 is shown in Figure 5.16 (2). It was observed that the dye removal capability for the M 2 improved when tested under UV radiation as the amount of dye removed increased from 34.8 % (under dark) to 66.3 % (UV light radiation). This is because of the photodegradation of MB dye by MoO_3 NPs in the UV light (Chithambararaj *et al.* 2013). That is, the electrons (e⁻) from

valence band gets excited to the conduction band by the incidence of the photon, thereby creating the holes (h^+) in the valence band. The water or hydroxide ions formed reacts with the holes created in the valence band to produce free radicals like hydroxyl radicals (•OH), and hydroperoxyl radicals (•O_2H). This hydroxyl radical (•OH), can, in turn, causes degradation of MB (Zhuo *et al.* 2008).
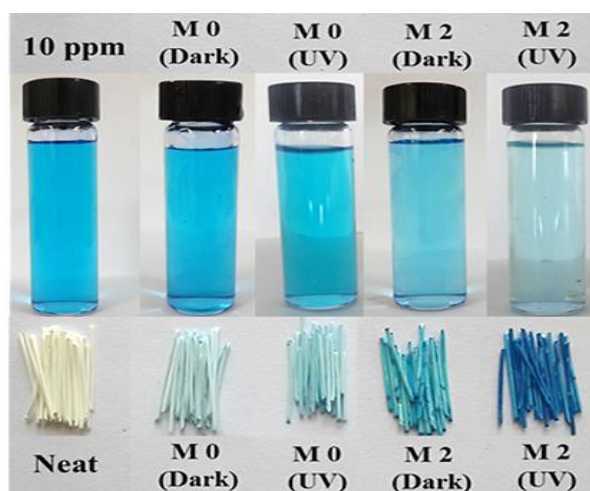
Figure 5.15 Digital images of MB solution and HF membranes after dye removal
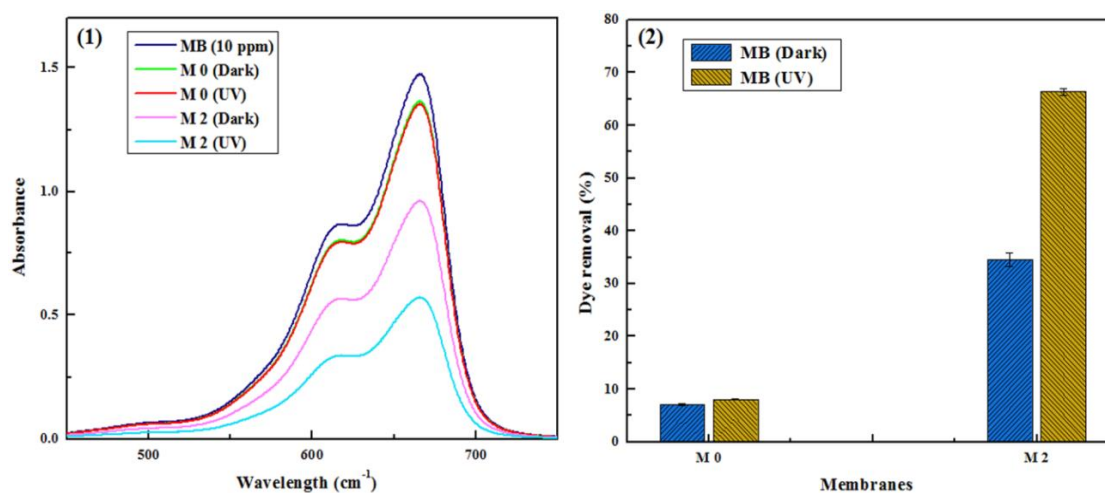
Figure 5.16 (1) UV absorbance spectra of MB dye solution, and (2) MB removal by M 0 and M 2

5.4. CONCLUSIONS

A series of HF membranes were fabricated by dry-wet spinning by varying the concentration of MoO_3 NPs. The results revealed that modified membranes displayed

enhanced hydrophilicity and permeability. The permeation experiments showed that PWF of the HF membrane with MoO_3 NPs was better than pristine membranes with the highest flux of 89 $Lm^{-2}h^{-1}$. The HF membranes with 2 wt. % of MoO_3 NPs, i.e. M 2 exhibited improved antifouling property with FRR and FDR value of 83.34 % and 53.92 %, respectively. The antibiofouling experiment showed the resistance of M 2 membranes to the bacterial strains such as *M. smegmatis*, *S. aureus,* and *E. coli.* The HF membrane demonstrated the capacity to adsorb the heavy metal ion such as Pb^{2+} and Cd^{2+}, thereby showing the rejection towards the Pb^{2+} and Cd^{2+} ions. Furthermore, M 2 showed rejection of MB dye, with 66.3 % dye removal by M 2 on exposure to UV light radiation. Thus MoO_3 NPs is an effective additive for removal of the cationic dye from wastewater.

CHAPTER 6

IMPACT OF HYDROPHILIC ADDITIVES ON THE THIN FILM COMPOSITE POLYAMIDE NANOFILTRATION MEMBRANES FOR DESALINATION

Abstract: *This chapter deals with the fabrication of PA TFC membranes by the interfacial polymerization of MPD and TMC. The effect of hydrophilic additives containing amine group such as glycine and L-glutamine in the diamine solution during the interfacial polymerization was investigated. The performances of hydrophilic TFC NF membranes were tested for desalination.*

6.1 INTRODUCTION

The NF is an effective method for desalination and wastewater treatment, with low operational cost and energy (Van der Bruggen and Vandecasteele 2003). The aromatic PA membranes are highly sought as TFC membrane, which is extensively used for RO and NF applications. TFC membranes generally contain an active layer formed by interfacial polymerization on the porous support. TFC PA membranes are generally prepared by the interfacial polymerization of a diamine and an acid chloride on a membrane support (Ghosh *et al.* 2008, Lau *et al.* 2012).
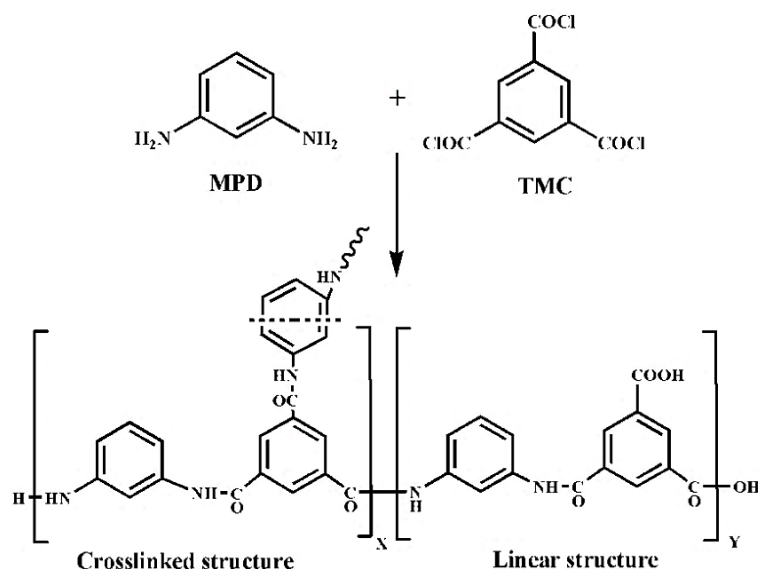
Scheme 6.1 Interfacial polymerization reaction of MPD and TMC (Jin and Su 2009)

The MPD and TMC are two monomers which are widely used for the formation of PA layer by interfacial polymerization (Scheme 6.1). The MPD in aqueous phase when comes in contact with TMC in the organic phase, leads to the formation of polyamide structure at the organic phase due to the high and low solubility of MPD in an organic medium and TMC in an aqueous medium, respectively (Soroush *et al.*

2012). The structure of PA is affected by factors such as reaction temperature, monomer composition, monomer concentration, reaction time, and curing conditions. Hence varying any of these factors can result in the formation of TFC membranes of desired characteristics.

Development of the hydrophilic aromatic PA TFC membranes with good flux has been a major concern over the past decades. Attempts are made to modify TFC PA layer or the porous substrate to produce a membrane with improved performance in terms of permeability, rejection, and better anti-fouling nature. The extent of fouling is influenced by the membrane features like smoothness, charge, and hydrophilicity of membrane surface (Vrijenhoek *et al.* 2001). Also, the pore size and hydrophilicity of the porous substrate can influence the membrane performance. Therefore, tailoring TFC membranes based on the required characteristics for water purification can be brought about by changing the monomer composition or concentration, usage of the hydrophilic substrate, by the functionalization of PA layer, and by incorporation of hydrophilic additives.

Roh *et al.* (2006) prepared TFC membrane by interfacial polymerization of MPD and TMC. The studies were conducted on the effect of variation in concentration of MPD and TMC from 0.1–1.0 wt. % in PA layer formation. They observed increased PA layer thickness with the increase in TMC, with higher surface hydrophilicity. But the increase in MPD caused decreased hydrophilicity with a small increase in thickness. However, the prominent decrease in water flux was observed for an increase in MPD concentration, while the increase in the concentration of TMC showed lower effect.

Xie *et al.* (2012) optimized the concentration of MPD within 1.5–2.0 wt. % to obtain supreme performing membranes having 0.4 ± 0.1 % of NaCl passage and a permeate flux of $42 \pm 3 \, \text{Lm}^{-2}\text{h}^{-1}$. They also prepared TFC PA membranes from S-BAPS, as diamine substitute. The membrane showed NaCl passage of 12 % and a permeate flux of $55 \, \text{Lm}^{-2}\text{h}^{-1}$. However, the highly cross-linked network formed from the aromatic compounds of MPD and TMC caused poor hydrophilicity which in turn resulted in a considerably inferior water flux for NF membranes.

An *et al.* (2013) synthesized N-aminoethyl piperazine propane sulfonate (AEPPS) zwitterion and designed a series of TFC membranes with AEPPS by interfacial polymerization of PIP with TMC (Scheme 6.2). It was found that the water flux improved on increasing the concentration of zwitterionic additive whereas rejection of K_2SO_4 remained around 97 %.
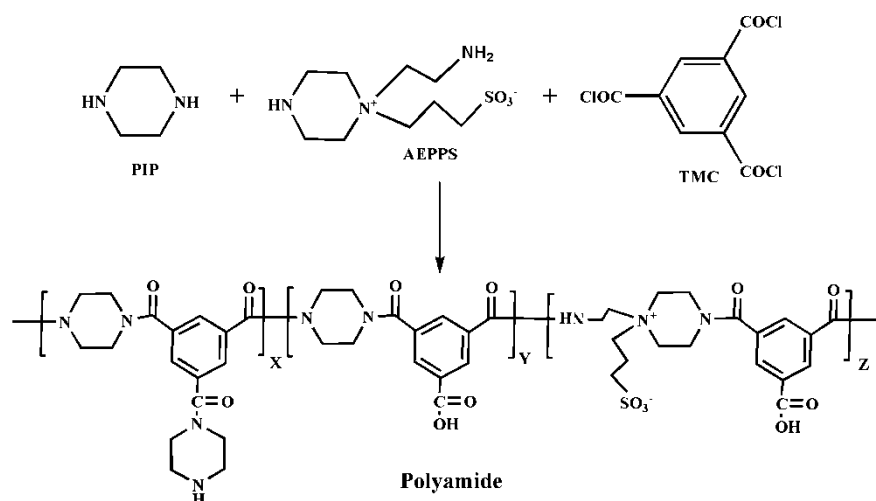
Scheme 6.2 Interfacial polymerization of PIP and AEPPS with TMC (An *et al.* 2013)

Zaho *et al.* (2013) used hydrophilic additives (Figure 6.1) to fabricate high-flux RO membranes. Moreover, these hydrophilic additives used could also bring about charge repulsion for high salt rejection. The prepared membranes displayed a flux of 52.6 gal.ft.$^{-2}$day^{-1} and a salt rejection of 98.8 % or greater.
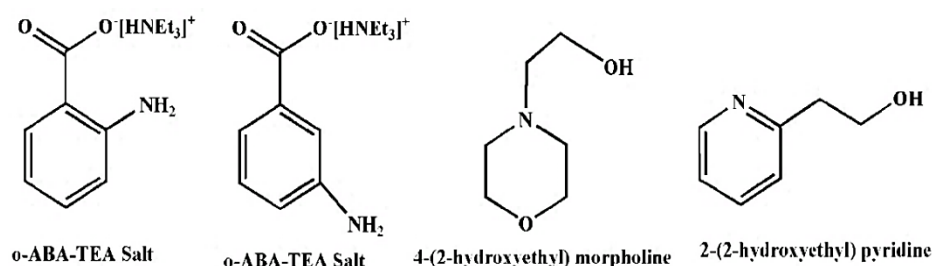
Figure 6.1 Structures of hydrophilic additives used during polymerization (Zhao *et al.* 2013)

Hermans *et al.* (2014) developed PA membranes via interfacial polymerization in a single step. The amine solution was added to the coagulation bath that caused the phase inversion and impregnation of support layer with amine simultaneously. Then

the TMC was used for the PA layer formation. However, the single step technique showed the same effect as the conventional method. They also studied the effect of additives like triethylamine (TEA) and sodium dodecyl sulfate. They observed that the addition of TEA accelerated the rate of PA formation as the HCl produced while the interfacial polymerization is neutralized by the base (Scheme 6.3) (Hermans *et al.* 2015). The membrane performance improved with an increase in the curing temperature due to crosslinking, wherein the increase in the reaction time showed no effect.
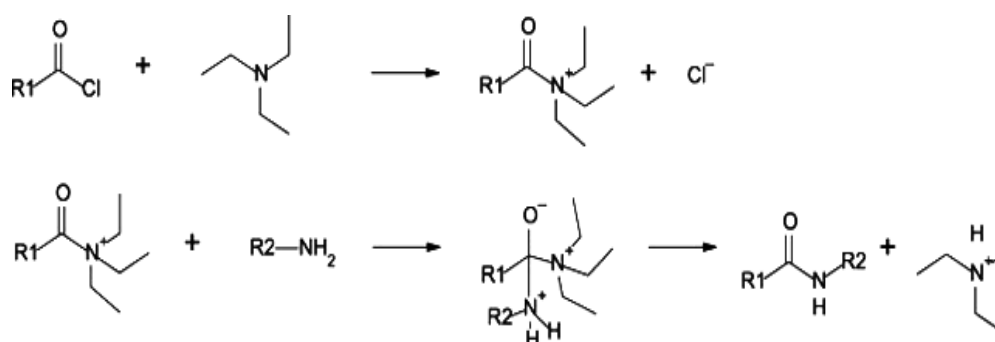
Scheme 6.3 PA formation with TEA as a catalyst (Hermans *et al.* 2015).

Pandian *et al.* (2015) studied the efficacy of some additives such as tryptophan (TRP), adenosine monophosphate (AMP), and phenethylamine (PEA) on the surface of PA membrane for improved salt rejection through the density functional theory. It was found that the carboxylate and phosphate groups contributed to better binding of metal ions (Figure 6.2). PA surface bound to TRP and AMP showed efficient salt removal. Similarly, various hydrophilic additives are used both in thin films and substrate to improve the membrane characteristics like permeability, rejection, and its anti-fouling nature (Hirose and Ikeda 1996, Yung *et al.* 2010, Kim *et al.* 2013). Later, Weng *et al.* (2015) studied the effect of polymerization of diamines such as PIP, N-aminoethyl piperazine, or N-aminoethyl piperazine propane sulfonate with TMC to develop TFC membranes. The membrane developed with zwitterionic diamine showed better hydrophilicity and antifouling property with the flux of 80.3 $Lm^{-2}h^{-1}$.
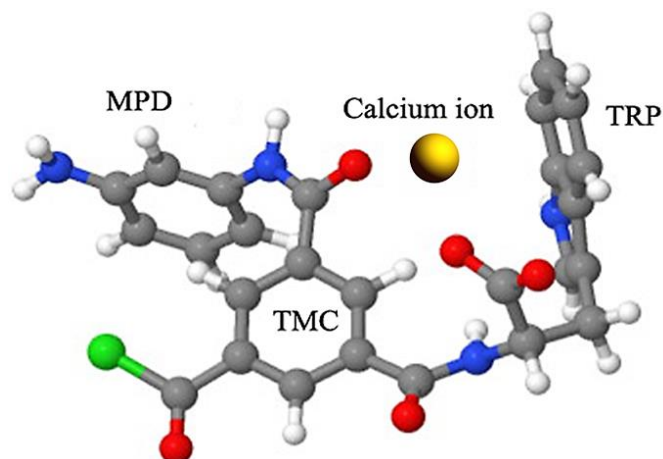
Figure 6.2 Optimized geometry of the TRP bound polyamide surface interacting with the Ca^{2+} ion (Pandian *et al.* 2015)

Khorshidi *et al.* (2017) studied the influence of monohydric and polyhydric alcohols on the permeability and salt rejection property of TFC PA membranes. It was studied that the water flux could be appreciably improved by the use of alcohols at low molar volume, i.e. ethanol and ethylene glycol, whereas it decreased after certain concentration. This is due to the complex interaction between the hydrophilic hydroxyl groups and hydrophobic aliphatic carbon chain present in the large alcohol molecules.

In this chapter, amino acids such as glycine and L-glutamine are selected and used as hydrophilic additives to improve the performance of TFC membranes. The TFC membranes were fabricated by the interfacial polymerization of MPD and TMC on PSF/sPPSU (85:15) substrate. The hydrophilic additives were introduced into the MPD solution to bring about the increased affinity of membrane surface for water and charge repulsion during salt rejection. The effects of concentrations of the hydrophilic additives on TFC membrane performance were also evaluated. The additives are expected to demonstrate a good salt separation capability with high PWF.

6.2 EXPERIMENTAL

6.2.1 Materials

PSF (Mw ~ 35,000) and MPD were procured from Sigma-Aldrich, India. PPSU (Radel R-5000) (Avg Mw ~ 50,000 g.mol^{-1}) was purchased from Solvay Advanced

Polymer (Belgium). NMP, H_2SO_4, glycine, NaCl, $MgSO_4$, and Na_2SO_4 were procured from Merck India. BSA (Mw ~ 69 kDa) obtained from CDH Chemicals Ltd TMC was purchased from Alfa Aser with 98% purity. TEA and L-glutamine were purchased from Spectrochem, India.

6.2.2 Fabrication of thin film composite membranes

W 15 (PSF/sPPSU (85:15)) UF membrane as mentioned in Chapter 3 was chosen as the substrate for the TFC membranes. The PA layer was synthesized by interfacial polymerization of the MPD and TMC on the W 15 substrate (Figure 6.3).
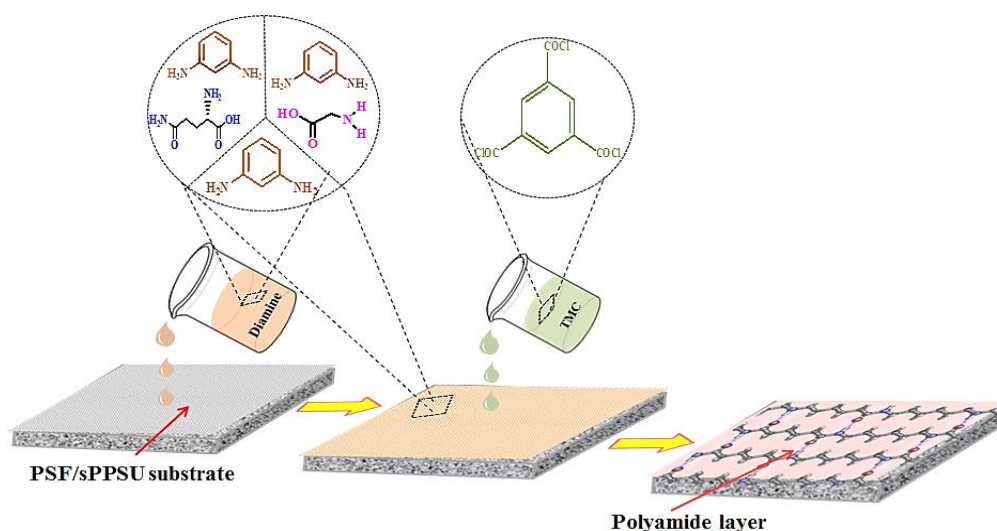
Figure 6.3 Schematic representation for preparation of TFC membrane

The membrane substrate was initially fixed onto a glass plate and soaked in DI water for 30 s. The membrane substrate was impregnated in amine solution for 15 min, which was prepared by dissolving MPD/TEA/hydrophilic additives in DI water as mentioned in Table 6.1. After 15 min, the amine solutions were poured out and excess of the solution was removed using rubber roller. The interfacial polymerization reaction was initiated by dipping impregnated membrane substrate in 0.1 wt. % of TMC in hexane for 1 min. The excess of TMC solution was then drained off and dried overnight at RT. Subsequently, the membrane was cured in an oven for 10 min at 50 °C and the TFC membranes were finally stored in DI water in dark after washing with DI water (Hermans *et al.* 2015).

Table 6.1 Compositions for PA membrane

Membrane code	MPD / TEA (wt. %)	TMC (wt. %)	Additive (wt. %)	
PA 0	2.0 / 1.0	0.1	NIL	
PA-Gly1	2.0 / 1.0	0.1	Glycine	1.0
PA-Gly2	2.0 / 1.0	0.1		2.0
PA-Glu1	2.0 / 1.0	0.1	L-glutamine	1.0
PA-Glu2	2.0 / 1.0	0.1		2.0

6.2.3 Membrane characterization

The morphology and structural characterization of PA layer of TFC membranes were performed by SEM, AFM, and FTIR spectroscopy. The FTIR spectra were carried to identify the membrane modification using Alfa Eco-ATR FTIR spectrometer (Bruker). The dry membrane samples were scanned for the range of 4000-600 cm^{-1} by ATR-FTIR. The hydrophilicity of the TFC membrane surface was evaluated using FTA-200 dynamic contact angle analyzer by sessile droplet method.

The streaming potential was measured to determine the surface charge using SurPASS electrokinetic analyzer (Anton Paar, Graz, Austria) (Hebbar *et al.* 2017). The KCl solution of 1 mM concentration was taken as electrolyte and the pH titration was carried using 0.1 M aqueous NaOH and HCl solution.

The membrane hydrophilicity, filtration, and antifouling studies were conducted according to the procedure mentioned in Chapter 2. The TFC membranes were tested for the rejection of salts such as NaCl, $MgSO_4$, and Na_2SO_4 at 0.8 MPa TMP. The salt solutions of 1000 ppm concentration were prepared by dissolving 1 g of salt in 1000 mL of water.

6.3 RESULTS AND DISCUSSIONS

6.3.1 Membrane characterization

Scheme 6.4 demonstrates the plausible reaction scheme for the interfacial polymerization of MPD and TMC to form PA layer on the membrane substrate. Here,

PA 0 represents the PA without any additives while PA-Gly and PA-Glu are the PA layers formed with the addition of glycine and L-glutamine to the amine solution, respectively. The PA layer is produced by the interfacial polymerization of the amine (NH_2) of MPD and acyl chloride (COCl) from TMC through an amide linkage (CO-NH) by eliminating HCl. The incorporation of hydrophilic additives such as glycine and L-glutamine to the aqueous phase containing MPD generates hydrophilic active sites on the PA layer formed by reaction of NH_2 group present in additive with COCl of TMC.
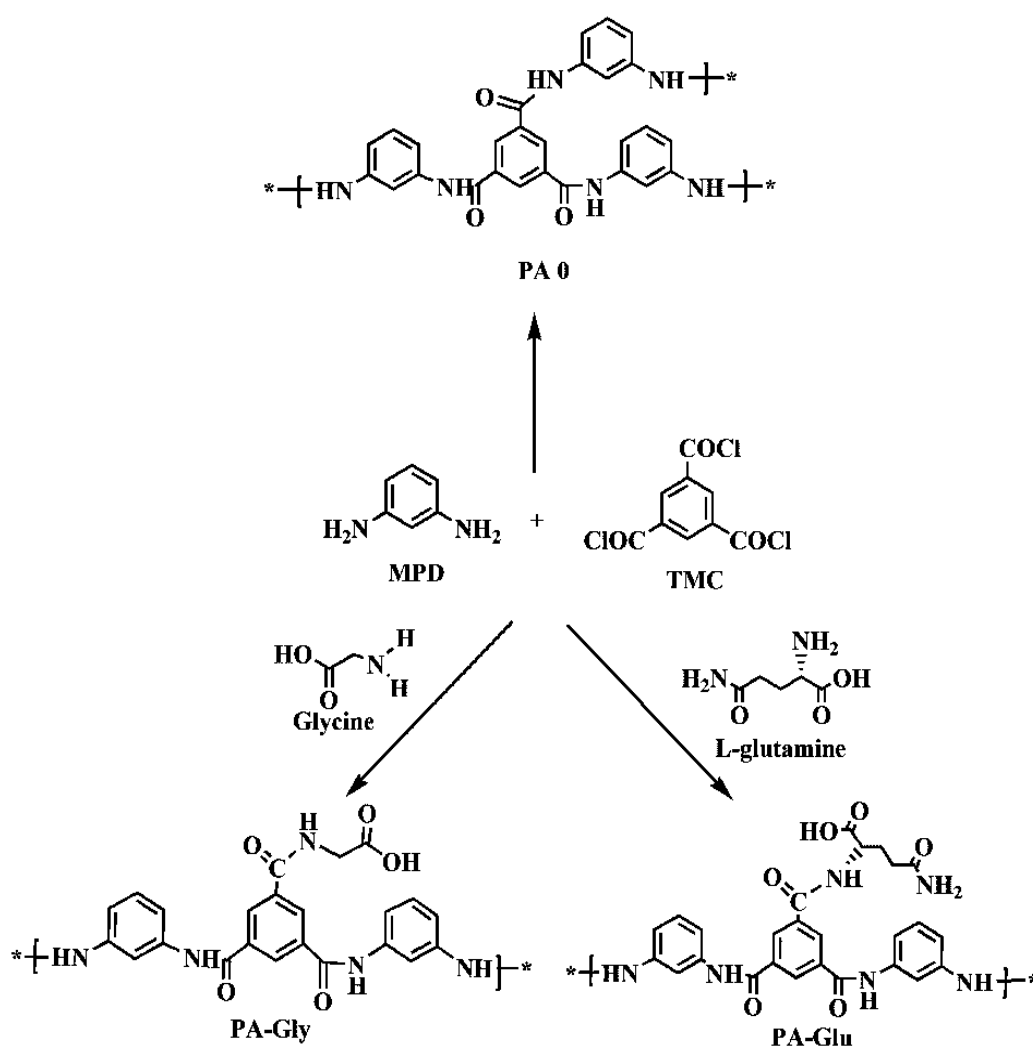
Scheme 6.4 Plausible scheme for synthesis of PA 0, PA-Gly, and PA-Glu

The formation of PA layer is confirmed by ATR-FTIR spectroscopic analysis of the membrane surface. The amide formation can be confirmed by the presence of

vibration peak around 3300 cm^{-1} and 1630-1660 cm^{-1} for NH stretching and C=O stretching, respectively (Figure 6.4). The generation of hydrophilic active sites on the incorporation of additives is detected by the vibration peak around 1700 cm^{-1}, for carbonyl group of carboxylic acid present in the additives.
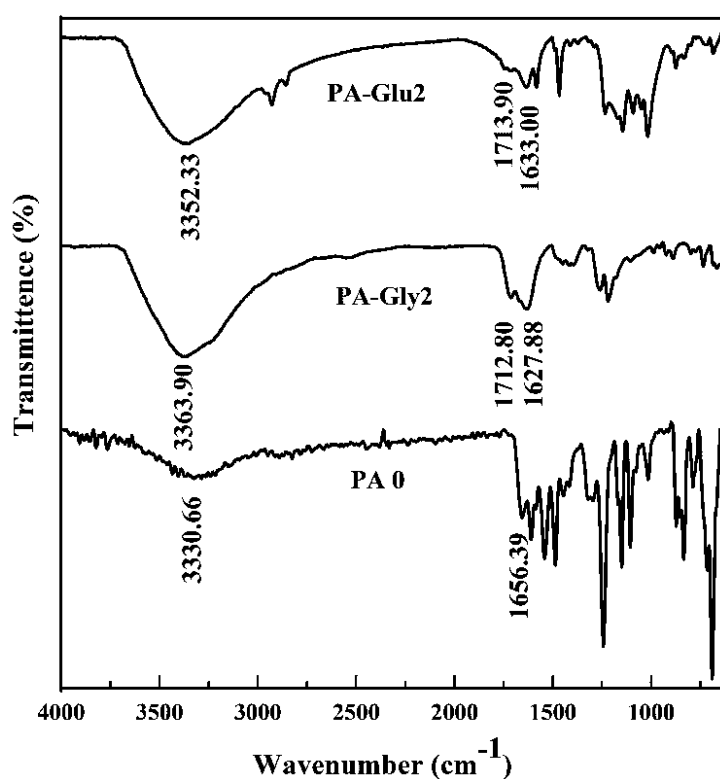
Figure 6.4 FTIR spectra of TFC membranes

The SEM images of membrane surface for the substrate and the TFC membranes are displayed in Figure 6.5. Development of PA layer was verified by the formation of a "ridge-and-valley" morphology over the smooth surface of the membrane substrate. The "ridge-and-valley" morphology of PA membranes showed white areas depicting the ridges and the black areas for the valley, which became less pronounced as the additive concentration is increased thereby indicating the formation of a smoother surface. The defect-free PA layer formation can also be observed from the surface image. It may be due to the presence of hydrophilic sulfonic group on the membrane substrate as it triggers the uniform diffusion of MPD (Zhang *et al.* 2016).
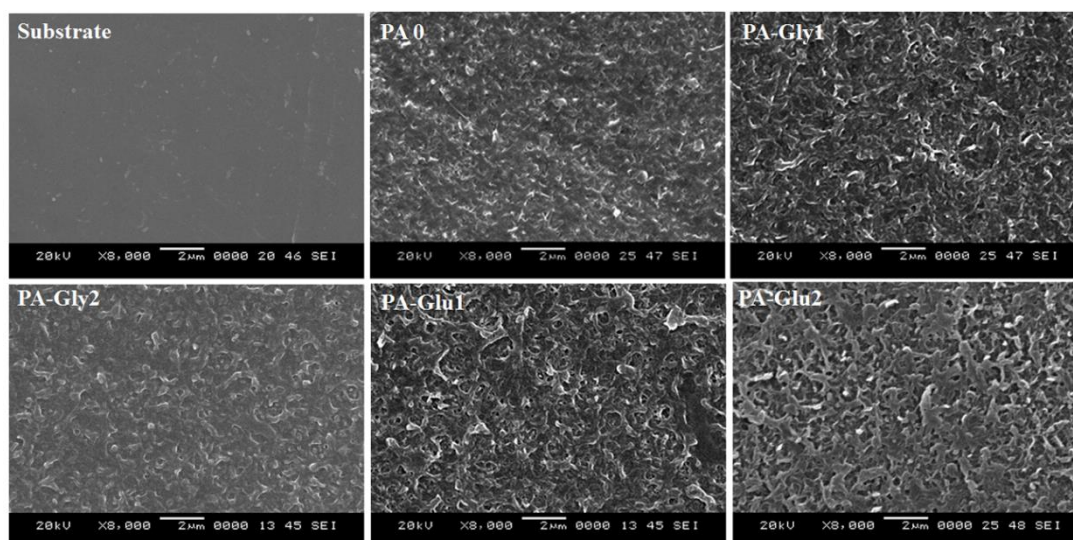
Figure 6.5 SEM images of membrane surface
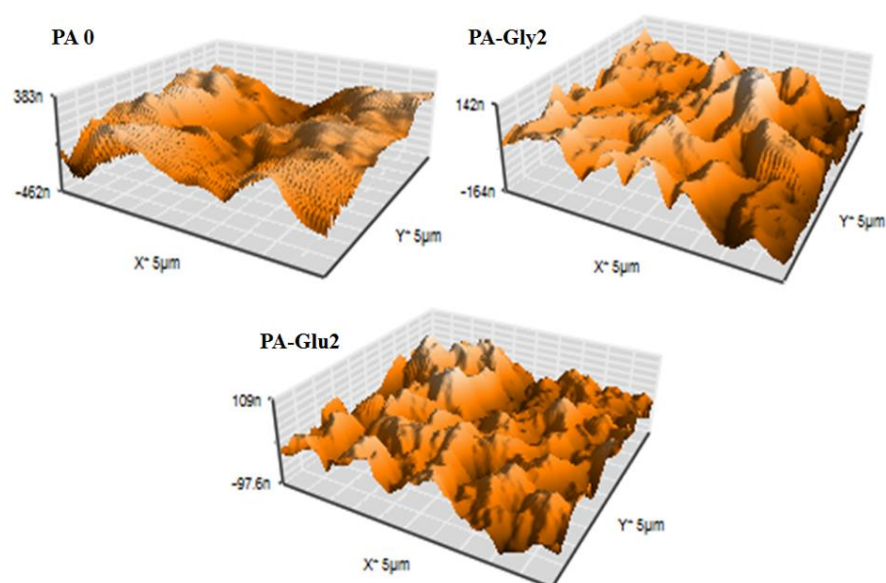
Figure 6.6 3D AFM images of PA 0, PA-Gly2, and PA-Glu2

Surface topography of the PA membranes prepared with and without the additives in the aqueous phase was studied using AFM (Figure 6.6). The peaks and valleys observed from the 3D AFM images display surface roughness of the membrane. The roughness parameters are also calculated to confirm the extent of surface roughness. It was observed that the roughness parameters decreased on the incorporation of hydrophilic additives in the aqueous phase. This is because the incorporation of additives decelerates the rigorous reaction between MPD and TMC

as they compete with MPD to give a smooth surface (Zhao and Ho 2014). Additionally, the R_a reduced from 93 nm to 37 nm and 30 nm on the addition of hydrophilic additives glycine and L-glutamine, respectively. The enhancement in the surface smoothness of the membranes can, in turn, benefit the antifouling performance.

Table 6.2 Roughness parameter of the membranes

Membrane code	Roughness Parameters (nm)	
	R_a	R_q
PA 0	93.37	113.60
PA-Gly2	37.48	49.68
PA-Glu2	30.49	39.05

The streaming ZP of the membrane surface was analyzed to determine the surface charge on the PA membrane. Figure 6.7 displays the effect of pH on the ZP value, where the membranes showed positive ZP at lower pH and negative ZP at higher pH. This is because of the protonation and deprotonation of free $-NH_2$ and $-COOH$ group, respectively present on the PA layer. The TFC membranes showed ZP of -38 mV, -60 mV and -62 mV at pH=9 for PA 0, PA-Gly2, and PA-Glu2, respectively. The ZP at pH=9 is associated with the total surface charge of the membrane, as the complete deprotonation of the carboxylic acid group is likely to take place at pH 9 (Tang *et al.* 2009). Moreover, it can be observed that the membranes showed higher negative ZP on the incorporation of the additives. This can be attributed to a large number of free carboxylic acid groups introduced on the membrane surface by incorporation of hydrophilic additives. Hence, it confirms the presence of hydrophilic sites on the PA layer formed. The increased amount of carboxylic acid group also facilitated the improvement in hydrophilicity, flux, and rejection. All the TFC membranes showed isoelectric point (IEP) i.e. the pH at which net charge is zero, at pH range of 3.5-4.0.
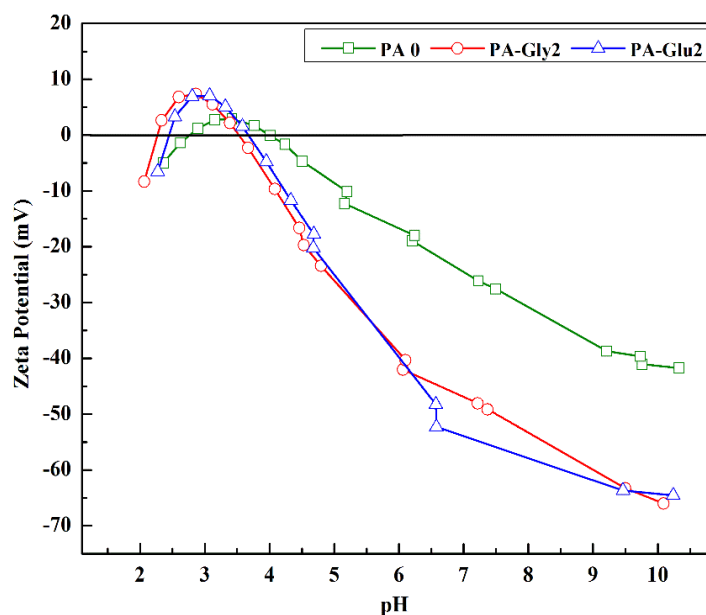
Figure 6.7 ZP of the TFC membranes

6.3.2 Membrane hydrophilicity and porosity

The WCA and water uptake capacity are measured to study the effect of the hydrophilic additives on the hydrophilicity of the PA membranes. The WCA of PA membranes decreased on the incorporation of glycine and L-glutamine to amine solution. This increase in the surface hydrophilicity of membrane surface is due to the carboxylic acid group introduced on the surface of PA layer with the of hydrophilic additives (Scheme 6.4). The carboxylic group enhances the interaction of PA layer and water due to the formation of a hydration layer over the active layer of the membrane. Moreover, lower WCA is observed for the PA layer formed by incorporation of L-glutamine than that of glycine as an additive. This is due to the higher hydrophilicity offered by the additional -NH_2 group present in the PA layer on incorporating L-glutamine (Scheme 6.4). Hence the WCA dropped from 87° for PA 0 to 81° and 73° for PA-Gly2 and PA-Glu2, respectively (Figure 6.8). The improved membrane hydrophilicity also benefitted its antifouling nature.

The water uptake capacity of the prepared membranes was calculated by dry weight technique and measurements are presented in Figure 6.8. The water uptake capacity of the membranes increased with the addition of additives and it further enhanced with the rise in the additive concentration. The improvement in water

uptake capacity is due to the enhanced surface hydrophilicity of membrane in the presence of the hydrophilic group, which is in agreement with the WCA results.
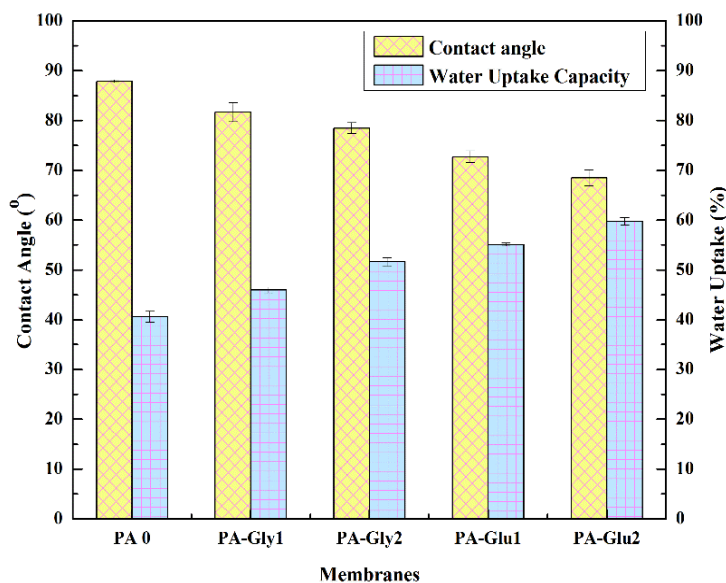
Figure 6.8 WCA and water uptake capacity of prepared TFC membranes

6.3.3 Filtration study

The NF behavior of the PA TFC membrane was studied by permeate flux and salt rejection. The TFC membranes follow Donnan and size exclusion mechanism in its transport pathway which makes them highly selective for the charge and size, respectively (Bera and Jewrajka 2016). Figure 6.9 demonstrates the time-dependent PWF for TFC membranes with and without additives at 0.8 MPa TMP. There is a significant rise in PWF observed with the addition of hydrophilic additives in the aqueous amine solution. This is because of the improved surface hydrophilicity due to the functionalization of PA layer by carboxylic acid groups in hydrophilic additives. The permeate flux of salt solutions was recorded and a similar trend was observed (Figure 6.10). However, the PWF for salt solutions were in the order: $NaCl > MgSO_4 > Na_2SO_4$, which is in accordance with the size of the salt ions. Therefore, the highest flux of 36.23 $Lm^{-2}h^{-1}$, 14.47 $Lm^{-2}h^{-1}$, 14.96 $Lm^{-2}h^{-1}$, and 21.44 $Lm^{-2}h^{-1}$ was shown by PA-Glu2 membrane for pure water, Na_2SO_4, $MgSO_4$, and NaCl solution, respectively.
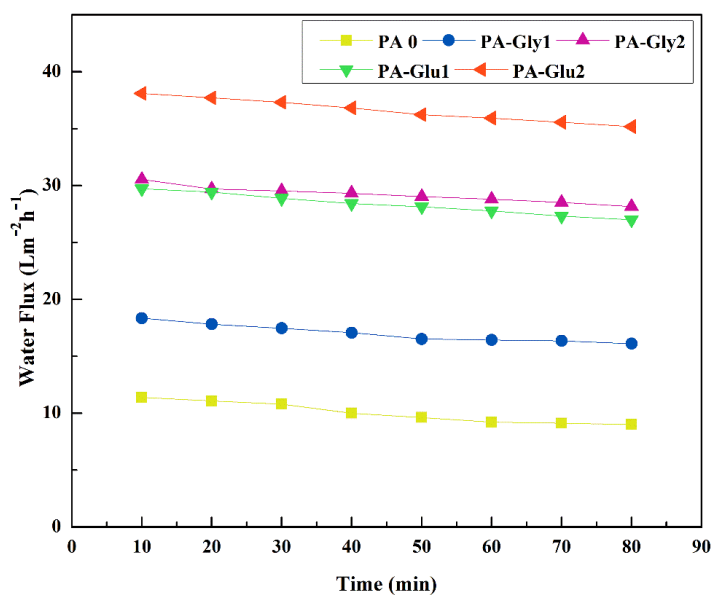
Figure 6.9 PWF of TFC membrane at 0.8 MPa TMP
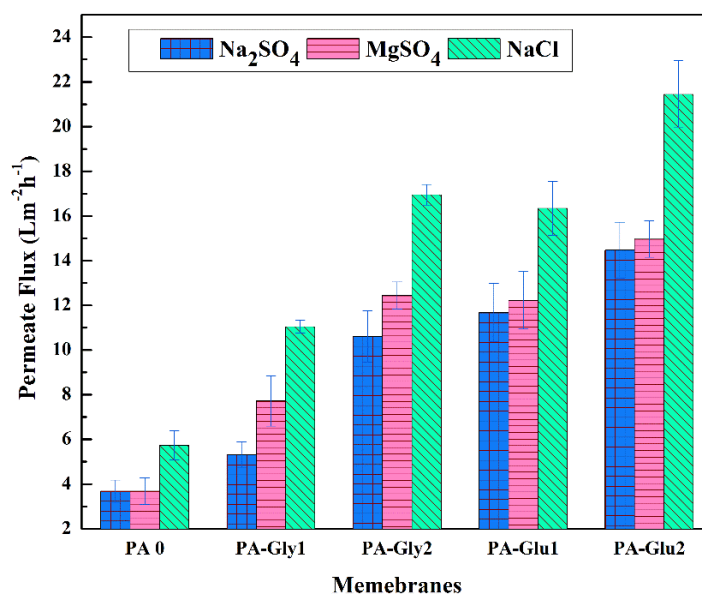
Figure 6.10 Permeate flux of salt solution at 0.8 MPa TMP

Figure 6.11 shows the rejection of $MgSO_4$, Na_2SO_4, and NaCl during the desalination of feed solution studied separately. The order of salt rejection is observed as $MgSO_4 > Na_2SO_4 > NaCl$. The retention of salt by the TFC is based on the Donnan exclusion principle which functions on the charge of the components and membranes. Figure 6.11 indicates higher rejection of $MgSO_4$ and Na_2SO_4 than NaCl, as membrane surface showed strong electrostatic repulsion for divalent SO_4^{2-} than the

monovalent Cl^- present in NaCl. The rejection of $MgSO_4$ is observed to be highest, as the divalent Mg^{2+} showed stronger binding than monovalent Na^+, due to their superior electrophilic nature than the monovalent cations (Remko *et al.* 2010, Pandian *et al.* 2015).
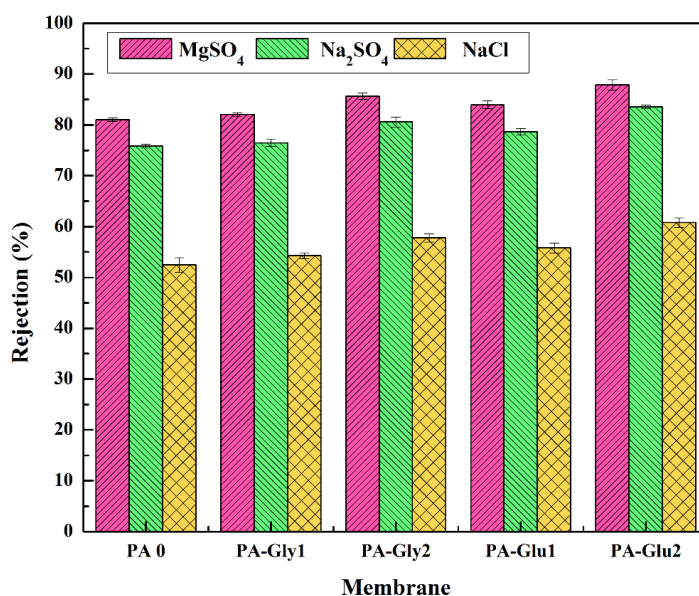
Figure 6.11 Salt rejection by TFC membranes at 0.8 MPa TMP

Pristine TFC membranes showed salt rejection of 81.04 %, 75.83 %, and 52.47 % for $MgSO_4$, Na_2SO_4, and NaCl, respectively, which improved with the incorporation of hydrophilic additives to the amine solution. This is because the incorporation of additive functionalizes the PA layer with the carboxylic acid group present in glycine and L-glutamine (Scheme 6.4). This, in turn, resulted in a negative surface charge on the PA TFC membranes. Thus, electrostatic interactions between the salt ions and negatively charged membranes caused the rejection of salt ions based on Donnan exclusion principle. The negative ZP of PA membranes prepared with glycine and L-glutamine as additives in amine solution supported the trend in the salt rejection behavior. Moreover, the PA membrane functionalized with L-glutamine showed higher rejection due to the collective effect of $-COO^-$ groups and an extra -NH_2 group present in L- glutamine (Singh *et al.* 2011). Hence, the PA-Glu2 showed the highest rejection of 87.87 %, 83.50 % and 60.77 % for $MgSO_4$, Na_2SO_4, and NaCl, respectively.

6.3.4 Antifouling study

The antifouling property of the TFC membranes was assessed by comparing the flux of water before and after passing the BSA solution (1000 ppm). Figure 6.12 illustrates the sudden decline in the flux by all the prepared membranes as the fouling occurred at an instant after exposure to the BSA rich feed. The extent of fouling and reusability of prepared membranes were found out by calculating the FRR (Figure 6.13). The TFC membranes showed good FRR which further increased with the incorporation of the hydrophilic additive into amine solution. The functionalization of PA surface with –COOH group on the incorporation of additives elevated the negative surface charge. This is attributed to the strong electrostatic repulsion between the negatively charged BSA molecules and membrane surface. Moreover, the hydrophilic carboxyl group present on the surface of TFC membranes resulted in the formation of hydration layer over the surface of PA membrane, making it difficult for the foulant to adhere on the membrane surface. On comparing FRR of the membranes prepared with L-glutamine and glycine as additives, PA-Glu membrane showed better antifouling result than PA-Gly (Figure 6.13). This fouling resistance offered is attributed to the lower surface roughness of the PA-Glu than PA-Gly which is observed by AFM images (Figure 6.6). Furthermore, the rougher surface is prone to the fouling as the foulant get adsorbed in the valley. Therefore, the lower surface roughness and higher surface charge of the membrane result in membranes with the enhanced antifouling property. The PA-Glu2 showed good fouling resistance with a highest FRR value of 89.18 %.

The R_{rev} and R_{irr} fouling of the membrane is also calculated to study the reusability of the membranes (Figure 6.13). The lower R_{irr} displays enhanced antifouling nature exhibited by the membranes. This is because of the hydrophilic surface of the modified membrane that makes it easy for the removal of adsorbed foulant by simple hydraulic washing. Therefore, R_{irr} fouling of the TFC membranes could be brought down from 23.33 % to 10.81 % by the incorporation of additives to the amine solution.
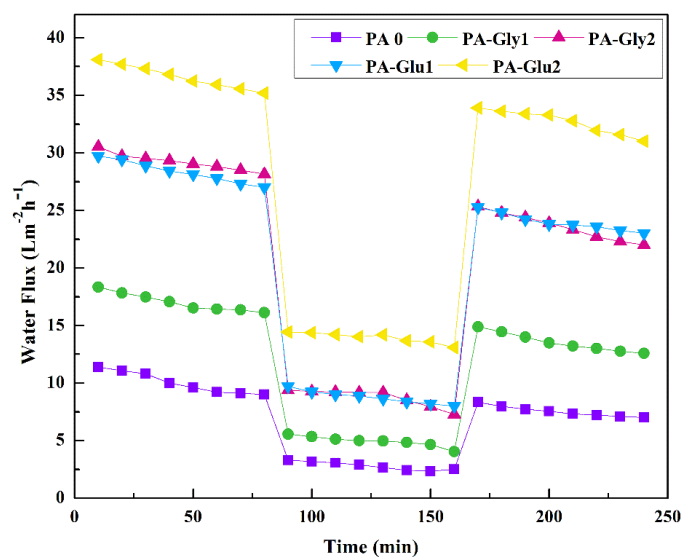
Figure 6.12 Flux vs. time for TFC membranes before and after passing BSA at 0.8 MPa TMP
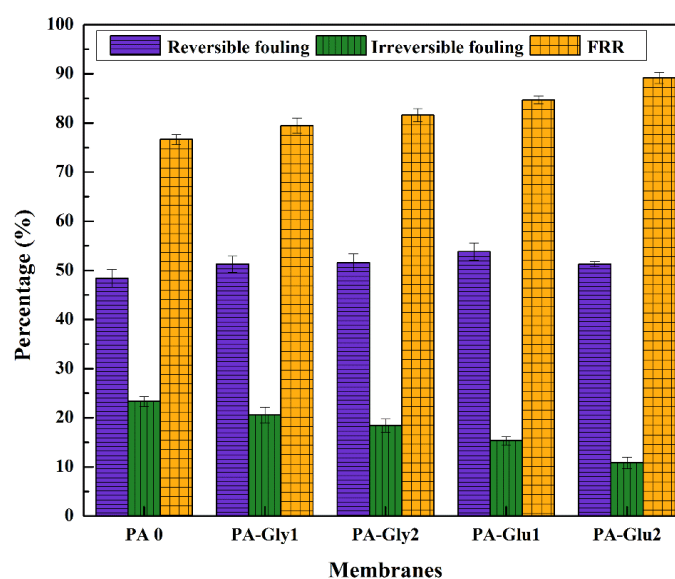
Figure 6.13 Fouling behavior of the PA TFC membranes

6.4 CONCLUSIONS

TFC NF membranes were fabricated by the interfacial polymerization of MPD and TMC, on the sPPSU/PSF membranes as substrate. The effect of hydrophilic additives such as glycine and L-glutamine on membrane performance is studied. The additives functionalized the membrane surface with –COOH groups that improved the hydrophilicity and surface charge of the membrane. The membrane performance

improved with an increase in the additive concentration as the number of functionalized –COOH group increased. The incorporation of hydrophilic additives resulted in the smoother membranes with the enhanced antifouling property, where R_{irr} declined from 24 % to 11 %. Therefore PA-Glu2 was found to be the best performing membrane among the series of TFC membranes, with a good salt rejection capability of 87.87 %, 83.50 % and 60.77% for $MgSO_4$, Na_2SO_4, and NaCl, respectively, and highest water flux of 36.23 $Lm^{-2}h^{-1}$. Hence, incorporation of additives modified the surface of the membrane as the active sites of hydrophilic additive alter the surface property, thereby improving flux and rejection.

CHAPTER 7

SUMMARY AND CONCLUSIONS

Abstract: This chapter deals with the summary of the entire research work and presents a concise comparison between synthesized membranes in terms of their properties and performance. It also enlists the major conclusions drawn from the work.

7.1 SUMMARY

The polyarylsulfone base membranes were fabricated by non-solvent induced phase inversion techniques using NMP as solvent and water as non-solvent. Five series of polyarylsulfone based membranes were prepared which include 17 FS and 11 HF membranes. The classifications of these membranes are given in Table 7.1. These membranes were the result of various modification techniques such as blending, coating, compositing, chemical modification or their combination.

Table 7.1 Series of membranes prepared

Membrane series	Membrane codes	Modification	Type of membrane	
MS 1	P0-P, P75-P, P100-P, P75-G0.5, P75-G1, P75-G2	Blending	UF	FS
MS 2	W5, W10, W15, G15, N15, S15	Combined technique (Chemical + Blending)		
MS 3	HF0, HF0.05, HF0.15, HF0.30, Ag-HF0.05, Ag-HF0.15, Ag-HF0.3	Nanocomposite		HF
MS 4	M 0, M 1, M 2, M 3			
MS 5	PA 0, PA-Gly1, PA-Gly2, PA-Glu1, PA-Glu2	Coating (i.e. TFC)	NF-FS	

In series MS 1, the polymer PPSU and PSF were blended to obtain membranes with better performance than their pristine forms. The effect of GB as a hydrophilic additive was studied on the performance of PPSU/PSF (75:25) blend UF membrane. It was seen that 1 wt. % of GB in the dope solution exhibited better membrane

performance which is reflected by the high rejection of 87.51 %, 80.23 %, and 71.45 % for BSA, Pb^{2+}, and Cd^{2+}, respectively. Here, the heavy metal ion rejection was performed using PEUF process.

MS 2 series reflects the effect of sulfonation (chemical modification) of PPSU on the performance of the membrane. The blending of 15 wt. % of sPPSU with PSF resulted in good permeation, hydrophilicity, fouling resistance, and rejection. The effect of coagulation bath, namely an aqueous solution of GB, NaCl, or NMP on the morphology of the membrane was also studied. It was found that the presence of GB in the coagulation bath resulted in the membrane with the highest flux and protein rejection of 66.3 %, 74.0 %, and 91.2 % for trypsin, pepsin, and BSA, respectively. The PEUF rejection of Pb^{2+} and Cd^{2+} ranged between 76-90 % and 65-79 %, respectively.

MS 3 and 4 are the nanocomposite HF membranes. In MS 3, CNPs and Ag-CNPs incorporated PPSU HF membrane were tested for dye rejection and antibiofouling. CNP and Ag-CNP impart a positive surface charge to the membrane, hence they are suitable for removal of anionic dyes from the feed. They also showed good antibacterial activity against *S. aureus, M. smegmatis,* and *E. coli*. MS 4 had MoO_3 NPs incorporated PPSU HF membranes, where negative charge induced by the NPs was responsible for cationic dye removal. Furthermore, these membranes also exhibited photodegradation of MB dye with 66.3 % removal on exposure to UV radiation. The antibiofouling experiment showed the resistance of these membranes towards the bacterial strains such as *M. smegmatis*, *S. aureus,* and *E. coli.*

In MS 5 series, TFC NF membranes were prepared by the interfacial polymerization of MPD and TMC, with sPPSU/PSF blend membranes as a porous substrate. The effect of hydrophilic additives such as glycine and L-glutamine on the membrane performance was studied. The addition of additives leads to the functionalization of membrane surface with -COOH groups which improve hydrophilicity and surface charge. Among the prepared membranes, PA-Glu2 showed good salt rejection capability of 87.87 %, 83.50 %, and 60.77 % for $MgSO_4$, Na_2SO_4, and NaCl, respectively. The comparison of the all the membranes prepared in 5 series based on WCA, water uptake capacity, PWF, and FRR are given below.

The surface hydrophilicity and wettability of the prepared membranes were evaluated by comparing their WCA (Figure 7.1) and water uptake capacity (Figure 7.2), where all the modified membranes showed lower contact angle and higher water uptake capacity than their pristine form. Hence, it can be said that the modifications affected the hydrophilicity of the prepared membranes. The nanocomposite HF membranes with 0.3 wt. % of Ag-CNP from MS 3 showed superior hydrophilicity with least WCA and maximum water uptake capacity.
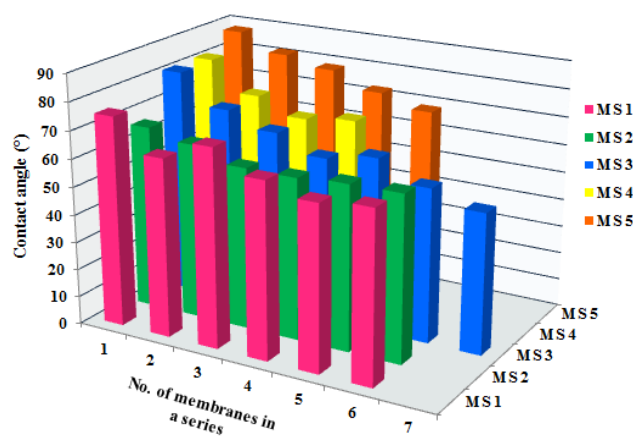
Figure 7.1 WCA of the prepared membranes
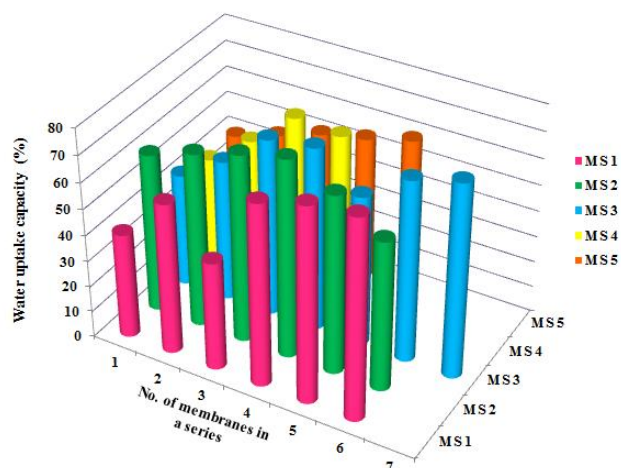
Figure 7.2 Water uptake capacity of membranes

Figure 7.3 shows the PWF of the UF membranes measured at 0.2 MPa and found that the modification of membranes could bring about higher PWF than their pristine forms. The PWF for FS membranes in MS 1 and MS 2 membranes was measured using dead-end filtration setup while the HF membranes in MS 3 and MS 4

were studied by cross-flow filtration setup. The membranes from MS 2 series showed the highest flux of 148.50 $Lm^{-2}h^{-1}$ among the FS membranes, while for HF membranes, the highest flux of 118.36 $Lm^{-2}h^{-1}$ was observed for AHF 0.15 of MS 3 series.
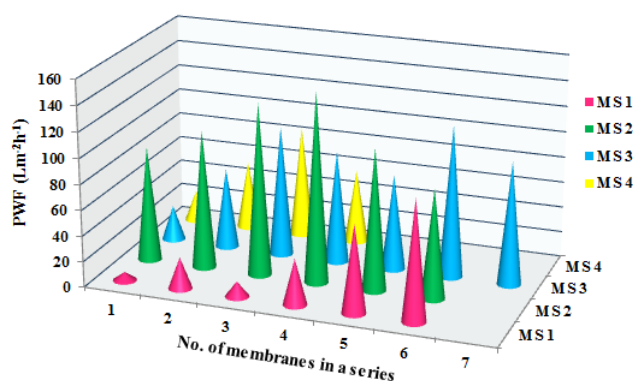
Figure 7.3 PWF of UF membranes at 0.2 MPa

The antifouling property and reusability of the membranes were determined by measuring the FRR as given in Figure 7.4. The increase in FRR of membranes was visible on modification, where NF membranes with 2 wt. % of L-glutamine additive showed highest FRR of 89.18 %.
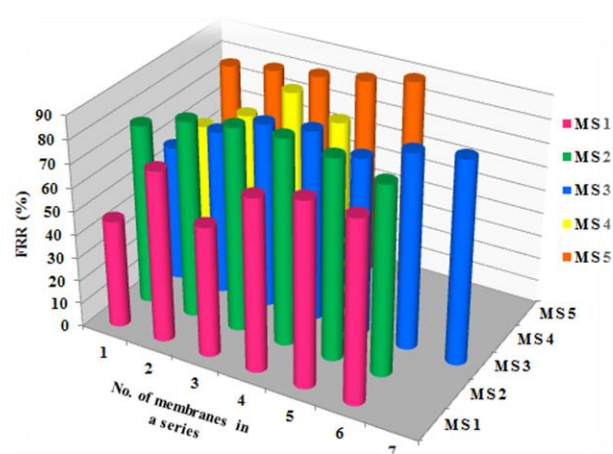
Figure 7.4 FRR of the prepared membranes

7.2 CONCLUSIONS

The polyarylsulfone base membranes were modified to improve the hydrophilicity and flux. The ability of membranes to selectively reject salt, heavy

metal ions, dyes, and proteins was exhibited with a judicial selection of modification techniques. The relation between the modification techniques and property and performance of the membranes drawn from the conducted research are listed below:

1. The blending of polymers could bring about change in the membrane morphology and porosity as it affects the segmental gap.

2. The chemical modification of the polymers imparts the polar functionality to the membranes that leads to enhancement in the hydrophilicity as the water molecules interact with the functional groups.

3. Variation in the coagulation bath composition can bring about change in the rate of liquid-liquid demixing during the phase inversion which can, in turn, affect the membrane morphology and pore elongation.

4. Incorporation of hydrophilic additives such as zwitterions and nanoparticles to the polymer dope solution can result in increased hydrophilicity and selectivity, as these additives diffuse or migrate to the membrane surface to impart its property.

5. Surface charge developed on the membranes by the modifications could bring about higher selectivity, as there is an electrostatic interaction between the solutes and the charged surface.

6. The increased hydrophilicity resulted in membranes with better antifouling property due to the formation of hydration layer that weakens the interaction between the membrane surface and foulant.

7. The interfacial polymerization results in TFC membranes, which have a selective rejection of solutes based on either Donnan or size exclusion.

Present research work gives a glimpse of endless possibilities within the purview of capabilities of different modification techniques in developing membranes with specific properties that can be tuned based on targeted applications. As much more is to be explored, the future work will be devoted to further understanding of the effect of modification techniques on the morphology to property relation of membranes. Subsequently, the developed membranes will be tested for long-term performance, durability, the stability of polymer in adverse conditions and will be optimized for superior antifouling and antibiofouling property for water purification.

REFERENCES

Akhavan, O. and Ghaderi, E. (2010). "Toxicity of graphene and graphene oxide nanowalls against bacteria." *ACS Nano*, 4(10), 5731-5736.

Al Hamouz, O. C. S. and Ali, S. A. (2012). "Removal of heavy metal ions using a novel cross-linked polyzwitterionic phosphonate." *Sep. Purif. Technol.*, 98, 94-101.

Ali, S. W., Rajendran, S. and Joshi, M. (2011). "Synthesis and characterization of chitosan and silver loaded chitosan nanoparticles for bioactive polyester." *Carbohydr. Polym.*, 83(2), 438-446.

Allogho, G. G. and Ashrit, P. (2012). "Wettability and photochromic behaviour of Molybdenum oxide thin films." *Thin Solid Films*, 520(6), 2326-2330.

Alsalhy, Q. F., Ali, J. M., Abbas, A. A., Rashed, A., Bruggen, B. V. d. and Balta, S. (2013). "Enhancement of poly (phenyl sulfone) membranes with ZnO nanoparticles." *Desalin. Water Treat.*, 51(31-33), 6070-6081.

An, Q. F., Sun, W. D., Zhao, Q., Ji, Y. L. and Gao, C. J. (2013). "Study on a novel nanofiltration membrane prepared by interfacial polymerization with zwitterionic amine monomers." *J. Membr. Sci.*, 431, 171-179.

Arockiasamy, D. L., Nagendran, A. and Mohan, D. (2008). "Studies on cellulose acetate/aminated poly (ether imide) blend ultrafiltration membranes." *Int. J. Polym. Mater.*, 57(11), 997-1018.

Arockiasamy, D. L., Nagendran, A., Shobana, K. and Mohan, D. (2009). "Preparation and characterization of cellulose acetate/aminated polysulfone blend ultrafiltration membranes and their application studies." *Sep. Sci. Technol.*, 44(2), 398-421.

Arockiasamy, D. L., Alhoshan, M., Alam, J., Muthumareeswaran, M., Figoli, A. and Kumar, S. A. (2017). "Separation of proteins and antifouling properties of polyphenylsulfone based mixed matrix hollow fiber membranes." *Sep. Purif. Technol.*, 174, 529-543.

Aroua, M. K., Zuki, F. M. and Sulaiman, N. M. (2007). "Removal of chromium ions from aqueous solutions by polymer-enhanced ultrafiltration." *J. Hazard. Mater.*, 147(3), 752-758.

Arumugham, T., Kaleekkal, N. J. and Doraiswamy, M. (2015). "Development of new hybrid ultrafiltration membranes by entanglement of macromolecular PPSU-SO₃H chains: Preparation, morphologies, mechanical strength, and fouling resistant properties." *J. Appl. Polym. Sci.*, 132(20), 1-9.

Arumugham, T., Kaleekkal, N. J., Rana, D. and Doraiswamy, M. (2016). "Separation of oil/water emulsions using nano MgO anchored hybrid ultrafiltration membranes for environmental abatement." *J. Appl. Polym. Sci.*, 133(1), 1-12.

Baker, R. W. (2004). "Overview of membrane science and technology." *Membrane Technology and Applications, Second Edition*, John Wiley & Sons Ltd., England, 1-14.

Bashir, A., Ahad, S. and Pandith, A. H. (2016). "Soft Template Assisted Synthesis of Zirconium Resorcinol Phosphate Nanocomposite Material for the Uptake of Heavy-Metal Ions." *Ind. Eng. Chem. Res.*, 55(17), 4820-4829.

Bechhold, H. (1908). "Ultrafiltration." *Colloid Polym. Sci.*, 3(5), 226-228.

Begon, M., Townsend, C. R. and Harper, J. L. (2006). *Ecology: from individuals to ecosystems,* Wiley-Blackwell, UK.

Bera, A. and Jewrajka, S. K. (2016). "Tailoring polyamide thin film composite nanofiltration membranes by polyethyleneimine and its conjugates for the enhancement of selectivity and antifouling property." *RSC Adv.*, 6(6), 4521-4530.

Bodzek, M., Korus, I. and Loska, K. (1999). "Application of the hybrid complexation-ultrafiltration process for removal of metal ions from galvanic wastewater." *Desalination*, 121(2), 117-121.

Bowry, S. K., Gatti, E. and Vienken, J. (2011). "Contribution of polysulfone membranes to the success of convective dialysis therapies." *In High-Performance Membrane Dialyzers Vol. 173*, Karger, Basel, 110-118.

Breitbach, L., Hinke, E. and Staude, E. (1991). "Heterogeneous functionalizing of polysulfone membranes." *Macromol. Mater. Eng.*, 184(1), 183-196.

Buonomenna, M., Macchi, P., Davoli, M. and Drioli, E. (2007). "Poly (vinylidene fluoride) membranes by phase inversion: the role the casting and coagulation conditions play in their morphology, crystalline structure and properties." *Eur. Polym. J.*, 43(4), 1557-1572.

Cadotte, J., Petersen, R., Larson, R. and Erickson, E. (1980). "A new thin-film composite seawater reverse osmosis membrane." *Desalination*, 32, 25-31.

Cao, C. Y., Qu, J., Yan, W. S., Zhu, J. F., Wu, Z. Y. and Song, W. G. (2012). "Low-cost synthesis of flowerlike α-Fe_2O_3 nanostructures for heavy metal ion removal: adsorption property and mechanism." *Langmuir*, 28(9), 4573-4579.

Cao, X., Ma, J., Shi, X. and Ren, Z. (2006). "Effect of TiO_2 nanoparticle size on the performance of PVDF membrane." *Appl. Surf. Sci.*, 253(4), 2003-2010.

Cao, X., Tang, M., Liu, F., Nie, Y. and Zhao, C. (2010). "Immobilization of silver nanoparticles onto sulfonated polyethersulfone membranes as antibacterial materials." *Colloids Surf., B*, 81(2), 555-562.

Chan, K. H., Wong, E. T., Irfan, M., Idris, A. and Yusof, N. M. (2015). "Enhanced Cu (II) rejection and fouling reduction through fabrication of PEG-PES nanocomposite ultrafiltration membrane with PEG-coated cobalt doped iron oxide nanoparticle." *J. Taiwan Inst. Chem. Eng.*, 47, 50-58.

Chehbouni, M. and Apblett, A. W. (2005). "Molybdenum-Oxide Based Sorbants for Toxic Metals." *Environmental Issues and Waste Management Technologies in the Ceramic and Nuclear Industries XI, Volume 176*, John Wiley & Sons, England, 15-23.

Chen, C., Li, X., Ma, W., Zhao, J., Hidaka, H. and Serpone, N. (2002). "Effect of transition metal ions on the TiO_2-assisted photodegradation of dyes under visible irradiation: a probe for the interfacial electron transfer process and reaction mechanism." *J. Phys. Chem. B*, 106(2), 318-324.

Chen, Y., Lu, C., Xu, L., Ma, Y., Hou, W. and Zhu, J. J. (2010). "Single-crystalline orthorhombic molybdenum oxide nanobelts: synthesis and photocatalytic properties." *CrystEngComm*, 12(11), 3740-3747.

Chen, Y., Hu, X., Hu, X., Zhang, S. and Zhang, Y. (2015). "Polymeric hollow fiber membranes prepared by dual pore formation mechanism." *Mater. Lett.*, 143, 315-318.

Cheng, L., Shao, M., Wang, X. and Hu, H. (2009). "Single-Crystalline Molybdenum Trioxide Nanoribbons: Photocatalytic, Photoconductive, and Electrochemical Properties." *Chem. Eur. J.*, 15(10), 2310-2316.

Chernousova, S. and Epple, M. (2013). "Silver as antibacterial agent: ion, nanoparticle, and metal." *Angew. Chem. Int. Ed.*, 52(6), 1636-1653.

Chithambararaj, A., Sanjini, N., Bose, A. C. and Velmathi, S. (2013). "Flower-like hierarchical h-MoO$_3$: new findings of efficient visible light driven nano photocatalyst for methylene blue degradation." *Catal. Sci. Tech.*, 3(5), 1405-1414.

Chithambararaj, A., Sanjini, N., Velmathi, S. and Bose, A. C. (2013). "Preparation of h-MoO$_3$ and α-MoO$_3$ nanocrystals: comparative study on photocatalytic degradation of methylene blue under visible light irradiation." *Phys Chem Chem Phys*, 15(35), 14761-14769.

Chun, K. Y., Jang, S. H., Kim, H. S., Kim, Y. W., Han, H. S. and Joe, Y. i. (2000). "Effects of solvent on the pore formation in asymmetric 6FDA–4, 4′ ODA polyimide membrane: terms of thermodynamics, precipitation kinetics, and physical factors." *J. Membr. Sci.*, 169(2), 197-214.

Daraei, P., Madaeni, S. S., Ghaemi, N., Salehi, E., Khadivi, M. A., Moradian, R. and Astinchap, B. (2012). "Novel polyethersulfone nanocomposite membrane prepared by PANI/Fe$_3$O$_4$ nanoparticles with enhanced performance for Cu(II) removal from water." *J. Membr. Sci.*, 415-416, 250-259.

Darvishmanesh, S., Jansen, J. C., Tasselli, F., Tocci, E., Luis, P., Degrève, J., Drioli, E. and Van der Bruggen, B. (2011). "Novel polyphenylsulfone membrane for potential use in solvent nanofiltration." *J. Membr. Sci.*, 379(1-2), 60-68.

Darvishmanesh, S., Tasselli, F., Jansen, J. C., Tocci, E., Bazzarelli, F., Bernardo, P., Luis, P., Degrève, J., Drioli, E. and Van der Bruggen, B. (2011). "Preparation of solvent stable polyphenylsulfone hollow fiber nanofiltration membranes." *J. Membr. Sci.*, 384(1), 89-96.

Deimede, V., Nikitopoulou, K., Voege, A. and Kallitsis, J. (2015). "Study of polymer blend membranes composed of sulfonated polysulfone and PEO-grafted aromatic polyether with controllable morphology." *Eur. Polym. J.*, 63, 113-122.

Di Vona, M., Sgreccia, E., Tamilvanan, M., Khadhraoui, M., Chassigneux, C. and Knauth, P. (2010). "High ionic exchange capacity polyphenylsulfone (SPPSU) and polyethersulfone (SPES) cross-linked by annealing treatment: thermal stability, hydration level and mechanical properties." *J. Membr. Sci.*, 354(1), 134-141.

Dong, W. and Dunn, B. (1998). "Sol–gel synthesis of monolithic molybdenum oxide aerogels and xerogels." *J. Mater. Chem.*, 8(3), 665-670.

Du, W. L., Niu, S. S., Xu, Y. L., Xu, Z. R. and Fan, C. L. (2009). "Antibacterial activity of chitosan tripolyphosphate nanoparticles loaded with various metal ions." *Carbohydr. Polym.*, 75(3), 385-389.

Dzinun, H., Othman, M. H. D., Ismail, A., Puteh, M. H., Rahman, M. A. and Jaafar, J. (2015). "Morphological study of co-extruded dual-layer hollow fiber membranes incorporated with different TiO_2 loadings." *J. Membr. Sci.*, 479, 123-131.

Ennigrou, D. J., Gzara, L., Romdhane, M. R. B. and Dhahbi, M. (2009). "Cadmium removal from aqueous solutions by polyelectrolyte enhanced ultrafiltration." *Desalination*, 246(1-3), 363-369.

Fakhri, A. and Nejad, P. A. (2016). "Antimicrobial, antioxidant and cytotoxic effect of molybdenum trioxide nanoparticles and application of this for degradation of ketamine under different light illumination." *J. Photochem. Photobiol.*, 159, 211-217.

Fang, B., Ling, Q., Zhao, W., Ma, Y., Bai, P., Wei, Q., Li, H. and Zhao, C. (2009). "Modification of polyethersulfone membrane by grafting bovine serum albumin on

the surface of polyethersulfone/poly (acrylonitrile-co-acrylic acid) blended membrane." *J. Membr. Sci.*, 329(1), 46-55.

Feng, Q., Wu, J., Chen, G., Cui, F., Kim, T. and Kim, J. (2000). "A mechanistic study of the antibacterial effect of silver ions on *Escherichia coli* and *Staphylococcus aureus*." *J. Biomed. Mater. Res.*, 52(4), 662-668.

Feng, Y., Lin, X., Li, H., He, L., Sridhar, T., Suresh, A. K., Bellare, J. and Wang, H. (2014). "Synthesis and characterization of chitosan-grafted BPPO ultrafiltration composite membranes with enhanced antifouling and antibacterial properties." *Ind. Eng. Chem. Res.*, 53(39), 14974-14981.

Feng, Y., Han, G., Chung, T. S., Weber, M., Widjojo, N. and Maletzko, C. (2017). "Effects of polyethylene glycol on membrane formation and properties of hydrophilic sulfonated polyphenylenesulfone (sPPSU) membranes." *J. Membr. Sci.*, 531, 27-35.

Fick, A. (1855). "Ueber Diffusion." *Annalen der Physik*, 170, 59-86.

Ganguly, A. and George, R. (2007). "Synthesis, characterization and gas sensitivity of MoO_3 nanoparticles." *Bull. Mater. Sci*, 30(2), 183-185.

Gao, F., Liu, G. and Yuan, S. (2017). "The effect of betaine on the foam stability: Molecular simulation." *Appl. Surf. Sci.*, 407, 156-161.

Garcia-Ivars, J., Alcaina-Miranda, M. I., Iborra-Clar, M. I., Mendoza-Roca, J. A. and Pastor-Alcañiz, L. (2014). "Enhancement in hydrophilicity of different polymer phase-inversion ultrafiltration membranes by introducing PEG/Al_2O_3 nanoparticles." *Sep. Purif. Technol.*, 128, 45-57.

Ghosh, A. K., Jeong, B. H., Huang, X. and Hoek, E. M. (2008). "Impacts of reaction and curing conditions on polyamide composite reverse osmosis membrane properties." *J. Membr. Sci.*, 311(1), 34-45.

Ghosh, A. K. and Hoek, E. M. (2009). "Impacts of support membrane structure and chemistry on polyamide–polysulfone interfacial composite membranes." *J. Membr. Sci.*, 336(1), 140-148.

Gleick, P. H. (1993). *Water in crisis: a guide to the world's fresh water resources,* Oxford University Press, Inc., UK.

Graham, T. (1866). "LV. On the absorption and dialytic separation of gases by colloid septa." *The London, Edinburgh, and Dublin Philosophical Magazine and Journal of Science*, 32(218), 401-420.

Hamouda, T. and Baker, J. (2000). "Antimicrobial mechanism of action of surfactant lipid preparations in enteric Gram-negative bacilli." *J. Appl. Microbiol.*, 89(3), 397-403.

Han, M. J. and Nam, S. T. (2002). "Thermodynamic and rheological variation in polysulfone solution by PVP and its effect in the preparation of phase inversion membrane." *J. Membr. Sci.*, 202(1), 55-61.

Hasegawa, T., Iwasaki, Y. and Ishihara, K. (2001). "Preparation and performance of protein-adsorption-resistant asymmetric porous membrane composed of polysulfone/phospholipid polymer blend." *Biomaterials*, 22(3), 243-251.

Hasegawa, T., Iwasaki, Y. and Ishihara, K. (2002). "Preparation of blood-compatible hollow fibers from a polymer alloy composed of polysulfone and 2-methacryloyloxyethyl phosphorylcholine polymer." *J. Biomed. Mater. Res.*, 63(3), 333-341.

Hebbar, R. S., Isloor, A. M. and Ismail, A. (2014). "Preparation of antifouling polyetherimide/hydrolysed PIAM blend nanofiltration membranes for salt rejection applications." *RSC Adv.*, 4(99), 55773-55780.

Hebbar, R. S., Isloor, A. M. and Ismail, A. (2014). "Preparation and evaluation of heavy metal rejection properties of polyetherimide/porous activated bentonite clay nanocomposite membrane." *RSC Adv.*, 4(88), 47240-47248.

Hebbar, R. S., Isloor, A. M., Ananda, K. and Ismail, A. (2016). "Fabrication of polydopamine functionalized halloysite nanotube/polyetherimide membranes for heavy metal removal." *J. Mater. Chem. A*, 4(3), 764-774.

Hebbar, R. S., Isloor, A. M., Ananda, K., Abdullah, M. S. and Ismail, A. (2017). "Fabrication of a novel hollow fiber membrane decorated with functionalized Fe_2O_3 nanoparticles: towards sustainable water treatment and biofouling control." *New J. Chem.*, 41(10), 4197-4211.

Hebbar, R. S., Isloor, A. M., Zulhairun, A., Abdullah, M. S. and Ismail, A. (2017). "Efficient treatment of hazardous reactive dye effluents through antifouling polyetherimide hollow fiber membrane embedded with functionalized halloysite nanotubes." *J. Taiwan Inst. Chem. Eng.*, 72, 244-252.

Hermans, S., Mariën, H., Dom, E., Bernstein, R. and Vankelecom, I. F. (2014). "Simplified synthesis route for interfacially polymerized polyamide membranes." *J. Membr. Sci.*, 451, 148-156.

Hermans, S., Bernstein, R., Volodin, A. and Vankelecom, I. F. (2015). "Study of synthesis parameters and active layer morphology of interfacially polymerized polyamide–polysulfone membranes." *React. Funct. Polym.*, 86, 199-208.

Huang, J. H., Zeng, G. M., Zhou, C. F., Li, X., Shi, L. J. and He, S.-B. (2010). "Adsorption of surfactant micelles and Cd^{2+}/Zn^{2+} in micellar-enhanced ultrafiltration." *J. Hazard. Mater.*, 183(1), 287-293.

Huang, J. H., Zeng, G. M., Zhou, C. F., Li, X., Shi, L. J. and He, S. B. (2010). "Adsorption of surfactant micelles and Cd^{2+}/Zn^{2+} in micellar-enhanced ultrafiltration." *J. Hazard. Mater.*, 183(1-3), 287-93.

Hussain, S. M., Hess, K. L., Gearhart, J. M., Geiss, K. T. and Schlager, J. J. (2005). "In vitro toxicity of nanoparticles in BRL 3A rat liver cells." *Toxicology in vitro*, 19(7), 975-983.

Hwang, L. L., Tseng, H. H. and Chen, J. C. (2011). "Fabrication of polyphenylsulfone/polyetherimide blend membranes for ultrafiltration applications: The effects of blending ratio on membrane properties and humic acid removal performance." *J. Membr. Sci.*, 384(1-2), 72-81.

Hwang, L. L., Chen, J. C. and Wey, M. Y. (2013). "The properties and filtration efficiency of activated carbon polymer composite membranes for the removal of humic acid." *Desalination*, 313, 166-175.

Isloor, A. M., Shenvi, S. S., Ismail, A. F., Shilton, S. J. and Al-Ahmad, D. A. (2015). "Humic Acid Based Biopolymeric Membrane for Effective Removal of Methylene Blue and Rhodamine B." *Ind. Eng. Chem. Res.*, 54(18,), 4965-4975

Jansen, J., Macchione, M. and Drioli, E. (2005). "High flux asymmetric gas separation membranes of modified poly (ether ether ketone) prepared by the dry phase inversion technique." *J. Membr. Sci.*, 255(1), 167-180.

Jia, Z. and Xu, W. (2001). "Synthesis and antibacterial activities of quaternary ammonium salt of chitosan." *Carbohydr. Res.*, 333(1), 1-6.

Jin, X., Huang, X. and Hoek, E. M. (2009). "Role of specific ion interactions in seawater RO membrane fouling by alginic acid." *Environ. Sci. Technol.*, 43(10), 3580-3587.

Jin, Y. and Su, Z. (2009). "Effects of polymerization conditions on hydrophilic groups in aromatic polyamide thin films." *J. Membr. Sci.*, 330(1), 175-179.

Jones, P. J., Paslay, L. C. and Morgan, S. E. (2010). "Effects of chain conformation on miscibility, morphology, and mechanical properties of solution blended substituted polyphenylene and polyphenylsulfone." *Polymer*, 51(3), 738-747.

Julien, C., Khelfa, A., Hussain, O. and Nazri, G. (1995). "Synthesis and characterization of flash-evaporated MoO_3 thin films." *J. Cryst. Growth*, 156(3), 235-244.

Kajekar, A. J., Dodamani, B., Isloor, A. M., Karim, Z. A., Cheer, N. B., Ismail, A. and Shilton, S. J. (2015). "Preparation and characterization of novel PSf/PVP/PANI-nanofiber nanocomposite hollow fiber ultrafiltration membranes and their possible applications for hazardous dye rejection." *Desalination*, 365, 117-125.

Kaner, P., Rubakh, E. and Asatekin, A. (2017). "Zwitterion-containing polymer additives for fouling resistant ultrafiltration membranes." *J. Membr. Sci.*, 533, 141-159

Kapnisti, M. G., Noli, F. G., Arvanitidis, J. and Hatzidimitriou, A. G. (2016). "Thermally modified molybdenum oxide as a potential sorbent for the removal of metal cations from aqueous solutions." *J. Radioanal. Nucl. Chem.*, 307(1), 555-565.

Khorshidi, B., Soltannia, B., Thundat, T. and Sadrzadeh, M. (2017). "Synthesis of thin film composite polyamide membranes: Effect of monohydric and polyhydric alcohol additives in aqueous solution." *J. Membr. Sci.*, 523, 336-345.

Kiani, S., Mousavi, S. M., Shahtahmassebi, N. and Saljoughi, E. (2015). "Hydrophilicity improvement in polyphenylsulfone nanofibrous filtration membranes through addition of polyethylene glycol." *Appl. Surf. Sci.*, 359, 252-258.

Kim, H. J., Nah, S. S. and Min, B. R. (2002). "A new technique for preparation of PDMS pervaporation membrane for VOC removal." *Adv. Environ. Res.*, 6(3), 255-264.

Kim, I. C., Jeong, B. R., Kim, S. J. and Lee, K. H. (2013). "Preparation of high flux thin film composite polyamide membrane: the effect of alkyl phosphate additives during interfacial polymerization." *Desalination*, 308, 111-114.

Kim, J. D., Donnadio, A., Jun, M. S. and Di Vona, M. L. (2013). "Crosslinked SPES-SPPSU membranes for high temperature PEMFCs." *Int. J. Hydrogen Energy*, 38(3), 1517-1523.

Kim, J. and Van der Bruggen, B. (2010). "The use of nanoparticles in polymeric and ceramic membrane structures: review of manufacturing procedures and performance improvement for water treatment." *Environ. Pollut.*, 158(7), 2335-2349.

Kim, W. S., Kim, H. C. and Hong, S. H. (2010). "Gas sensing properties of MoO_3 nanoparticles synthesized by solvothermal method." *J. Nanopart. Res*, 12(5), 1889-1896.

Kolff, W., Berk, H., Welle, N. M., Ley, A., Dijk, E. and Noordwijk, J. (1944). "The artificial kidney: a dialyser with a great area." *Acta Med. Scand.*, 117(2), 121-134.

Krishnamoorthy, K., Veerapandian, M., Zhang, L. H., Yun, K. and Kim, S. J. (2012). "Antibacterial efficiency of graphene nanosheets against pathogenic bacteria via lipid peroxidation." *The Journal of Physical Chemistry C*, 116(32), 17280-17287.

Kumar, R., Isloor, A. M., Ismail, A. F. and Matsuura, T. (2013). "Performance improvement of polysulfone ultrafiltration membrane using N-succinyl chitosan as additive." *Desalination*, 318, 1-8.

Kumar, R., Isloor, A. M., Ismail, A. F., Rashid, S. A. and Al Ahmed, A. (2013). "Permeation, antifouling and desalination performance of TiO_2 nanotube incorporated PSf/CS blend membranes." *Desalination*, 316, 76-84.

Kumar, R., Isloor, A. M., Ismail, A. F., Rashid, S. A. and Matsuura, T. (2013). "Polysulfone–Chitosan blend ultrafiltration membranes: preparation, characterization, permeation and antifouling properties." *RSC Adv.*, 3(21), 7855-7861.

Kumar, R., Ismail, A. F., Kassim, M. A. and Isloor, A. M. (2013). "Modification of PSf/PIAM membrane for improved desalination applications using Chitosan coagulation media." *Desalination*, 317, 108-115.

Kumar, R., Isloor, A. M. and Ismail, A. (2014). "Preparation and evaluation of heavy metal rejection properties of polysulfone/chitosan, polysulfone/N-succinyl chitosan and polysulfone/N-propylphosphonyl chitosan blend ultrafiltration membranes." *Desalination*, 350, 102-108.

Lalia, B. S., Kochkodan, V., Hashaikeh, R. and Hilal, N. (2013). "A review on membrane fabrication: Structure, properties and performance relationship." *Desalination*, 326, 77-95.

Lau, W. J., Ismail, A. F., Misdan, N. and Kassim, M. A. (2012). "A recent progress in thin film composite membrane: a review." *Desalination*, 287, 190-199.

Li, H., Lin, Y., Luo, Y., Yu, P. and Hou, L. (2011). "Relating organic fouling of reverse osmosis membranes to adsorption during the reclamation of secondary

effluents containing methylene blue and rhodamine B." *J. Hazard. Mater.*, 192(2), 490-499.

Li, N. N., Fane, A. G., Ho, W. W. and Matsuura, T. (2011). *Advanced membrane technology and applications,* John Wiley & Sons, Canada.

Li, Q., Xu, Z. L. and Liu, M. (2011). "Preparation and characterization of PVDF microporous membrane with highly hydrophobic surface." *Polymer. Adv. Tech.*, 22(5), 520-531.

Li, Z., Zhuang, X. P., Liu, X. F., Guan, Y. L. and De Yao, K. (2002). "Study on antibacterial O-carboxymethylated chitosan/cellulose blend film from LiCl/N, N-dimethylacetamide solution." *Polymer*, 43(4), 1541-1547.

Liau, S., Read, D., Pugh, W., Furr, J. and Russell, A. (1997). "Interaction of silver nitrate with readily identifiable groups: relationship to the antibacterial action of silver ions." *Lett Appl Microbiol*, 25(4), 279-283.

Liu, G., Zhang, L., Mao, S., Rohani, S., Ching, C. and Lu, J. (2015). "Zwitterionic chitosan–silica–PVA hybrid ultrafiltration membranes for protein separation." *Sep. Purif. Technol.*, 152, 55-63.

Liu, J. and Hurt, R. H. (2010). "Ion release kinetics and particle persistence in aqueous nano-silver colloids." *Environ. Sci. Technol.*, 44(6), 2169-2175.

Liu, J., Ma, Y., Xu, T. and Shao, G. (2010). "Preparation of zwitterionic hybrid polymer and its application for the removal of heavy metal ions from water." *J. Hazard. Mater.*, 178(1-3), 1021-9.

Liu, Y., Yue, X., Zhang, S., Ren, J., Yang, L., Wang, Q. and Wang, G. (2012). "Synthesis of sulfonated polyphenylsulfone as candidates for antifouling ultrafiltration membrane." *Sep. Purif. Technol.*, 98, 298-307.

Liu, Y., Zhang, S., Zhou, Z., Ren, J., Geng, Z., Luan, J. and Wang, G. (2012). "Novel sulfonated thin-film composite nanofiltration membranes with improved water flux for treatment of dye solutions." *J. Membr. Sci.*, 394, 218-229.

Liu, Y., Zhang, S. and Wang, G. (2013). "The preparation of antifouling ultrafiltration membrane by surface grafting zwitterionic polymer onto poly(arylene ether sulfone) containing hydroxyl groups membrane." *Desalination*, 316, 127-136.

Lonsdale, H. (1982). "The growth of membrane technology." *J. Membr. Sci.*, 10(2), 81-181.

Lou, X. W. and Zeng, H. C. (2002). "Hydrothermal synthesis of α-MoO$_3$ nanorods via acidification of ammonium heptamolybdate tetrahydrate." *Chem. Mater.*, 14(11), 4781-4789.

Lutchmiah, K., Lauber, L., Roest, K., Harmsen, D. J., Post, J. W., Rietveld, L. C., van Lier, J. B. and Cornelissen, E. R. (2014). "Zwitterions as alternative draw solutions in forward osmosis for application in wastewater reclamation." *J. Membr. Sci.*, 460, 82-90.

Ma, Y., Zhou, T. and Zhao, C. (2008). "Preparation of chitosan–nylon-6 blended membranes containing silver ions as antibacterial materials." *Carbohydr. Res.*, 343(2), 230-237.

Ma, Y., Shi, F., Ma, J., Wu, M., Zhang, J. and Gao, C. (2011). "Effect of PEG additive on the morphology and performance of polysulfone ultrafiltration membranes." *Desalination*, 272(1-3), 51-58.

Madaeni, S. and Rahimpour, A. (2005). "Effect of type of solvent and non-solvents on morphology and performance of polysulfone and polyethersulfone ultrafiltration membranes for milk concentration." *Polymers for advanced technologies*, 16(10), 717-724.

Mahon, H. I. (1966). "Permeability separatory apparatus and process utilizing hollow fibers." 3,228,877.

Majewska-Nowak, K. (1989). "Synthesis and properties of polysulfone membranes." *Desalination*, 71(2), 83-95.

Malaisamy, R., Mohan, D. R. and Rajendran, M. (2002). "Polyurethane and sulfonated polysulfone blend ultrafiltration membranes: I. Preparation and characterization studies." *J. Colloid Interface Sci.*, 254(1), 129-140.

Malaisamy, R., Mohan, D. R. and Rajendran, M. (2002). "Polyurethane and Sulfonated Polysulfone Blend Ultrafiltration Membranes." *J. Colloid Interface Sci.*, 254(1), 129-140.

Malaisamy, R., Mohan, D. R. and Rajendran, M. (2003). "Polyurethane and sulfonated polysulfone blend ultrafiltration membranes: II. Application studies." *Polym. Int.*, 52(3), 412-419.

Manivel, A., Lee, G. J., Chen, C. Y., Chen, J. H., Ma, S. H., Horng, T. L. and Wu, J. J. (2015). "Synthesis of MoO_3 nanoparticles for azo dye degradation by catalytic ozonation." *Mater. Res. Bull.*, 62, 184-191.

Martín, A., Arsuaga, J. M., Roldán, N., de Abajo, J., Martínez, A. and Sotto, A. (2015). "Enhanced ultrafiltration PES membranes doped with mesostructured functionalized silica particles." *Desalination*, 357, 16-25.

Mbareck, C., Nguyen, Q. T., Alaoui, O. T. and Barillier, D. (2009). "Elaboration, characterization and application of polysulfone and polyacrylic acid blends as ultrafiltration membranes for removal of some heavy metals from water." *J. Hazard. Mater.*, 171(1-3), 93-101.

Mbareck, C., Nguyen, Q. T., Alaoui, O. T. and Barillier, D. (2009). "Elaboration, characterization and application of polysulfone and polyacrylic acid blends as ultrafiltration membranes for removal of some heavy metals from water." *J. Hazard. Mater.*, 171(1), 93-101.

Mi, B. and Elimelech, M. (2010). "Organic fouling of forward osmosis membranes: fouling reversibility and cleaning without chemical reagents." *J. Membr. Sci.*, 348(1), 337-345.

Michailovski, A., Grunwaldt, J. D., Baiker, A., Kiebach, R., Bensch, W. and Patzke, G. R. (2005). "Studying the solvothermal formation of MoO_3 fibers by

complementary in situ EXAFS/EDXRD techniques." *Angew. Chem. Int. Ed. Engl.*, 44(35), 5643-5647.

Molinari, R., Gallo, S. and Argurio, P. (2004). "Metal ions removal from wastewater or washing water from contaminated soil by ultrafiltration-complexation." *Water Res*, 38(3), 593-600.

Molinari, R., Poerio, T. and Argurio, P. (2008). "Selective separation of copper (II) and nickel (II) from aqueous media using the complexation–ultrafiltration process." *Chemosphere*, 70(3), 341-348.

Mulder, M. (1996). "Membrane Processes." *Basic Principles of Membrane Technology Second Edition,* Kluwer Academic Publishers, Netherlands, 280-412.

Müller, R., Jacobs, C. and Kayser, O. (2001). "Nanosuspensions as particulate drug formulations in therapy: rationale for development and what we can expect for the future." *Adv. Drug Deliv. Rev.*, 47(1), 3-19.

Nazri, G. A. and Julien, C. (1992). "Far-infrared and Raman studies of orthorhombic MoO 3 single crystal." *Solid State Ionics*, 53, 376-382.

Ngah, W. W., Teong, L. and Hanafiah, M. (2011). "Adsorption of dyes and heavy metal ions by chitosan composites: A review." *Carbohydr. Polym.*, 83(4), 1446-1456.

Nollet, J. A. (1995). "Investigations on the causes for the ebullition of liquids." *J. Membr. Sci.*, 100(1), 1-3.

Oh, S. J., Kim, N. and Lee, Y. T. (2009). "Preparation and characterization of PVDF/TiO$_2$ organic–inorganic composite membranes for fouling resistance improvement." *J. Membr. Sci.*, 345(1), 13-20.

Pabby, A. K., Rizvi, S. S. and Requena, A. M. S. (2015). *Handbook of membrane separations: chemical, pharmaceutical, food, and biotechnological applications,* CRC press, London.

Padaki, M., Isloor, A. M. and Wanichapichart, P. (2011). "Polysulfone/N-phthaloylchitosan novel composite membranes for salt rejection application." *Desalination*, 279(1), 409-414.

Padaki, M., Isloor, A. M., Ismail, A. F. and Abdullah, M. S. (2012). "Synthesis, characterization and desalination study of novel PSAB and mPSAB blend membranes with Polysulfone (PSf)." *Desalination*, 295, 35-42.

Panda, S. R. and De, S. (2014). "Preparation, characterization and performance of $ZnCl_2$ incorporated polysulfone (PSF)/polyethylene glycol (PEG) blend low pressure nanofiltration membranes." *Desalination*, 347, 52-65.

Pandian, S., Katha, A. R., Moon, J. H., Kolake, S. M. and Han, S. (2015). "Exploring the effect of additives on polyamide membrane surface for seawater desalination using density functional tools." *Desalination*, 367, 28-36.

Paraguay-Delgado, F., Albiter, M., Huirache-Acuña, R., Verde, Y. and Alonso-Nuñez, G. (2007). "Optimization of the synthesis of α-MoO_3 nanoribbons and hydrodesulfurization (HDS) Catalyst Test." *J. Nanosci. Nanotechnol*, 7(10), 3677-3683.

Park, A. M., Wycisk, R. J., Ren, X., Turley, F. E. and Pintauro, P. N. (2016). "Crosslinked poly (phenylene oxide)-based nanofiber composite membranes for alkaline fuel cells." *J. Mater. Chem. A*, 4(1), 132-141.

Peighambardoust, S., Rowshanzamir, S. and Amjadi, M. (2010). "Review of the proton exchange membranes for fuel cell applications." *Int. J. Hydrogen Energy*, 35(17), 9349-9384.

Pellegrin, B., Mezzari, F., Hanafi, Y., Szymczyk, A., Remigy, J. C. and Causserand, C. (2015). "Filtration performance and pore size distribution of hypochlorite aged PES/PVP ultrafiltration membranes." *J. Membr. Sci.*, 474, 175-186.

Pereira, V. R., Isloor, A. M., Bhat, U. K. and Ismail, A. F. (2014). "Preparation and antifouling properties of PVDF ultrafiltration membranes with polyaniline (PANI) nanofibers and hydrolysed PSMA (H-PSMA) as additives." *Desalination*, 351, 220-227.

Pereira, V. R., Isloor, A. M., Al Ahmed, A. and Ismail, A. (2015). "Preparation, characterization and the effect of PANI coated TiO_2 nanocomposites on the

performance of polysulfone ultrafiltration membranes." *New J. Chem.*, 39(1), 703-712.

Pereira, V. R., Isloor, A. M., Zulhairun, A., Subramaniam, M., Lau, W. and Ismail, A. (2016). "Preparation of polysulfone-based PANI–TiO$_2$ nanocomposite hollow fiber membranes for industrial dye rejection applications." *RSC Adv.*, 6(102), 99764-99773.

Perkins, C. K., Barber, K. N. and Apblett, A. W. (2014). "Direct conversion of a nanometric suspension of molybdenum trioxide into nanometric lead molybdate." *Cryst. Eng. Comm.*, 16(14), 2869-2873.

Peyravi, M., Rahimpour, A. and Jahanshahi, M. (2012). "Thin film composite membranes with modified polysulfone supports for organic solvent nanofiltration." *J. Membr. Sci.*, 423-424, 225-237.

Phuruangrat, A., Chen, J. S., Lou, X. W., Yayapao, O., Thongtem, S. and Thongtem, T. (2012). "Hydrothermal synthesis and electrochemical properties of α-MoO$_3$ nanobelts used as cathode materials for Li-ion batteries." *Appl. Phys. A*, 107(1), 249-254.

Pinnau, I. and Freeman, B. (2000). "Formation and modification of polymeric membranes: overview." *Membrane Formation and Modification*, 744, 1-22.

Pollack, N., Cunningham, A. R. and Rosenkranz, H. S. (2003). "Environmental persistence of chemicals and their carcinogenic risks to humans." *Mutat Res Fund Mol Mech Mut*, 528(1), 81-91.

Praneeth, K., James, T. and Sridhar, S. (2014). "Design of novel ultrafiltration systems based on robust polyphenylsulfone hollow fiber membranes for treatment of contaminated surface water." *Chem. Eng. J.*, 248, 297-306.

Qi, L., Xu, Z., Jiang, X., Hu, C. and Zou, X. (2004). "Preparation and antibacterial activity of chitosan nanoparticles." *Carbohydr. Res.*, 339(16), 2693-2700.

Qin, J. and Chung, T. S. (1999). "Effect of dope flow rate on the morphology, separation performance, thermal and mechanical properties of ultrafiltration hollow fibre membranes." *J. Membr. Sci.*, 157(1), 35-51.

Quinn, R., Laciak, D. and Pez, G. (1997). "Polyelectrolyte-salt blend membranes for acid gas separations." *J. Membr. Sci.*, 131(1), 61-69.

Ramalingam, B., Khan, M. M. R., Mondal, B., Mandal, A. B. and Das, S. K. (2015). "Facile Synthesis of Silver Nanoparticles Decorated Magnetic-Chitosan Microsphere for Efficient Removal of Dyes and Microbial Contaminants." *ACS Sustain. Chem. Eng.*, 3(9), 2291-2302.

Razmjou, A., Mansouri, J. and Chen, V. (2011). "The effects of mechanical and chemical modification of TiO_2 nanoparticles on the surface chemistry, structure and fouling performance of PES ultrafiltration membranes." *J. Membr. Sci.*, 378(1-2), 73-84.

Razmjou, A., Resosudarmo, A., Holmes, R. L., Li, H., Mansouri, J. and Chen, V. (2012). "The effect of modified TiO_2 nanoparticles on the polyethersulfone ultrafiltration hollow fiber membranes." *Desalination*, 287, 271-280.

Reid, C. E. and Breton, E. J. (1959). "Water and ion flow across cellulosic membranes." *J. Appl. Polym. Sci.*, 1(2), 133-143.

Remko, M., Fitz, D. and Rode, B. M. (2010). "Effect of metal ions (Li^+, Na^+, K^+, Mg^{2+}, Ca^{2+}, Ni^{2+}, Cu^{2+} and Zn^{2+}) and water coordination on the structure and properties of l-histidine and zwitterionic l-histidine." *Amino Acids*, 39(5), 1309-1319.

Roh, I. J., Greenberg, A. R. and Khare, V. P. (2006). "Synthesis and characterization of interfacially polymerized polyamide thin films." *Desalination*, 191(1-3), 279-290.

Rucka, M., Poźniak, G., Turkiewicz, B. and Trochimczuk, W. (1996). "Ultrafiltration membranes from polysulfone/aminated polysulfone blends with proteolytic activity." *Enzyme Microb. Technol.*, 18(7), 477-481.

Sajitha, C., Mahendran, R. and Mohan, D. (2002). "Studies on cellulose acetate–carboxylated polysulfone blend ultrafiltration membranes—Part I." *Eur. Polym. J.*, 38(12), 2507-2511.

Saljoughi, E., Amirilargani, M. and Mohammadi, T. (2009). "Effect of poly (vinyl pyrrolidone) concentration and coagulation bath temperature on the morphology,

permeability, and thermal stability of asymmetric cellulose acetate membranes." *J. Appl. Polym. Sci.*, 111(5), 2537-2544.

Sengur, R., de Lannoy, C. F., Turken, T., Wiesner, M. and Koyuncu, I. (2015). "Fabrication and characterization of hydroxylated and carboxylated multiwalled carbon nanotube/polyethersulfone (PES) nanocomposite hollow fiber membranes." *Desalination*, 359, 123-140.

Shafaei, S., Dörrstein, J., Guggenbichler, J. P. and Zollfrank, C. (2017). "Cellulose acetate-based composites with antimicrobial properties from embedded molybdenum trioxide particles." *Lett Appl Microbiol*, 64(1), 43-50.

Shannon, M. A., Bohn, P. W., Elimelech, M., Georgiadis, J. G., Marinas, B. J. and Mayes, A. M. (2008). "Science and technology for water purification in the coming decades." *Nature*, 452(7185), 301-310.

Shenvi, S., Ismail, A. and Isloor, A. M. (2014). "Enhanced Permeation Performance of Cellulose Acetate Ultrafiltration Membranes by Incorporation of Sulfonated Poly (1, 4-phenylene ether ether sulfone) and Poly (styrene-co-maleic anhydride)." *Ind. Eng. Chem. Res.*, 53(35), 13820-13827.

Shenvi, S. S., Rashid, S. A., Ismail, A. F., Kassim, M. A. and Isloor, A. M. (2013). "Preparation and characterization of PPEES/chitosan composite nanofiltration membrane." *Desalination*, 315, 135-141.

Shi, Q., Su, Y., Zhao, W., Li, C., Hu, Y., Jiang, Z. and Zhu, S. (2008). "Zwitterionic polyethersulfone ultrafiltration membrane with superior antifouling property." *J. Membr. Sci.*, 319(1-2), 271-278.

Shukla, A. K., Alam, J., Alhoshan, M., Dass, L. A. and Muthumareeswaran, M. (2017). "Development of a nanocomposite ultrafiltration membrane based on polyphenylsulfone blended with graphene oxide." *Scientific Reports*, 7, 1-12.

Silver, S. (2003). "Bacterial silver resistance: molecular biology and uses and misuses of silver compounds." *FEMS Microbiol. Rev.*, 27(2-3), 341-353.

Singh, P., Rao, A., Ray, P., Bhattacharya, A., Singh, K., Saha, N. and Reddy, A. (2011). "Techniques for characterization of polyamide thin film composite membranes." *Desalination*, 282, 78-86.

Sivakumar, M., Mohan, D. R., Rangarajan, R. and Tsujita, Y. (2005). "Studies on cellulose acetate–polysulfone ultrafiltration membranes: I. Effect of polymer composition." *Polym. Int.*, 54(6), 956-962.

Sivakumar, M., Mohan, D. R. and Rangarajan, R. (2006). "Studies on cellulose acetate-polysulfone ultrafiltration membranes: II. Effect of additive concentration." *J. Membr. Sci.*, 268(2), 208-219.

Sondi, I. and Salopek-Sondi, B. (2004). "Silver nanoparticles as antimicrobial agent: a case study on *E. coli* as a model for Gram-negative bacteria." *J. Colloid Interface Sci.*, 275(1), 177-182.

Soroush, A., Barzin, J., Barikani, M. and Fathizadeh, M. (2012). "Interfacially polymerized polyamide thin film composite membranes: Preparation, characterization and performance evaluation." *Desalination*, 287, 310-316.

Staude, E. and Breitbach, L. (1991). "Polysulfones and their derivatives: materials for membranes for different separation operations." *J. Appl. Polym. Sci.*, 43(3), 559-566.

Stefancich, S., Delben, F. and Muzzarelli, R. (1994). "Interaction of soluble chitosans with dyes in water. I. Optical evidence." *Carbohydr. Polym.*, 24(1), 17-23.

Strathmann, H. and Kock, K. (1977). "The formation mechanism of phase inversion membranes." *Desalination*, 21(3), 241-255.

Sun, Q., Su, Y., Ma, X., Wang, Y. and Jiang, Z. (2006). "Improved antifouling property of zwitterionic ultrafiltration membrane composed of acrylonitrile and sulfobetaine copolymer." *J. Membr. Sci.*, 285(1-2), 299-305.

Sunu, S., Prabhu, E., Jayaraman, V., Gnanasekar, K., Seshagiri, T. and Gnanasekaran, T. (2004). "Electrical conductivity and gas sensing properties of MoO_3." *Sens Actuators B Chem*, 101(1), 161-174.

Susanto, H. and Ulbricht, M. (2009). "Characteristics, performance and stability of polyethersulfone ultrafiltration membranes prepared by phase separation method using different macromolecular additives." *J. Membr. Sci.*, 327(1-2), 125-135.

Takagishi, T., Okuda, S., Kuroki, N. and Kozuka, H. (1985). "Binding of metal ions by polyethylenimine and its derivatives." *J. Polym. Sci. Polym. Chem. Ed.*, 23(8), 2109-2116.

Tang, C. Y., Kwon, Y. N. and Leckie, J. O. (2009). "Effect of membrane chemistry and coating layer on physiochemical properties of thin film composite polyamide RO and NF membranes: II. Membrane physiochemical properties and their dependence on polyamide and coating layers." *Desalination*, 242(1-3), 168-182.

Tang, E., Huang, M. and Lim, L. (2003). "Ultrasonication of chitosan and chitosan nanoparticles." *Int. J. Pharm.*, 265(1), 103-114.

Tang, Y., Widjojo, N., Shi, G. M., Chung, T. S., Weber, M. and Maletzko, C. (2012). "Development of flat-sheet membranes for C1–C4 alcohols dehydration via pervaporation from sulfonated polyphenylsulfone (sPPSU)." *J. Membr. Sci.*, 415, 686-695.

Teli, S. B., Molina, S., Calvo, E. G., Lozano, A. E. and de Abajo, J. (2012). "Preparation, characterization and antifouling property of polyethersulfone–PANI/PMA ultrafiltration membranes." *Desalination*, 299, 113-122.

Thombre, A., Cardinal, J., DeNoto, A. and Gibbes, D. (1999). "Asymmetric membrane capsules for osmotic drug delivery II. In vitro and in vivo drug release performance." *J. Controlled Release*, 57(1), 65-73.

Traube, M. (1867). "Physiologie und wissenschaftliche Medizin." *Arch. An. Physiol*, 87.

Van der Bruggen, B. and Vandecasteele, C. (2003). "Removal of pollutants from surface water and groundwater by nanofiltration: overview of possible applications in the drinking water industry." *Environ. Pollut.*, 122(3), 435-445.

Vatanpour, V., Madaeni, S. S., Moradian, R., Zinadini, S. and Astinchap, B. (2011). "Fabrication and characterization of novel antifouling nanofiltration membrane prepared from oxidized multiwalled carbon nanotube/polyethersulfone nanocomposite." *J. Membr. Sci.*, 375(1), 284-294.

Venkatesan, J., Lee, J. Y., Kang, D. S., Anil, S., Kim, S. K., Shim, M. S. and Kim, D. G. (2017). "Antimicrobial and anticancer activities of porous chitosan-alginate biosynthesized silver nanoparticles." *Int. J. Biol. Macromol.*, 98, 515-525.

Vijayalakshmi, A., Arockiasamy, D. L., Nagendran, A. and Mohan, D. (2008). "Separation of proteins and toxic heavy metal ions from aqueous solution by CA/PC blend ultrafiltration membranes." *Sep. Purif. Technol.*, 62(1), 32-38.

Vrijenhoek, E. M., Hong, S. and Elimelech, M. (2001). "Influence of membrane surface properties on initial rate of colloidal fouling of reverse osmosis and nanofiltration membranes." *J. Membr. Sci.*, 188(1), 115-128.

Wang, P., Ma, J., Wang, Z., Shi, F. and Liu, Q. (2012). "Enhanced separation performance of PVDF/PVP-g-MMT nanocomposite ultrafiltration membrane based on the NVP-grafted polymerization modification of montmorillonite (MMT)." *Langmuir*, 28(10), 4776-4786.

Wang, X., Zhang, L., Sun, D., An, Q. and Chen, H. (2008). "Effect of coagulation bath temperature on formation mechanism of poly (vinylidene fluoride) membrane." *J. Appl. Polym. Sci.*, 110(3), 1656-1663.

Wei, G., Yu, H., Quan, X., Chen, S., Zhao, H. and Fan, X. (2014). "Constructing all carbon nanotube hollow fiber membranes with improved performance in separation and antifouling for water treatment." *Environ. Sci. Technol.*, 48(14), 8062-8068.

Weng, T. H., Tseng, H. H. and Wey, M. Y. (2008). "Preparation and characterization of PPSU/PBNPI blend membrane for hydrogen separation." *Int. J. Hydrogen Energy*, 33(15), 4178-4182.

Weng, T. H., Tseng, H. H. and Wey, M. Y. (2010). "Effects of crosslinking modification on the O_2/N_2 separation characteristics of poly (phenyl sulfone)/poly

(bisphenol A-co-4-nitrophthalic anhydride-co-1, 3-phenylenediamine) blend membranes." *J. Appl. Polym. Sci.*, 116(3), 1254-1263.

Weng, X., Ji, Y., Zhao, F., An, Q. and Gao, C. (2015). "Tailoring the structure of polyamide thin film composite membrane with zwitterions to achieve high water permeability and antifouling property." *RSC Adv.*, 5(120), 98730-98739.

White, A. and Jiang, S. (2010). "Local and bulk hydration of zwitterionic glycine and its analogues through molecular simulations." *J. Phys. Chem. B*, 115(4), 660-667.

Wongchitphimon, S., Wang, R., Jiraratananon, R., Shi, L. and Loh, C. H. (2011). "Effect of polyethylene glycol (PEG) as an additive on the fabrication of polyvinylidene fluoride-co-hexafluropropylene (PVDF-HFP) asymmetric microporous hollow fiber membranes." *J. Membr. Sci.*, 369(1-2), 329-338.

Wu, F. C., Tseng, R. L. and Juang, R. S. (2010). "A review and experimental verification of using chitosan and its derivatives as adsorbents for selected heavy metals." *J. Environ. Manage.*, 91(4), 798-806.

Wu, P. and Imai, M. (2012). *Novel biopolymer composite membrane involved with selective mass transfer and excellent water permeability,* INTECH Open Access Publisher, Croatia,

Wu, Y., Yang, W., Wang, C., Hu, J. and Fu, S. (2005). "Chitosan nanoparticles as a novel delivery system for ammonium glycyrrhizinate." *Int. J. Pharm.*, 295(1), 235-245.

Xie, W., Geise, G. M., Freeman, B. D., Lee, H. S., Byun, G. and McGrath, J. E. (2012). "Polyamide interfacial composite membranes prepared from m-phenylene diamine, trimesoyl chloride and a new disulfonated diamine." *J. Membr. Sci.*, 403, 152-161.

Xu, J., Tang, Y., Wang, Y., Shan, B., Yu, L. and Gao, C. (2014). "Effect of coagulation bath conditions on the morphology and performance of PSf membrane blended with a capsaicin-mimic copolymer." *J. Membr. Sci.*, 455, 121-130.

Xu, X., Yang, Y. Q., Xing, Y. Y., Yang, J. F. and Wang, S. F. (2013). "Properties of novel polyvinyl alcohol/cellulose nanocrystals/silver nanoparticles blend membranes." *Carbohydr Polym*, 98(2), 1573-7.

Xu, Z. L. and Qusay, F. A. (2004). "Polyethersulfone (PES) hollow fiber ultrafiltration membranes prepared by PES/non-solvent/NMP solution." *J. Membr. Sci.*, 233(1), 101-111.

Yam-Cervantes, M., Santiago-García, J., Loría-Bastarrachea, M., Duarte-Aranda, S., Alberto Ruiz-Treviño, F. and Aguilar-Vega, M. (2017). "Sulfonated polyphenylsulfone asymmetric membranes: Effect of coagulation bath (acetic acid-NaHCO$_3$/isopropanol) on morphology and antifouling properties." *J. Appl. Polym. Sci.*, 134(8),

Yang, S. and Liu, Z. (2003). "Preparation and characterization of polyacrylonitrile ultrafiltration membranes." *J. Membr. Sci.*, 222(1), 87-98.

Yang, X., Du, Y., Zhang, X., He, A. and Xu, Z. K. (2017). "Nanofiltration Membrane with a Mussel-Inspired Interlayer for Improved Permeation Performance." *Langmuir*, 33(9), 2318-2324.

Yu, L. Y., Xu, Z. L., Shen, H. M. and Yang, H. (2009). "Preparation and characterization of PVDF–SiO$_2$ composite hollow fiber UF membrane by sol–gel method." *J. Membr. Sci.*, 337(1-2), 257-265.

Yu, Z., Zhao, Y., Gao, B., Liu, X., Jia, L., Zhao, F. and Ma, J. (2015). "Performance of novel a Ag-n-TiO$_2$/PVC reinforced hollow fiber membrane applied in water purification: in situ antibacterial properties and resistance to biofouling." *RSC Adv.*, 5(118), 97320-97329.

Yuliwati, E., Ismail, A. F., Matsuura, T., Kassim, M. A. and Abdullah, M. S. (2011). "Characterization of surface-modified porous PVDF hollow fibers for refinery wastewater treatment using microscopic observation." *Desalination*, 283, 206-213.

Yuliwati, E., Ismail, A. F., Matsuura, T., Kassim, M. A. and Abdullah, M. S. (2011). "Effect of modified PVDF hollow fiber submerged ultrafiltration membrane for refinery wastewater treatment." *Desalination*, 283, 214-220.

Yung, L., Ma, H., Wang, X., Yoon, K., Wang, R., Hsiao, B. S. and Chu, B. (2010). "Fabrication of thin-film nanofibrous composite membranes by interfacial polymerization using ionic liquids as additives." *J. Membr. Sci.*, 365(1), 52-58.

Yunos, M. Z., Harun, Z., Basri, H. and Ismail, A. F. (2014). "Studies on fouling by natural organic matter (NOM) on polysulfone membranes: Effect of polyethylene glycol (PEG)." *Desalination*, 333(1), 36-44.

Zeng, X., Zhang, X., Yang, M. and Qi, Y. (2013). "A facile hydrothermal method for the fabrication of one-dimensional MoO_3 nanobelts." *Mater. Lett.*, 112, 87-89.

Zha, S., Yu, J., Zhang, G., Liu, N. and Lee, R. (2015). "Polyethersulfone (PES)/cellulose acetate butyrate (CAB) composite hollow fiber membranes for BTEX separation from produced water." *RSC Adv.*, 5(128), 105692-105698.

Zhang, L., Yu, J. C., Yip, H. Y., Li, Q., Kwong, K. W., Xu, A. W. and Wong, P. K. (2003). "Ambient light reduction strategy to synthesize silver nanoparticles and silver-coated TiO_2 with enhanced photocatalytic and bactericidal activities." *Langmuir*, 19(24), 10372-10380.

Zhang, X., Lv, Y., Yang, H.-C., Du, Y. and Xu, Z. K. (2016). "Polyphenol Coating as an Interlayer for Thin-Film Composite Membranes with Enhanced Nanofiltration Performance." *ACS Appl. Mater. Interfaces*, 8(47), 32512-32519.

Zhao, J., He, X., Wang, L., Tian, J., Wan, C. and Jiang, C. (2007). "Addition of NH_4HCO_3 as pore-former in membrane electrode assembly for PEMFC." *Int. J. Hydrogen Energy*, 32(3), 380-384.

Zhao, L., Chang, P. C. Y. and Ho, W. W. (2013). "High-flux reverse osmosis membranes incorporated with hydrophilic additives for brackish water desalination." *Desalination*, 308, 225-232.

Zhao, L. and Ho, W. W. (2014). "Novel reverse osmosis membranes incorporated with a hydrophilic additive for seawater desalination." *J. Membr. Sci.*, 455, 44-54.

Zhao, S., Wang, Z., Wei, X., Zhao, B., Wang, J., Yang, S. and Wang, S. (2012). "Performance improvement of polysulfone ultrafiltration membrane using well-dispersed polyaniline–poly (vinylpyrrolidone) nanocomposite as the additive." *Ind. Eng. Chem. Res.*, 51(12), 4661-4672.

Zhao, S., Wang, Z., Wang, J. and Wang, S. (2014). "The effect of pH of coagulation bath on tailoring the morphology and separation performance of polysulfone/polyaniline ultrafiltration membrane." *J. Membr. Sci.*, 469, 316-325.

Zhong, P. S., Widjojo, N., Chung, T. S., Weber, M. and Maletzko, C. (2012). "Positively charged nanofiltration (NF) membranes via UV grafting on sulfonated polyphenylenesulfone (sPPSU) for effective removal of textile dyes from wastewater." *J. Membr. Sci.*, 417, 52-60.

Zhu, J., Tian, M., Zhang, Y., Zhang, H. and Liu, J. (2015). "Fabrication of a novel "loose" nanofiltration membrane by facile blending with Chitosan–Montmorillonite nanosheets for dyes purification." *Chem. Eng. J. (Lausanne)*, 265, 184-193.

Zhu, J., Zhao, X. and He, C. (2015). "Zwitterionic SiO_2 nanoparticles as novel additives to improve the antifouling properties of PVDF membranes." *RSC Adv.*, 5(66), 53653-53659.

Zhu, L. P., Xu, L., Zhu, B. K., Feng, Y. X. and Xu, Y. Y. (2007). "Preparation and characterization of improved fouling-resistant PPESK ultrafiltration membranes with amphiphilic PPESK-graft-PEG copolymers as additives." *J. Membr. Sci.*, 294(1), 196-206.

Zhu, X., Tang, L., Wee, K. H., Zhao, Y. H. and Bai, R. (2011). "Immobilization of silver in polypropylene membrane for anti-biofouling performance." *Biofouling*, 27(7), 773-786.

Zhuo, Q., Ma, H., Wang, B. and Fan, F. (2008). "Degradation of methylene blue: Optimization of operating condition through a statistical technique and environmental estimate of the treated wastewater." *J. Hazard. Mater.*, 153(1), 44-51.

Zinadini, S., Zinatizadeh, A., Rahimi, M., Vatanpour, V., Zangeneh, H. and Beygzadeh, M. (2014). "Novel high flux antifouling nanofiltration membranes for dye removal containing carboxymethyl chitosan coated Fe_3O_4 nanoparticles." *Desalination*, 349, 145-154.

Zollfrank, C., Gutbrod, K., Wechsler, P. and Guggenbichler, J. P. (2012). "Antimicrobial activity of transition metal acid MoO_3 prevents microbial growth on material surfaces." *Mater. Sci. Eng., C*, 32(1), 47-54.

Zulhairun, A., Ng, B., Ismail, A., Murali, R. S. and Abdullah, M. (2014). "Production of mixed matrix hollow fiber membrane for CO_2/CH_4 separation." *Sep. Purif. Technol.*, 137, 1-12.

LIST OF PUBLICATIONS

1. Moideen K, I., Isloor, A. M., Ismail, A., Obaid, A. and Fun, H. K. (2015). "Fabrication and characterization of new PSF/PPSU UF blend membrane for heavy metal rejection." *Desalin. Water Treat.*, 57, 19810-19819.

2. Moideen K, I., Isloor, A. M., Garudachari, B. and Ismail, A. (2016). "The effect of glycine betaine additive on the PPSU/PSF ultrafiltration membrane performance." *Desalin. Water Treat.*, 57, 24788-24798.

3. Moideen K, I. and Isloor, A. M. " Separation of heavy metal and protein from wastewater by sulfonated polyphenylsulfone ultrafiltration membrane process prepared by glycine betaine enriched coagulation bath" *Revised manuscript under revision in Korean J. Chem. Eng.*

4. Moideen K, I. and Isloor, A. M. "Design of new antibiofouling hollow fiber membranes for dye rejection by embedding Chitosan and Silver-impregnated chitosan nanoparticles" *Communicated to. Environ. Chem. Lett.*

5. Moideen K, I. and Isloor, A. M. "Fabrication and chemical investigations of novel hollow fiber membranes containing molybdenum trioxide nanoparticles for the better removal of dye and heavy metal" *Communicated to J. Hazard. Mater.*

6. Moideen K, I. and Isloor, A. M. "Impact of hydrophilic additives in the thin film composite polyamide nanofiltration membrane for desalination" *Communicated to Desalination.*

LIST OF CONFERENCES ATTENDED

1. Moideen K, I. and Isloor, A. M. (2015) "Synthesis and characterization of PSF/PPSU based polymer blend ultrafiltration membrane for heavy metal rejection" at International Conference on membrane-based separations (MEMSEP-2015), The Maharaja Sayajirao University of Baroda, Gujarat, India.

2. Moideen K, I. and Isloor, A. M. (2016) "The effect of glycine betaine additive on the PPSU/PSF ultrafiltration membrane performance" at National conference on recent trends in chemical sciences (NCRTCS-2016), Manipal University, Manipal, Karnataka, India.

3. Moideen K, I. and Isloor, A. M. (2016) "Preparation, characterization of sulfonated polyphenylsulfone (sPPSU) ultrafiltration membranes for protein and toxic heavy metal separation" at International Conference on Advanced Polymer for science and technology (APST-2016), Vellore Institute of Technology, Vellore, Tamil Nadu, India.

4. Moideen K, I. and Isloor, A. M. (2017) "Fabrication of hollow fiber membrane encrusted with chitosan nanoparticle and Ag loaded chitosan nanoparticle for dye rejection and antibiofouling property" at International Conference on Recent Trends in Chemical Science (ICRCS-17), Govt. Engineering College, Bikaner, Rajasthan, India.

BIODATA

Irfana Moideen K

Phone: +91-9611316956

Email: irfanamk@gmail.com

OBJECTIVES
A skilled and hardworking researcher aiming to pursue career in research and development of novel membranes

RESEARCH INTEREST
• Polymer Science • Membrane Technology • Nanotechnology

EXPERIENCE

Organization	Description	Year
National Institute of Technology Karnataka (NITK) Surathkal	Conducted laboratory practical classes for B.Tech. and M.Sc. students	2013-17
Advanced Membrane Technology Research Centre (AMTEC), Universiti Teknologi Malaysia, Skudai, Johor, Malaysia	Worked as a research student intern for two moths	2016
Indian Institute of Science (IISc.), Bangalore	Worked as summer intern for 2 months	2012

EDUCATION

Degree	Institution	Year
Ph.D. Chemistry	National Institute of Technology Karnataka	2013-2017
M.Sc. Chemistry	National Institute of Technology Karnataka	20011-2013
B.Sc.	St Aloysius College, Mangalore	2008-2011

SKILLS		
Polymer synthesis	Membrane fabrication	Instrumentation analysis

PUBLICATIONS

1. Moideen K, I., Isloor, A. M., Ismail, A., Obaid, A. and Fun, H. K. (2015). "Fabrication and characterization of new PSF/PPSU UF blend membrane for heavy metal rejection." *Desalin. Water Treat.*, 57, 19810-19819.

2. Moideen K, I., Isloor, A. M., Garudachari, B. and Ismail, A. (2016). "The effect of glycine betaine additive on the PPSU/PSF ultrafiltration membrane performance." *Desalin. Water Treat.*, 57, 24788-24798.

CONFERENCES

1. Moideen K, I. and Isloor, A. M. (2015) "Synthesis and Characterization of PSF/PPSU based polymer blend ultrafiltration membrane for heavy metal rejection" at International Conference on membrane-based separations (MEMSEP-2015), The Maharaja Sayajirao University of Baroda, Gujarat, India.

2. Moideen K, I. and Isloor, A. M. (2016) "The Effect of Glycine Betaine additive on the PPSU/PSF Ultrafiltration membrane performance" at National conference on recent trends in chemical sciences (NCRTCS-2016), Manipal University, Manipal, Karnataka, India.

3. Moideen K, I. and Isloor, A. M. (2016) "Preparation, characterization of sulfonated polyphenylsulfone (sPPSU) ultrafiltration membranes for protein and toxic heavy metal separation" at International Conference on Advanced Polymer for science and technology (APST-2016), Vellore Institute of Technology, Vellore, Tamil Nadu, India.

4. Moideen K, I. and Isloor, A. M. (2017) "Fabrication of Hollow Fiber Membrane Encrusted with Chitosan Nanoparticle and Ag Loaded Chitosan Nanoparticle for Dye Rejection and Antibiofouling Property" at International Conference on Recent Trends in Chemical Science (ICRCS-17), Govt. Engineering College, Bikaner, Rajasthan, India.

AWARDS AND ACHIEVEMENTS

1. Best poster in International Conference on Recent Trends in Chemical Science (ICRCS-17), GEC, Bikaner, Rajasthan, India.

2. Best poster at International Conference on Advanced Polymer for science and technology (APST-2016), VIT, Vellore, Tamil Nadu, India.

3. IASc "Summer Research Fellowship 2012".

4. Received "merit of excellence" (2008, 2009 & 2010).

PERSONAL DETAILS

Address for correspondence	#203, Abode Apartment, Kalpana Road, Falnir, Mangalore.
Date of birth	17/02/1990
Sex	Female
Nationality	Indian
Languages known	English, Hindi, Malayalam, Kannada,

REFERENCES

Dr. Arun M. Isloor

Associate Professor

Dept. of Chemistry

NITK-Surathkal, Mangalore

Phone no: +91-9448523990

Email: isloor@yahoo.com

Prof. (Dr.) A. F. Ismail

Director

Advanced Membrane Technology Centre (AMTEC)

Universiti Teknologi, Malaysia

Phone no: +60-97775545

Email: afauzi@utm.my